Title

Understanding multi-kingdom communication in plant-microbe endosymbiosis

Author

Serrano, Karen

Publication Date

2024

Peer reviewed|Thesis/dissertation

Understanding Multi-Kingdom Communication in Plant-Microbe Endosymbiosis

By

Karen Serrano

A dissertation submitted in partial satisfaction of the

requirements for the degree of

Doctor of Philosophy

in

Plant Biology

in the

Graduate Division

of the

University of California, Berkeley

Committee in charge:

Professor Henrik Vibe Scheller, Chair
Professor N. Louise Glass
Professor Devin Coleman-Derr

Spring 2024

Abstract

Understanding multi-kingdom communication in plant-microbe endosymbiosis

by

Karen Serrano

Doctor of Philosophy in Plant Biology

University of California, Berkeley

Henrik Vibe Scheller

Microbes, plants, and humans are globally interconnected through dynamic symbiotic relationships that influence ecosystem balance, agricultural productivity, and human health. Among these interactions, endosymbiosis, characterized by microorganisms residing within the cells of other species, represents a critical relationship that requires sustained communication across kingdoms. This thesis explores the connections between microbes, plants, and humans and examines recently developed approaches to the study of endosymbiosis and their implications for plant productivity and human nutrition. Starting with a discussion of the new methods by which scientists are beginning to target crop genetic engineering for certain beneficial effects on the human gut microbiome and moving to a discussion of new available RNA-sequencing technologies and their applications in plant-microbe endosymbiosis, I present unique avenues to symbiosis research that overcome barriers to prior investigations. Applying single-nuclei and spatial transcriptomic technologies to the arbuscular mycorrhizal symbiosis, I demonstrate the utility of such approaches in the identification of symbiosis-responsive cell populations from both species and present hundreds of new targets for further functional characterization and genetic engineering of an improved symbiosis. Lastly, I analyze the effects of such genetic modifications on symbiotic interactions in agriculturally-relevant plant species, contributing to the development of strategies to enhance symbiosis in agricultural settings. In essence, this thesis presents fundamental discoveries about previously unknown aspects of cross-species communication during symbiosis and offers insights into the latest methodologies applied to analyze symbiosis at a cellular level.

Table of Contents

List of Figures

List of Tables

Acknowledgements

I would first like to thank my esteemed supervisor – Dr. Henrik Vibe Scheller for his invaluable support during the course of my Ph.D. degree. His insight, optimism, and patience during my doctorate transformed what is typically a difficult process into an enjoyable journey. My gratitude extends to Dr. Benjamin Cole and Dr. Margot Bezrutcyzk who provided extensive technical and professional guidance and aide, as well as Dr. N. Louise Glass and Dr. Devin Coleman-Derr, for their continuous advice and feedback which shaped my thesis research.

I would also like to express gratitude to all of my colleagues who have taught me more than I could have ever imagined learning and have helped me without question every time I asked. Thank you to Victoria Vera, Tomo Yoshino, Lorenzo Washington, Dr. Christopher Gee, and Dr. Jutta Dalton, as well as all of the Feedstockers at the Joint Bioenergy Institute, Lawrence Berkeley National Laboratory. Special thanks to Dr. Simona Radutoiu, Dr. Jens Stougaard, and Dr. Stig U. Andersen, and Dr. Francesca Tedeschi, and all other colleagues in the Department of Molecular Biology and Genetics at Aarhus University for welcoming me to their laboratories, collaborating on research projects, and introducing me to all of the strange aspects of Danish culture. I'd also like to thank all of the following co-authors: Danielle Goudeau, Dr. Thai Dao, Dr. Ronan O'Malley, Dr. Rex Malmstrom, and Dr. Axel Visel. All of these scientists and mentors have encouraged me daily in my academic research and daily life.

I am additionally grateful for the research funding I received from the U. S. Department of Energy, Office of Science, Office of Biological and Environmental Research, through contract DE-AC02-05CH11231 between Lawrence Berkeley National Laboratory and the U.S. Department of Energy, by the project Molecular Mechanisms and Dynamics of Plant-Microbe Interactions at the Root-Soil Interface (InRoot), supported by the Novo Nordisk Foundation grant no. NNF19SA0059362, the Latinxs and the Environment Fellowship at UC Berkeley, the Chicanx and Latinx Student Development Center, and the Berkeley Fellowship.

Last but definitely not least, I'd like to thank all of my family and loved ones who encouraged and supported me throughout my entire academic journey. To my dad, Dr. Rafael Serrano, thank you for setting the best example in every single aspect and also being the most reliable chauffeur from kindergarten to graduate school. To my mom, Mary Munoz, thank you for teaching me tenacity and independence and for also allowing me to call you and complain to you over every slight inconvenience. To my sisters, thank you for keeping me humble. To my partner, Erick, thank you for always being my number one fan and for all of the bear hugs. To all of my friends and fellow students, especially the Berkeley Coven, thank you for all the days and nights spent commiserating and laughing at our situations. You all made the Ph.D. so worth it.

Introduction

Plant productivity, both in natural and agricultural ecosystems, is critical to global health and nutrition and relies heavily on services and functions carried out by microorganisms that live in the phyllosphere (the aerial surface of the plant), the endosphere (inside or between plant cells), and the rhizosphere (soil around the plant root system)[1]. These microorganisms influence plant developmental and health processes. For example, plant microbial pathogens can invade and quickly deteriorate the health of a plant, causing devastating agricultural crop losses, while other microorganisms can provide tolerance against pathogen infection[2]. Microbes can also influence plant productivity by modulating plant response to abiotic stress, such as soil salinity or drought[3]. Lastly, a plant's microbiome can impact the efficiency of photosynthesis and photosynthetic product breakdown, by affecting the absorption of atmospheric carbon dioxide, the allocation of photosynthetic carbon within the plant and beyond, and carbon storage within the soil[4–7].

Among all plant-microbe interactions, endosymbiosis represents the most intimate relationship as it is characterized by the microorganism co-existing within the plant's own cellular structure and requires sustained multi-kingdom communication between species. Endosymbiosis is an ancient process which had an immense impact on eukaryote evolution as free-living prokaryotes were taken up by eukaryotic cells and transformed into subcellular compartments which evolved into permanent organelles[8]. In the same fashion, microorganisms are allowed entry into the plant body in which they traverse across and between cells until they reach a final destination, at which point the plant creates symbiosis-specific cellular structures that will house and maintain the microbe throughout the symbiosis. There are two main plant root endosymbioses that are widespread among vascular plants and are credited for enhancing nutrition of major plant micronutrients.

The first is the interaction between roots and Glomeromycota fungi, termed the "Arbuscular Mycorrhizal" or "AM" symbiosis. The AM symbiosis is credited for the evolution of land plants, as it has been suggested the earliest land plants were dependent on the fungal symbiont's capabilities for foraging of soil nutrients and water. In present-day, more than 80% of all vascular land plants are capable of participating in this symbiosis and the AM symbiosis has been reported in all terrestrial ecosystems[9]. This interaction is initiated by plant phosphate stress-induced signaling and recruitment of germinating and branching AM fungi from the soil to the root surface[10]. Once physical contact between the species has been established, AM fungal hyphae traverse between and across plant root cells to the inner cortical cell layer in which the plant and fungus coordinate to build a plant-derived peri-arbuscular membrane (PAM) around a highly-branched hyphal structure called an arbuscule within the cell. It is across this PAM that the majority of metabolite exchange occurs between the two species, enabled by PAM-localized transporters from both partners[11]. Through the creation of this extra- and intra-radical hyphal network, AM fungi are able to extend the root surface area and scavenge nutrients and water, particularly phosphorus, from the surrounding soil for the plant. In return, the plant host rewards their symbiont with a supply of photosynthetic carbon, in the form of lipids and sugars, which sustains the hyphal network and maintains the symbiosis.

The second interaction occurs between leguminous plant roots and rhizobial bacteria, termed the rhizobial symbiosis. The rhizobial symbiosis is thought to have evolved from the AM symbiosis, as many genetic components of the symbiotic interaction are shared between or co-opted from those of the AM symbiosis[12,13]. It is initiated by the production and exudation of flavonoid signaling compounds from plant roots into the soil, which activates rhizobial production and exudation of their own signals, called Nod factors[14]. Upon perception of Nod factors, the plant initiates the creation of a new organ called a nodule. This process begins with the curling of root hairs to form an infection thread, root cortical cell division, and eventual nodule primordium formation. Rhizobia are then able to enter cortical cells via this infection thread and travel to the nodule primordium where they are then maintained in plant-derived cell compartments called symbiosomes[15]. In these structures, rhizobia convert atmospheric nitrogen (N2) into ammonia, a form of nitrogen usable by the plant. In return, the legume will supply the bacteria with photosynthetic carbon. Similarly, the symbiosis between *Frankia* bacteria with actinorhizal plant species also leads to nodule formation and nitrogen-fixation and transfer from bacteria to plant[16].

The similarities between these two types of endosymbiosis are clear. Both involve two species from different kingdoms developing and sustaining communication to coordinate physical contact and metabolite trade, with the microbe supplying otherwise unreachable or unusable nutrients and water from the soil and the plant host allocating a portion of the carbon from its own photosynthetic capabilities to the microbe in order to enable the microbe's activities. This mutualistic relationship, or contract, between the two species, is contingent upon both species benefiting from the arrangement. In the case of AM fungi, the fungus is an obligate biotroph, dependent on the symbiosis with the plant host to complete its full life-cycle[9]. For both rhizobia and AM fungi, the microbes depend on the carbon supply from the host to carry out sufficient growth, development, and metabolic activities[17,18]. For plant hosts, the metabolites and other benefits derived from this interaction must offset the loss of photosynthetic carbon as well as the energy and physical space devoted to house the symbiont[19]. For example, it has been demonstrated that in environments with sufficient soil phosphorus concentration, plants will "turn off" this symbiotic programming, suppressing mycorrhization when it is not needed[20]. Likewise, AM fungi have been shown to preferentially select different plant hosts, allocating more resources to "higher quality" hosts[21]. Research has shown similar processes for the rhizobial symbiosis, as legumes monitor and respond to the performance of rhizobial symbionts, punishing low-nitrogen fixing bacteria by breaking down nodules[22].

How do these different species communicate with each other during symbiosis? This question has been the primary focus of symbiosis research for the past few decades, with many discoveries revealing the identity and functions of various signaling components in both symbioses[12,20,23–31]. Additionally, emphasis has been placed on understanding the gene expression changes associated with symbiosis, with many research groups utilizing a broad array of RNA-sequencing technologies to analyze symbiosis-specific transcriptome signatures[32–44]. This thesis focuses on the development and application of novel genetic and transcriptomic technologies to study host-plant-microbe interactions, particularly the aforementioned AM and rhizobial endosymbiosis in order to better understand cross-species communication and identify candidates for genetic engineering for improved symbiosis. There are four main chapters in this thesis. **Chapter 1,** entitled "Soil to stomach: The "one health" approach to host-microbe interactions", will serve as an overview of how plant-microbe interactions can impact human

health and nutrition, particularly by examining the impact of raw vegetables and fruit consumption on the human gut microbiome[45] and how researchers are beginning to target genetic engineering of crops to improve plant endophytic microbial communities**. Chapter 2,** "Unraveling plant-microbe endosymbiosis with single-cell and spatial transcriptomics", is a research review that covers advances in single-cell and spatial transcriptomic technologies and their recent applications to the AM and rhizobial endosymbiosis. **Chapter 3,** "Spatial co-transcriptomics reveals discrete stages of the arbuscular mycorrhizal symbiosis", will describe my main thesis work combining single-nuclei and spatial transcriptomics to the analysis of the AM symbiosis between the model legume *Medicago truncatula* and the AM fungus *Rhizophagus irregularis*[46]. **Chapter 4,** "Effects of plant host genetic modification on the arbuscular mycorrhizal colonization capacity of *Rhizophagus irregularis* on *Oryza sativa* and *Sorghum bicolor*" describes two research projects conducted to analyze the effects of genetic engineering for various desired phenotypes on the symbiotic ability of two major agriculturally-relevant plant species: *Oryza sativa* and *Sorghum bicolor.*

Chapter 1. Soil to Stomach: The "One Health" Approach to Host-Microbe Interactions

Including material from published work from **Karen Serrano** and Margot Bezrutzyck. "Genome to gut: crop engineering for human microbiomes". Nature Reviews Microbiology. 2023 Mar; 21(3):132. doi: 10.1038/s41579-022-00850-6.

1.1 Introduction

For living organisms on planet Earth, there is no such thing as "isolation". No matter the domain of life, living organisms exist in an interdependent manner, interacting with and influencing the other inhabitants of each ecosystem. The scale and extent of this interaction can vary dramatically. A human crushing hundreds of ants with one heavy step on an anthill is one example of this interconnectedness between species, while two archaeal species surviving extreme temperatures within the same hot spring represent another. In recent years, much attention has been focused on this concept of interdependence between organisms, especially the microbial organisms that humans cannot easily see. Published in the *Proceedings of the National Academy of Sciences in* 2018, researchers profiled the biomass distribution in gigatons of carbon for all living organisms on Earth[47] and found that plants constitute the majority of global biomass (450 Gt C), with bacteria (70 Gt C) and fungi (12 Gt C), constituting the top three most abundant kingdoms. Humans, for reference, constituted a mere 0.6 Gt C, representing less than 1% of life. Acknowledging the pervasiveness and enormity of the plant, bacterial, and fungal presence across the Earth, the "One Health" concept, first coined at a symposium held in 2004 by the Wildlife Conservation Society (https://oneworldonehealth.wcs.org/), is an approach which recognizes human health is linked with and reliant upon the health of other ecosystem components, including soil as well as other animals, plants, and microorganisms[48]. Microbes associate with humans, animals, and plants and can contribute to the health of these organisms, with microbial communities functioning as a "second genome"[49,50]. This approach extends beyond the classic study of microbial pathogens responsible for animal or plant disease to cover all microbial associations, whether detrimental, beneficial, or neutral, and their implications for ecosystem health[51].

The human gut microbiome, referring to the collective bacterial, archaeal, and eukaryotic microorganisms which colonize the gastrointestinal tract, represents on average more than 10^{14} microbial cells[52]. The gut microbiome is considered to have the most influence on human health of all human body microbiomes, serving a variety of functions. One of the main functions is to aid in food digestion and fermentation of indigestible nutrients, particularly the metabolism of non-digestible carbohydrates such as starches, cellulose, hemicellulose, and pectin, all major components of plant cells[53]. This allows for improved absorption for the human host while serving as an energy source for microbial growth. The gut microbiota can also provide protection from intestinal colonization by pathogens. Higher microbial diversity within the gut is associated with higher pathogen colonization resistance, and lower microbial diversity, a result of antibiotic treatment, can lead to reduced nutrient competition, leading to an increase in colonization and growth of pathogens[54]. The gut represents the largest immune organ in the human body[55]. Accordingly, the gut microbiome can affect the local mucosal immune system as well as systemic immune function[56]. Lastly, humans rely on their gut microbiota for the production of

amino acids and vitamins such as vitamin K, biotin, cobalamin, pantothenic acid, riboflavin, and thiamine[57]. On the other hand, the disturbance of gut microbial communities, known as "dysbiosis", can lead to adverse health effects for the human host. Inflammatory bowel disease, obesity, diabetes, autoimmune disease, and cardiovascular disease have all been linked to gut microbiome dysbiosis[58]. As humans age, gut microbiome communities become less stable and less diverse, resulting in increased frailty and decreased immune function[59].

What factors determine the health of the human gut microbiome? To answer this question, one must first define a "healthy" human gut microbiota, which is a difficult task given the high degree of variation across human individual gut microbial communities. However, research suggests that a "healthy" gut microbiome should exhibit two main characteristics. The first of these is high community diversity. Higher taxonomic diversity and higher microbial gene richness are associated with healthy individuals, while lower diversity is associated with dysbiosis and adverse health effects[60]. The second is community resilience, the ability to return to a stable state after a disturbance. Healthy individuals with more diverse microbiomes or with more stable core microbiomes display a higher level of resistance to perturbations when compared to microbiomes of individuals with disease[61]. Multiple studies have determined the dominant gut microbial phyla in healthy individuals to consist of Firmicutes, Bacteroidetes, and Actinobacteria[62,63]. Other phyla, such as Proteobacteria, Fusobacteria, and Verrucomicrobia are also represented. There are several environmental and genetic factors that influence gut microbial composition. Of these, environmental factors, such as diet and medication, have been demonstrated to have stronger influence on shaping the composition of the human gut microbiome, with host and genetic factors playing a minor role[58,64–66].

The idea that the human gut microbiome composition can be modulated by diet has garnered much attention and been the focus of many research studies in recent years. Dietary components such as protein, fats, digestible and non-digestible carbohydrates, as well as targeted dietary intervention such as prebiotics and probiotics, are all demonstrated to induce changes in the gut microbiome[67]. Probiotic foods or supplements contain live bacterial or fungal organisms that can be consumed to increase the proportion of beneficial intestinal microbes whereas prebiotics, sources of non-digestible oligosaccharides and polysaccharides, are administered to act as foods for probiotics within the gut microbiome[68]. Studies suggest that a diet high in fiber and other nondigestible carbohydrate prebiotics increase microbiota gene richness and community diversity, as these carbohydrates are readily accessible to gut microbiota for fermentation[69]. Plant-based diets such as those of vegans and vegetarians have unique impacts on the gut microbiome and have been reported to be associated with higher species richness compared to omnivore diets, specifically with higher abundance of protective microbial species[70,71]. This is due to their increased carbohydrate, fiber, and phytochemical content, and the high quantity of polyphenols in particular provides protection against pathogens and has anti-inflammatory effects[72].

When we consume plants, we are also consuming all of the microorganisms that these plants harbor which is referred to as the "edible plant microbiome". Fruits, vegetables, herbs, and nuts all are often consumed raw and harbor unique and diverse bacterial communities derived from the soil and surrounding environment[73]. Certain types of produce also share more similar microbial communities. For example, fruits and vegetables grown closer to the soil surface such

as sprouts, spinach, tomatoes and strawberries all had higher abundance of Enterobacteriaceae than other produce[74], and there are significant differences between conventionally and organically grown produce[75]. For years, scientists have hypothesized that the consumption of the edible plant microbiome could modulate the human gut microbiota, and the first evidence for raw fruit and vegetable consumption influencing the developing gut microbiota was provided by Wickasano et al. through the reconstruction of 156 fruit and vegetable metagenomes compared to 2,426 human gut microbiomes[76]. This connection between soil, plant, and human microbiomes exemplifies One Health principles and implies that factors which influence soil health and resulting fruit and vegetable microbiomes, such as agricultural practices, could affect human health. The following Genome Watch article published in Nature Reviews Microbiology[45], details how metagenomics aids in profiling plant-derived microorganisms and molecules that could have an impact on the composition and function of the human gut microbiome.

1.2 Genome to gut: crop engineering for human microbiomes

The microbial community structure within the human digestive system is linked to our health and nutrition, which highlights the influence of these organisms in metabolic homeostasis and disease prevention. The composition and diversity of the human gut microbiome is modulated through diet and medication. High consumption of plant-derived fibers and bioactive molecules have been shown to increase the abundance of beneficial microorganisms and expression of functional microbial genes within our gut that may have a positive impact on health[68]. Recent studies applying functional genomics to identify plant-derived microorganisms and molecules that may shape the human gut microbiome are transforming modern crop engineering by shifting focus to the manipulation of this symbiosis.

To identify genetic loci that contribute to *Sorghum bicolor* traits that could alter the composition of human gut microbial communities, Yang et al. developed a novel approach: automated in vitro microbiome screening (AiMS)[77]. The authors applied AiMS to 294 *Sorghum* recombinant inbred lines, identifying 10 significant loci associated with gut microbial composition. Two loci, linked to increased tannin content and dark seed colour, significantly affected the relative abundance of *Faecalibacterium prausnitzii*, the depletion of which is associated with inflammatory bowel disease. *F. prausnitzii* demonstrated consumption of condensed tannins in axenic culture, which supports the hypothesis that sorghum-derived tannins may stimulate growth of these protective bacteria. AiMS can be broadly applied to crop species, which increases our ability to study the effects of complex plant traits on the human microbiome. However, only a small number of human gut microbiome samples were applied in the AiMS analyses, and further experimental validation is needed to establish direct links between the sorghum-derived prebiotic fibres and gut microbial communities.

Human diets do not solely consist of the crops we consume, we also consume crop-associated microorganisms. The ‘edible plant microbiome’ refers to microorganisms associated with raw plant tissues that may influence human gut microbiomes and overall nutrition[78]. In 2017, Wassermann et al. pioneered using 16S rRNA sequencing to characterize the microbial composition of *Brassica* vegetables, uncovering possible human health-relevant microbial functions of the dominant genera[79]. Similarly, Soto-Giron et al. used shotgun metagenomics to profile microbial communities found in tomatoes, baby spinach, green olives and dry figs[80].

Taxonomic analysis revealed that Proteobacteria dominated all sample microbiomes, but major differences exist at the genus level between fruits and vegetables. Functional annotation uncovered the presence of metabolic pathways associated with human gut microbiome homeostasis, such as glutamate and biotin synthesis, and numerous carbohydrate-active enzymes (CAZymes), which supports the idea that plant-derived microorganisms and metabolites may provide a metabolic function to the human gut microbiome[80]. As the repertoire of edible plant microbiomes grows, it will be critical to consider the persistence of these microorganisms throughout digestion before assessing their impact on human nutrition.

Historically, genetic engineering of crops focused on increasing yield, whereas nutrition, resilience and other traits were considered secondarily. These studies highlight the incredible diversity of plant-derived microorganisms and molecules in our diets that may be modulating the composition and functionality of our gut microbiomes. It is exciting to imagine that in the near future, the relationship between human gut microorganisms and plant biochemistry will have a prominent role in crop breeding and the development of plant-based foods.

1.3 Significance Statement

This chapter focused broadly on the intersection of plant, microbial, and human health, establishing a direct link between soil, plant, and human microbial communities and microbial gene function. The edible plant microbiome is an exciting area of research that presents a novel direction for future crop breeding, genetic engineering, and development of agricultural practices. With the growing amount of evidence on the effects of diet on the human gut microbiome, consumers are increasingly adopting plant-based diets and purchasing prebiotic and probiotic products. The global market for prebiotic and probiotic food and supplements is expected to reach 85.4 billion dollars by 2027[81] and the plant-based food market is expected to reach 162 billion dollars by 2030[82] which holds immense potential for agricultural and biotechnology research. Further research into what plant host genetic components are linked to plant microbial composition, how these connections can be synthetically altered to improve human health upon composition, and longitudinal studies that establish a timeline for these changes within the gut microbiome will undoubtedly lead to the development of advanced food and dietary products. The remaining three chapters in this thesis continue to build upon the idea of symbiosis by focusing on beneficial plant-soil microbe endosymbiosis. These intimate, mutualistic relationships are another strong area of focus for crop engineering as they represent a direct interaction between plants and soil microbes that naturally provides a plethora of benefits to the plant host and could be manipulated to favor plant productivity.

Chapter 2. Unraveling Plant-Microbe Endosymbiosis with Single-cell and Spatial Transcriptomics

Including material from invited review manuscript from **Karen Serrano,** Francesca Tedeschi, Stig U. Andersen, and Henrik Vibe Scheller. "Unraveling plant-microbe endosymbiosis with single-cell and spatial transcriptomics." Trends in Plant Science, *submitted Jan 2024*.

2.1 Abstract

Plant-microbe symbioses require intense interaction and genetic coordination to successfully establish in specific cell types of the host and symbiont. Traditional RNA-sequencing methodologies lack the cellular resolution to fully capture these complexities, but single-cell and spatial transcriptomics are now allowing scientists to probe symbiotic interactions at an unprecedented level of detail. Here, we discuss the advantages that novel spatial and single-cell transcriptomic technologies provide in studying plant-microbe endosymbiosis and highlight key recent studies. Finally, we consider the remaining limitations of applying these approaches to symbiosis research, which are mainly related to simultaneous capture of both plant and microbial transcripts within the same cells.

2.2 Transcriptomic Investigations of Plant-Microbe Symbioses

The field of plant transcriptomics has experienced rapid growth and comprehensive reviews describe recent developments in plant single-cell transcriptomes[83–87]. Technological advances in single-cell (scRNA-seq) and spatial RNA-sequencing present new opportunities for research into complex plant-microbe interactions. scRNA-seq allows for the study of gene expression occurring in individual cells, rather than whole-tissue, providing more detail into heterogeneous cell populations. scRNA-seq can be applied to investigate the response of individual plant cells to symbiotic infection, revealing cell-type specific gene expression. Spatial transcriptomics enables analysis of individual cells in fixed positions within the tissue, providing the physical location of gene expression[88]. This methodology provides insight into the spatial organization of plant and symbiont gene expression during symbiosis. In this review, we focus on the utilization of high-throughput scRNA-seq and spatial RNA-seq technologies to investigate beneficial plant-microbe interactions.

2.3. Open Questions in Plant-Microbe Endosymbiosis

Plant species engage in mutually beneficial interactions with a wide array of microorganisms. A prevalent characteristic of such symbioses is the microorganisms' capacity to promote plant growth by facilitating the acquisition of scarce nutrients. By trading these nutrients, the microbe receives carbon generated by the plant. The legume-rhizobial bacteria and the plant-arbuscular mycorrhizal fungi (AMF) interactions are two of the most well-explored endosymbioses, characterized by intra-cellular accommodation of the symbiont (Fig. 2-1).

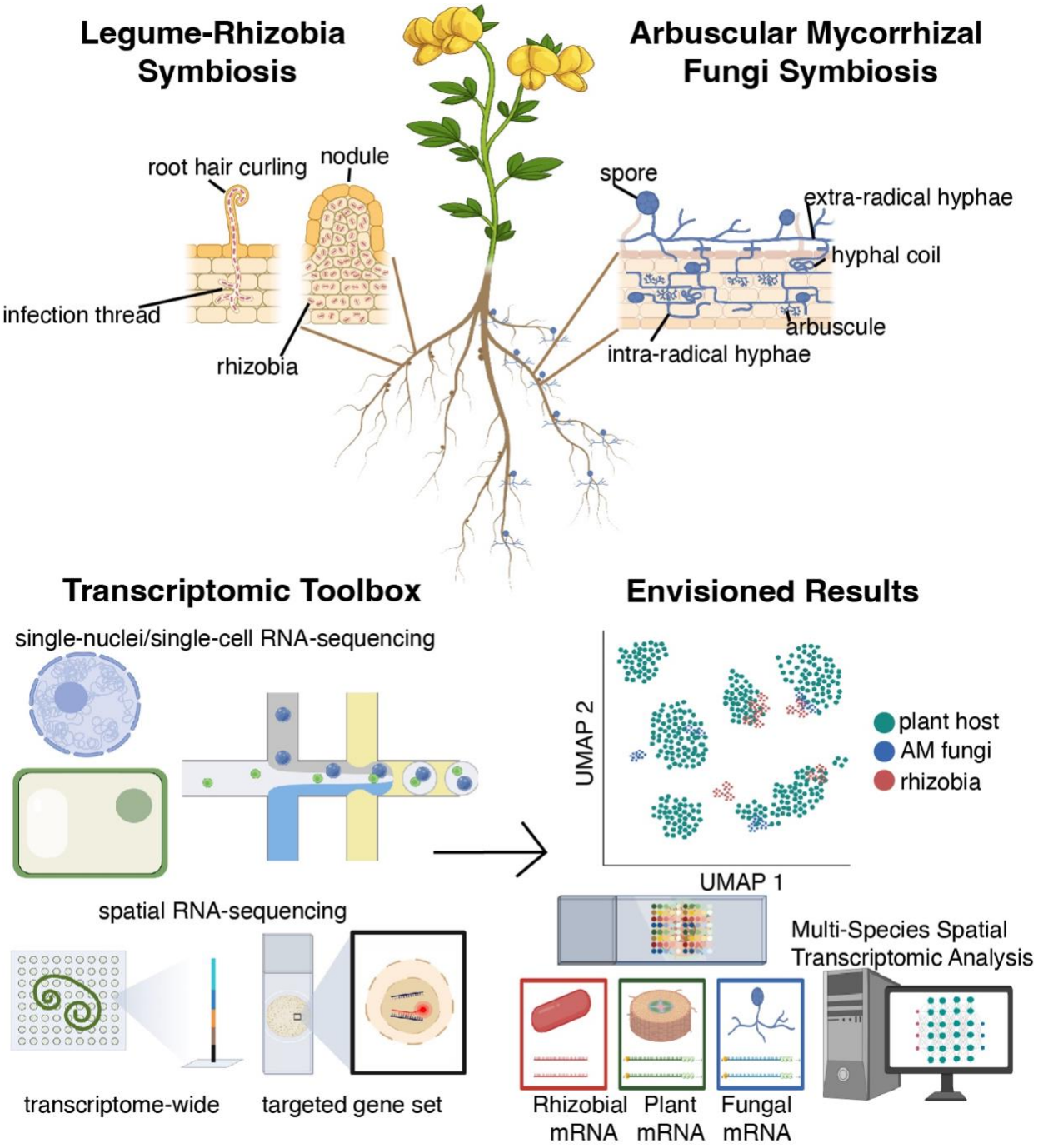

Figure 2.1. Transcriptomics as a Tool for Plant-Microbe Endosymbioses

An overview of the legume-rhizobia and plant-arbuscular mycorrhizae symbioses and the corresponding microbial structures. The legume-rhizobia symbiosis is characterized by rhizobial infection of root cells that causes curling of root hairs and the development of infection threads. Infection threads extend through the root hair into cortical cells and culminate in the formation of specialized structures called nodules in which bacteria convert atmospheric nitrogen into a form usable by plants. The legume rewards the bacteria with carbon. The arbuscular mycorrhizal fungi-plant symbiosis involves controlled intracellular and intercellular fungal hyphal

colonization of the plant root and culminates in the formation of arbuscules, highly branched fungal hyphal structures, in which soil nutrients are transferred from the fungus to the plant host in exchange for carbon. Single-cell and single-nuclei RNA-sequencing technologies and both targeted and non-targeted spatial RNA-sequencing technologies have evolved over recent years and hold great potential as tools to study the complexities of plant-microbe endosymbioses. The ultimate goal of such studies is to be able to simultaneously capture microbial endosymbiont and plant host RNA during these interactions in order to study cell-type specific infection expression patterns in a spatially-resolved manner. Figure created with BioRender.com.

The legume-rhizobia interaction is characterized by a complex biological process leading to the formation of specialized structures called nodules where the bacteria reside and convert atmospheric nitrogen into a form usable by plants. Nodulation has been extensively investigated at cellular, molecular, and physiological levels and requires the activation of temporally and spatially coordinated programs in a limited number of root cells [31,89]. This involves sophisticated communication, mediated by flavonoids and nodulation (Nod) factors. Legumes release flavonoids into the soil to recruit potential symbiotic partners. Rhizobia sense flavonoids and produce Nod factors in response. Nod factors, in turn, trigger a response in the root that leads to root hair curling and culminates in the formation of an infection pocket and development of infection threads (ITs). ITs extend through root hairs towards cortical cells and ramify in nodule primordia, which are formed by dividing cortical cells, facilitating the release of rhizobia into nodules. The perception of rhizobia in root hairs of legumes such as *Phaseolus, Glycine* and *Lotus spp* induce the formation of nodules that lose their meristematic activity over time (determinate nodules), while other legumes like *Pisum sativum* and *Medicago truncatula* form indeterminate nodules with a persistent meristem [90].

What are the requirements for successful intracellular rhizobial infection? How does the plant decide which root hair among thousands should respond to the rhizobia facilitating the initiation or progression of intracellular ITs? Classical transcriptomic approaches applied to whole roots and root hairs of legume models have brought us closer to answering these questions[40 91]. These studies were able to capture infected cells, but could not distinguish between the transcriptional signatures of root hairs that were successful in IT formation and those that were unsuccessful but still exhibit a symbiotic response.

The plant-AMF symbiosis is defined by the controlled fungal colonization of roots which culminates in both extra- and intra-radical hyphal networks as well as branched structures called arbuscules within cortical cells that facilitate metabolite transfer[92]. Intercellular passage and subsequent intracellular accommodation of the fungus involves novel gene expression in both colonized and non-colonized adjacent plant cells and continuous signaling between the partners[93–95]. Nutrient-stressed plant roots exude strigolactones into the soil which stimulate AMF spore germination and hyphal branching towards the root[96,97]. AMF exude Myc factors[98] in response, which trigger plant transcriptional and physiological responses. Following physical contact, hyphae enter the epidermal cell layer and subsequently travel inter- and intra-cellularly to the inner cortical cells in which arbuscules will form[99]. Once inside the cortical cell, the fungus penetrates the plant cell wall and the plant synthesizes a new peri-arbuscular membrane to surround the arbuscule, equipped with proteins responsible for facilitating metabolite exchange[99–101]. A suite of physiological changes occur in the cell to accommodate and maintain the arbuscule, including, but

not limited to, a reduction in vacuole size and organelle compaction[101]. Arbuscules are transient structures[102], thus the window for this exchange is limited.

Due to asynchronous colonization, multiple fungal structures exist within different cell types simultaneously, which precludes efforts to tackle the complexities of the transcriptional programs involved in this symbiosis with traditional RNA-sequencing methods. How can the individual stages of AM symbiotic development be distinguished when they are occurring simultaneously within the root tissue? How do colonized cells and adjacent non-colonized cells differ in their transcriptional signatures? How does the fungus control its development within the root and subsequent metabolite transfer from the soil? Many traditional transcriptomic studies of AMF-inoculated and mock-inoculated roots from many different plant and fungal partners have identified thousands of differentially regulated genes under mycorrhizal conditions[34,41,42,103–109]. Insights from studies utilizing laser-capture microdissection [94,95] have revealed the importance of including non-colonized cells adjacent to arbusculated cells. Furthermore, research regarding the genetic landscape and expression patterns of arbuscular mycorrhizal fungi[35,36,110–117] has greatly expanded our knowledge of the symbiont in this interaction. Advances in RNA-seq technology will enable research into cell-type specific responses from both partners.

The commonalities between these endosymbioses continue to emerge, supporting the theory that rhizobia co-opted existing cellular programs for the AMF symbiosis for bacterial accommodation[118,119]. Due to large differences in culturability between bacteria and fungi, research into endosymbioses has focused on the legume-rhizobia symbiosis. In particular, on the Common Symbiotic Signaling Pathway (CSSP) that includes genes with similar functions in both symbioses[30,89]. However, additional genes with roles in both symbioses that fall outside of this pathway and numerous genes within the pathway with fine distinctions in their functions exist in either pathway[30]. The details of how these two systems overlap and how each influences the other during co-infection will likely be revealed with further transcriptomic analysis.

2.4 A Transcriptomic Toolbox for Symbiosis Research

Novel transcriptomics technologies are revolutionizing gene expression analysis, providing unprecedented insights into the complexity of biological systems. These advancements mark a step forward to uncover fundamental cellular and molecular processes in symbiosis. However, as RNA-seq methodologies continue to rapidly diversify across various platforms, it is important to understand the unique features and applications of each method. This knowledge is crucial for making an informed choice on how to most effectively answer open questions in plant-microbe interactions.

scRNA-sequencing involves key steps such as single-cell (or single-nuclei) isolation and capture, cell lysis, reverse transcription, cDNA amplification, and library preparation. The first step, separating and isolating intact plant protoplasts or nuclei, is critical. If the integrity of these biological entities is compromised, this could decrease detection of Unique Molecular Identifiers (UMIs) and genes. There are distinct differences between cellular and nuclear transcriptomes in plants. The cellular transcriptome contains transcripts from the nuclear and organellar compartments, while the nuclear transcriptome is less complex and contains polyadenylated mRNA transcripts and ribosomal RNAs. Thus, while nuclei extraction is often quicker and more adaptable, the nuclear transcriptome may fail to capture important biological processes involved

in mRNA processing, RNA stability, and metabolism[84,120]. Protoplasting plant tissues, however, involves cell-wall degrading enzymes, which may induce artificial stress responses. Additionally, Van den Brink and colleagues [121] revealed dissociation-induced transcriptome changes as the potential outcome of the physical dissociation process during single-cell isolation in animal cells. To test the validity of protoplasting, researchers combined the scRNA-seq data of all captured cells from plant root into a pseudo-bulk dataset and compared this dataset with a conventional bulk RNA-seq dataset of non-protoplasted plant root tissues and found the two datasets highly correlated with each other, regardless the presence or absence of protoplasting-induced genes [122,123]. Despite their potential limitations, both single-cell and single-nuclei RNA-sequencing are valid methodologies.

To date, the main high-throughput technology for sn/scRNA-seq in plant single-cell transcriptomics is Chromium, a microfluidics-based method, provided by 10X Genomics [124]. In brief, single cells or single nuclei are encapsulated along with gel beads-containing barcoded oligonucleotides, reagents and oil to create GEMs (Gel bead-in-EMulsion) in which the reverse transcription of poly-adenylated mRNA occurs. When the GEMs are broken and the barcoded cDNAs are released, the entire cDNA content of a single cell or nucleus will have the same barcode, allowing the sequencing reads to be mapped back to their original single cell/nucleus of origin (https://www.10xgenomics.com). Emerging technologies that do not rely on complex instruments have been developed with the prospect of reducing costs and increasing accessibility. Particle-Templated Instant Partitions (PIPseq™) can simultaneously segregate complex cell mixtures into partitions with barcoded template particles that can be processed for scRNA-Seq (https://www.fluentbio.com/technology/). Another rising technique is Evercode™ from Parse Bioscience. The Evercode™ combinatorial barcoding technology uses particle-templated emulsification to enable single-cell encapsulation and barcoding of cDNA in droplet emulsions, providing a simple, flexible, and scalable next-generation workflow for scRNA-seq (https://www.parsebiosciences.com/technology).

Spatial transcriptomics enables the preservation of a cell's position and thus spatial tracking of gene expression[125]. Plant-microbe endosymbioses are restricted to specific cell types and manifest in various unique symbiotic structures within and between plant cells. Therefore, it is critical to preserve the spatial landscape. There are many reviews that cover all recently-developed spatial technologies[126–129], but here we focus on two main types: 1) Spatial barcoding-based transcriptome-wide and 2) targeted *in situ* hybridization (ISH)-based.

Untargeted technologies include Spatial Transcriptomics (ST)[130], Slide-Seq/V2[131,132], High-Definition Spatial Transcriptomics (HDST)[133], Deterministic Barcoding in Tissue (DBIT-seq)[134], Seq-Scope[135], and Stereo-Seq[136] (Table 2-1). All of these allow for transcriptome-wide capture of mRNA transcripts from fresh-frozen or Formalin-Fixed Paraffin-Embedded tissue sections and rely on positional next-generation sequencing to generate spatially-resolved transcriptomic libraries. These technologies differ greatly in their resolution, capture efficiency, and accessibility, all of which can significantly impact the quality of resulting libraries[137]. ST, first developed in 2016 and commercialized in 2018 by 10X Genomics as Visium, is the most widely used. Tissue sections are fixed to Spatial Gene Expression Slides engineered to enable spatially-barcoded mRNA capture from ~5000 voxels (barcoded oligo-capture spot). Cells are permeabilized directly on the slide, releasing mRNA onto the capture oligos within the voxels, and reverse transcription

and subsequent cDNA library construction is performed. Given that Visium is commercially available and relatively adaptable, the main limitation of this method is the resolution of ~55-um, which for many tissues is above single-cell. To date, two untargeted technologies can achieve sub-micron resolution: Seq-Scope and Stereo-Seq. Seq-Scope indirectly measures mRNA at ~0.6um resolution[135]. Another advantage of Seq-Scope is that its high capture efficiency (~4,700 UMIs/cell) is comparable to scRNA-seq methodologies[135]. Stereo-Seq, or Spatial Enhanced Resolution Omics-Sequencing, uses DNA nanoball (DNB) technology for RNA capture[136]. Stereo-Seq achieves the highest density of capture spots and highest resolution of all spatially-barcoded methods[136].

In situ hybridization-based methodologies all rely on direct labeling of transcripts within tissue sections to detect target gene expression. The main methodologies include MERFISH (MERSCOPE)[138], seqFISH/seqFISH+[139,140], Molecular Cartography[141], DSP[142], Split-FISH[143], EEL-FISH[144], and PHYTOMap[145] (Table 2-1). Building off the original single-molecule FISH (smFISH) technology[123,146], two methodologies were developed to allow simultaneous detection of dramatically more RNA molecules: seqFISH/seqFISH+ and MERFISH (now commercially available as MERSCOPE). Molecular Cartography is another commercially available smFISH-based technology. It has high sensitivity and is currently limited to a panel of 100 genes[141]. Lastly, PHYTOMap (plant hybridization-based targeted observation of gene expression map), was developed specifically for whole-mount plant tissue. In PHYTOMap, gene-targeted DNA probes are hybridized to targets directly within fixed whole-mount plant tissues and amplified *in situ*[145].

Technology	**Original Publication**	**Methodology**	**Commercially Available?**	**Capture Area Size**	**Resolution / Detection Limit(ISH)**
Spatial Transcriptomics	Stahl, P.L. et al. (2016) Visualization and analysis of gene expression in tissue sections by spatial transcriptomics.[56]	Untargeted, transcriptome - wide capture	Visium by 10X Genomics	6.5 x 6.5mm	55 um
Slide-seq	Rodriques, S.G. et al. (2019) Slide-seq: A scalable technology for measuring genome-wide expression at high spatial resolution.[57]	Untargeted, transcriptome - wide capture	See Slide-Seq V2.	66 tissue sections over 39x39 mm^2	10 um
High-Definition Spatial Transcriptomics	Vickovic, S. et al. (2019) High-definition spatial transcriptomics for in situ tissue profiling. [59]	Untargeted, transcriptome - wide capture	N/A	5.7 × 2.4mm	2 um
Deterministic Barcoding in Tissue	Liu, Y. et al. (2020) High-Spatial-Resolution Multi-Omics Sequencing	Untargeted, transcriptome - wide capture	AtlasXomics	3.8 x 3.8 mm	50, 25 and 10 um

	via Deterministic Barcoding in Tissue.[60]				
Seq-Scope	Cho, C. et al. (2021) Microscopic examination of spatial transcriptome using Seq-Scope. [61]	Untargeted, transcriptome - wide capture	N/A	0.8 × 1 mm	0.6 um
Slide-seq V2	Stickels, R. et al. (2021) Highly sensitive spatial transcriptomics at near-cellular resolution with Slide-seqV2. [58]	Untargeted, transcriptome - wide capture	Seeker by Curio Bioscience	3 x 3 mm or 10 x 10 mm	10 um
Stereo-Seq	Chen, A. et al. (2022) Spatiotemporal transcriptomic atlas of mouse organogenesis using DNA nanoball-patterned arrays. [62]	Untargeted, transcriptome - wide capture	STOmics by BGI	13.2 x 13.2 cm	0.22 um
MERFISH	Chen, K.H. et al. (2015) Spatially resolve, highly multiplexed RNA profiling in single cells.[64]	Targeted, *in situ* hybridization	MERSCOPE by Vizgen	2 x 1.5 cm	10,000 genes

seqFISH	Shah, S. et al. (2016) In Situ Transcription Profiling of Single Cells Reveals Spatial Organization of Cells in the Mouse Hippocampus.[65]	Targeted, *in situ* hybridization	See seqFISH+.	0.5 x 0.5 mm	250 genes
seqFISH+	Eng. C, et al. (2019) Transcriptome-scale super-resolved imaging in tissues by RNA seqFISH+.[66]	Targeted, *in situ* hybridization	GenePS by Spatial Genomics	1 x 1 mm	10,000 genes
Molecular Cartography	Groiss, S. et al. (2021) Highly resolved spatial transcriptomics for detection of rare events in cells. [67]	Targeted, *in situ* hybridization	Molecular Cartography by Resolve Biosciences	26 x 26 mm	300 nm/ 100 genes
Digital Spatial Profiling	Merritt, C.R. et al. (2020) Multiplex digital spatial profiling of proteins and RNA in fixed tissue.[68]	Targeted, *in situ* hybridization	GeoMX DSP by NanoString	35.3 × 14.1 mm	50 um/ whole transcriptome
split-FISH	Goh, J.J.L. et	Targeted, *in*	N/A	varies, 3 x	317 genes

	al. (2020) Highly specific multiplexed RNA imaging in tissues with split-FISH.[69]	*situ* hybridization		3 mm in original study	
EEL-FISH	Borm, L.E. et al. (2022) Scalable in situ single-cell profiling by electrophoretic capture of mRNA using EEL FISH.[70]	Targeted, *in situ* hybridization	Esper High Plex Assay by Rebus Biosystems	24 x 24 mm	5000 genes
PHYTOmap	Nobori, T. et al. (2023) Multiplexed single-cell 3D spatial gene expression analysis in plant tissue using PHYTOMap .[71]	Targeted, *in situ* hybridization	N/A	whole-mount	100 genes

Table 2-1. Overview of Transcriptome-Wide Spatial Methodologies

2.5 Decoding Symbiosis: Transcriptomic Research on the Legume-Rhizobial and Plant-Mycorrhizal Interactions

Pioneer scRNA-seq work in *A. thaliana* roots [123],[147],[148],[149],[150],[151] paved the way for transcriptomic investigation of different biological processes across diverse plant species. More recently, scRNA-seq and spatial RNA-seq transcriptomics have been applied to study plant-microbe endosymbioses (Figure 2-2, Table 2-2). Cervantes-Pérez et al. applied snRNA-seq to *M. truncatula* roots inoculated with the rhizobium *E. meliloti* at 2 dpi (days post-inoculation)[152]. This provided a comprehensive annotation of *M. truncatula* root cell type as well as analysis of the transcriptomic response of cells to rhizobial infection. Gene expression patterns were unique to specific cell types, indicating a cell-type specific role for certain genes in nodulation. This study confirmed decades

of research in legume nodulation, identifying key genes and pathways involved in nodulation, including genes related to cell division, signaling, and nutrient transport[152]. Moreover, it led to the discovery of genes that had not been previously highlighted by bulk transcriptome analyses. Another scRNA-seq analysis in *M. truncatula* infected with *Ensifer meliloti*, was conducted by Ye and colleagues using indeterminate *M. truncatula* nodule protoplasts at 14 dpi[39]. This study improved our understanding of the early stages of root nodulation through identification and characterization of 13 distinct nodule cell clusters. Additionally, pseudotime analysis revealed that two groups of apical meristematic cells diverge into symbiotic and non-symbiotic fates. Lastly, investigation of nitrogen assimilation in nodules provided insight into how uninfected cells may play a role in the overall nodule functioning. Taking a new approach, Liu and colleagues focused on the earliest stages of signaling between plants and bacteria. Liu applied time-course snRNA-seq to *M. truncatula* symbiotic roots at 30 min, 6 h, and 24 h after Nod factor treatment [44]. Significant reprogramming of gene expression in the epidermis and cortex was observed as early as 30 mpi, with the majority of these changes restored at 6 hours. A co-expression module enriched for known symbiotic nitrogen fixation genes was further explored and revealed the involvement of *MtFER* in rhizobial perception. The researchers demonstrated that *MtFER* can promote root growth and impact symbiotic and defense-related gene expression[44].

Two additional studies were conducted using legume species that form determinate nodules. Frank, Fechete et al. used scRNA-seq of *Lotus japonicus* at 10 dpi to define root hair and cortical cell populations involved in rhizobium infection[122]. More than 500 genes with enriched expression in nodulation-associated cells were identified, providing a valuable resource for further analysis. The researchers were also able to validate a new nodulation gene, *LjSYMRKL1*, with expression specific to infected root hair and cortical cells. Lastly, scRNA-seq of protoplasted root susceptible zones of the *cyclops* mutant allowed for the identification of gene expression associated with infection failure [122]. Liu et al.[43] combined snRNA-seq and spatial RNA-seq on nodules (12 and 21 dpi) in *G. max* as well as the root regions where nodules formed. While root cell types could be easily identified, the lack of marker genes for *G. max* nodules made it difficult to assign cell clusters. To tackle this issue, they utilized Stereo-Seq and tracked gene expression in nodules at the same developmental stage. Using histological features and deconvolution of spatial and snRNA-seq expression data, they classified most major cell types of the root and nodule[43].

Research on plant-pathogen interactions[40,87,153–155] demonstrated the utility of novel transcriptomic methodologies to analyze plant-fungal relationships. Single-nuclei and spatial transcriptomics were applied for the first time to the AMF symbiosis between *M. truncatula* and *R. irregularis*[46]. Serrano, Bezrutcyzk et al. combined Chromium and Visium to construct a spatially-resolved transcriptome map containing genes from both species at 28 dpi. Fungal nuclei were not captured by the Chromium platform. However, Visium did allow for plant and fungal transcripts to be captured simultaneously, with over 12,000 fungal transcripts captured across the nine capture areas[46]. The resulting datasets present a novel transcriptomic resource for the AM symbiosis community, however, the limited resolution of the spatial technology did not allow for cell-type specific analyses of the fungal transcripts, as most voxels may contain different cell types. Spatial technologies with increased resolution, such as Stereo-Seq and Seq-Scope, also have the potential to capture fungal transcripts and represent great tools for the AM community to disentangle the cell-type specific transcriptomic signature of the AM symbiosis.

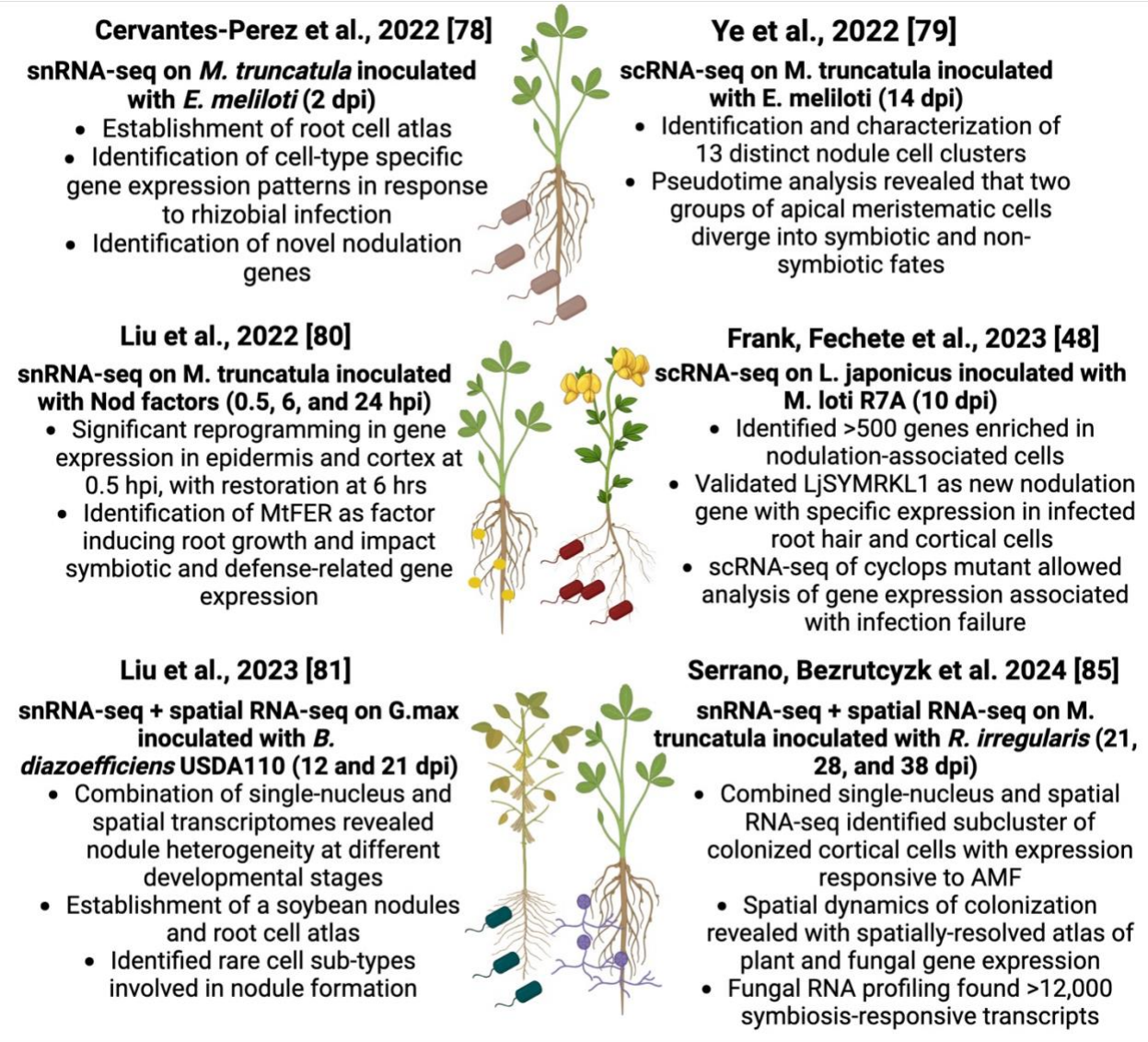

Figure 2-2. Recent Transcriptomic Discoveries in Plant-Microbe Endosymbioses

Summary of the key findings from recent literature analyzing plant-microbe endosymbiosis via single-cell/single-nuclei and spatial RNA-sequencing. Each publication is referenced using the author and publication date and is displayed next to a schematic of what symbiotic system was analyzed. Abbreviations: dpi, days post-inoculation; hpi, hours post-inoculation; mpi, minutes post-inoculations. Figure created with BioRender.com.

Original Publication	Cell/Nuclei Number	Median Gene per Cell/Nucleus
Cervantes-Pérez, S.A. et al. (2022) *Cell-specific pathways recruited for symbiotic nodulation in the Medicago truncatula legume*[78]	28,375 nuclei	1,053
Ye, Q. et al. (2022) *Differentiation trajectories and biofunctions of symbiotic and un-symbiotic fate cells in root nodules of Medicago truncatula*[79]	10,814 protoplasts	1,620
Liu, Z. et al. (2023) *Single-nucleus transcriptomes reveal spatiotemporal symbiotic perception and early response in Medicago*[80]	26,712 nuclei	1,018
Frank, M. et al. (2023) *Single-cell analysis identifies genes facilitating rhizobium infection in Lotus japonicus*[48]	25,024 protoplasts	1,500
Liu, Z. et al. (2023) *Integrated single-nucleus and spatial transcriptomics captures transitional states in soybean nodule maturation.*[81]	26,712 nuclei	1,342
Serrano and Bezrutcyzk. et al. (2024) *Spatial Co-transcriptomics Reveals Discrete Stages of the Arbuscular Mycorrhizal Symbiosis*[46]	16,890 nuclei	1,120

Table 2-2. sc/snRNA-seq Symbiosis Studies

2.6 Limitations to Transcriptomic Investigation of Symbiosis

Identifying cell types from transcriptome data relies on manual annotation of clusters using reference marker genes. For non-model plant, bacterial, and fungal species without an available curated database of marker genes, this can be a difficult and time-consuming task. This issue is exacerbated when profiling rare cell types, which require processing of large cell populations, adding to experimental costs. The capture of low abundance cells engaged in early responses within root hair or cortical cells may demand increased sequencing depth, subsequently elevating the overall expense and length of analyses.

scRNA-seq and spatial RNA-seq studies generate an immense amount of data. The need for standardized and accessible experimental workflows, data processing/analysis pipelines, and data deposition practices increases with the method's popularity. Many researchers are publishing transcriptome data for the same species using similar methodologies, but without a public centralized database for symbiosis research with established experimental standards, it is difficult to compare data across multiple studies. Recent efforts such as SpatialDB[156], a public web curation of spatially-resolved transcriptome data, and the Plant Cell Atlas Consortium[157], a scientific

focusing on building a single-cell multi-omics atlas of developing model plants, are laying the groundwork but standard repositories are for more specialized efforts.

Another major obstacle is that it is not currently possible to capture both plant and bacterial transcripts simultaneously in the same cells. Plant mRNA transcripts are relatively easy to separate from rRNAs because they are polyadenylated, but bacterial mRNAs are less abundant, less stable and lack polyadenylation [158]. Quantifying gene expression from bacterial symbionts using scRNA-seq requires very efficient counterselection against bacterial rRNAs, likely coupled with deep sequencing to detect bacterial mRNAs within an RNA pool dominated by plant transcripts. Furthermore, polyadenylation of bacterial mRNAs following rRNA depletion would be required to allow compatibility with standard scRNA-seq procedures, including the 10x Chromium protocols (https://www.10xgenomics.com). To capture bacterial single-cell data, bacterial cells would have to be physically separated from plant cells, as previously demonstrated in *A. thaliana* leaves [159], prior to application of prokaryotic scRNA-seq techniques, such as microSPLiT [160] and PETRI-seq [161], precluding simultaneous capture of information from both host and symbiont. Spatial transcriptomic methods have the same challenges with respect to detection of microbial mRNAs, but are able to capture polyadenylated fungal transcripts [162], and spatial metatranscriptomics (SmT) allows capture of bacterial and fungal microbial signatures for community structure analysis via 16S, 18S, and ITS probes [154]. Spatial, hybridization-based methods should in principle be able to capture both plant and bacterial mRNAs, but require design of specific probes, necessitating prior knowledge of both host and symbiont target genes.

AM fungi contain multinucleate hyphae in a connected cytoplasmic space and have an extremely high number of nuclei within each cell, ~2 orders of magnitude higher than any fungal relatives [163,164]. Additionally, the diameter size of these nuclei can vary significantly between species and between life stages of the same species[164], which can complicate nuclei capture and filtering during snRNA-seq workflows. However, AM fungi currently remain more amenable than rhizobia to within-host single-cell analysis because of their polyadenylated mRNAs. Capturing single-cell rhizobial transcriptional signatures, together with those of their host plant cells, in infection threads and nodules will have to await further technological developments where a likely first step would rely on spatial, *in situ* hybridisation-based technology (Table 2-1).

2.7 Concluding Remarks and Future Perspectives

Plant-microbial endosymbioses have distinct biological characteristics which limit the power of traditional transcriptomic approaches. Novel technologies present great potential for their application to studies of such symbiotic relationships as they enable cell-type and morphological-feature specific analyses of gene expression from both partners. Here, we provide an overview of the main single-cell and spatial methodologies that have emerged over recent years and speak to their advantages and disadvantages. Scientists applied some of these sc/snRNA-seq or ST approaches in isolation or in unison to analyze the gene expression occurring between two species in either the plant-mycorrhizal or legume-rhizobial symbiosis. This research enriched our understanding of plant-microbe endosymbiosis, particularly the legume-rhizobial symbiosis, to which many groups have applied sc/snRNA-seq and identified new marker genes for symbiotic structures and processes as well as new symbiosis-specific candidate genes for functional characterization. For the AM symbiosis, pioneering work that combined single-nuclei and spatial

RNA-seq constructed a spatially-resolved, high resolution map of gene expression from both species and identified thousands of symbiosis-responsive fungal transcripts for the first time. However, these studies are limited by the current technologies. Future method development, particularly the development of a spatially-resolved single-cell platform which allows for concurrent prokaryotic and eukaryotic transcript capture, will have increased power to answer outstanding questions. As data is generated, the creation of a public, centralized database with standards for data collection and analysis that allows users to browse scRNA-seq and spatial RNA-seq data across species will prove critical to the effort in building a single-cell gene expression atlas for endosymbiosis.

2.8 Acknowledgements

This study was supported by the DOE Joint BioEnergy Institute (http://www.jbei.org) supported by the U. S. Department of Energy, Office of Science, Office of Biological and Environmental Research, through contract DE-AC02-05CH11231 between Lawrence Berkeley National Laboratory and the U.S. Department of Energy, by Independent Research Fund Denmark (grant agreement no. 1026-00032B), and by the project Molecular Mechanisms and Dynamics of Plant-Microbe Interactions at the Root-Soil Interface (InRoot), supported by the Novo Nordisk Foundation grant no. NNF19SA0059362.

2.9 Competing Interests

The authors declare no competing interests.

2.10 Significance Statement

This chapter provided background information on the two most prevalent plant-microbe endosymbioses: the rhizobial-legume symbiosis and the arbuscular mycorrhizal symbiosis. There was a general overview of our current understanding of these symbioses and also a discussion of open questions regarding how exactly these interactions occur remaining in the field. We reviewed past and current RNA-sequencing technologies, comparing and contrasting their applications and advantages, with a focus on single-cell and single-nuclei as well as spatial RNA-sequencing technologies. Additionally, discussion of how these technologies have recently been applied to study plant-microbe endosymbiosis and what the main findings of those new publications added to our understanding of these interactions. Lastly, the current limitations of these technologies in reaching our desired goals of applying RNA-sequencing to analyze these multi-kingdom relationships were assessed and recommendations for the development of future technologies with enhanced capabilities were given. This chapter lays the groundwork and builds context for a full understanding of chapter 3, in which one of the recent publications applying single-cell and spatial transcriptomics to the arbuscular mycorrhizal symbioses that was briefly mentioned in this review will be expanded upon.

Chapter 3. Spatial Co-Transcriptomics Reveals Discrete Stages of the Arbuscular Mycorrhizal Symbiosis

Including material from the published manuscript from **Karen Serrano,** Margot Bezrutcyzk, Danielle Goudeau, Thai Dao, Ronan O'Malley, Rex Malmstrom, Axel Visel, Henrik Vibe Scheller, and Benjamin Cole. Spatial co-transcriptomics reveals discrete stages of the arbuscular mycorrhizal symbiosis. *Nat. Plants* (2024). https://doi.org/10.1038/s41477-024-01666-3.

3.1 Abstract

The symbiotic interaction of plants with arbuscular mycorrhizal fungi (AM fungi) is ancient and widespread. Plants provide AM fungi with carbon in exchange for nutrients and water, making this interaction a prime target for crop improvement. However, plant-fungal interactions are restricted to a small subset of root cells, precluding the application of most conventional functional genomic techniques to study the molecular bases of these interactions. Here we used single-nucleus and spatial RNA sequencing to explore both *Medicago truncatula* and *Rhizophagus irregularis* transcriptomes in AM symbiosis at cellular and spatial resolution. Integrated, spatially-registered single-cell maps revealed infected and uninfected plant root cell types. We observed that cortex cells exhibit distinct transcriptome profiles during different stages of colonization by AM fungi, indicating dynamic interplay between both organisms during establishment of the cellular interface enabling successful symbiosis. Our study provides insight into a symbiotic relationship of major agricultural and environmental importance and demonstrates a paradigm combining single-cell and spatial transcriptomics for the analysis of complex organismal interactions.

3.2 Introduction

Arbuscular mycorrhizal (AM) fungi occur in all major terrestrial ecosystems[165]. They are fundamental to agricultural production as they provide plants with nutrients, particularly nonrenewable phosphorus, as well as resistance to abiotic stress[166] and pathogens[167]. Plants reward these services by transferring carbohydrates and lipids to AM fungi which enables extension of extraradical mycelium in the soil[168]. Intense coordination between species is required for symbiotic recruitment, development and maintenance within the root. Preceding contact, signaling between plant roots and germinating fungal spores initiates hyphal branching towards the root at which a hyphopodium will form to initiate the symbiosis[93]. Upon contact, a plant-derived pre-penetration apparatus guides the fungus across and through the epidermis, with hyphae traveling both inter- and intra-cellularly to reach the inner-most cortical cells[10,169]. Hyphae then differentiate to form branched structures termed arbuscules within cortical cells[170]. The host plant restructures the cortex cell and builds a peri-arbuscular membrane (PAM)[168], creating an apoplastic space across which metabolite exchange occurs between species. As symbiosis develops, the carbon supply from the root allows for expansion of an intraradical and extraradical mycelium, through which soil minerals are transported into the plant[93].

Decades of research resulted in much progress regarding functional characterization of genes involved in the AM symbiosis[25,28,29,171–176], yet many remain to be characterized. Multiple characteristics of AM symbiosis complicate traditional transcriptomic approaches. As obligate biotrophs, AM fungi cannot complete their life cycles or be cultured independently in asymbiotic

conditions. Recent advances in asymbiotic sporulation of mycorrhizal fungi using bacterial fatty acids as stimuli are encouraging[177,178], but it remains challenging to develop axenic AM inoculums. Due to asynchronous colonization, many developmental stages exist simultaneously within the cortex. This limits the ability of whole-root transcriptomics to differentiate between transcriptional profiles of each stage[179]. Arbuscules are extremely transient structures, lasting only a few days before senescence[102,180], confounding efforts to distinguish discrete phases of interaction. Furthermore, arbuscule collapse and vesicle or spore formation indicates that the plant and fungus are assimilating exchanged nutrients, which creates the need to analyze root cells that appear to be non-colonized[181]. Several groups have elegantly addressed these challenges using laser capture microdissection (LCM) to obtain transcriptomes of cortex cells visually confirmed to be directly adjacent to fungal appressoria (early stage) and colonized cortex cells (late stage)[94,95]. One disadvantage of LCM is that it limits investigation to cell types already known to be involved, which creates the need for an unbiased approach to analyze all root cell types.

The rapid adoption of single-cell RNA-sequencing (scRNA-seq) or single-nuclei RNA-sequencing (snRNA-seq), with potential to identify novel cell types, model developmental trajectories, and analyze transcriptional activity of individual cells[182], has revolutionized plant biology. In both scRNA-seq and snRNA-seq, investigation of transcriptomes from all cell types is possible, rather than requiring manual selection of individual cells, as with LCM. Moreover, snRNA-seq's rapid protocols are robust to diverse organisms and tissue types. In addition, certain cell types are preferentially released as protoplasts during enzymatic digestion for scRNA-seq, but nuclei are extracted uniformly across cell types, leading to a more representative population of cell types in snRNA-seq datasets[126,183]. For example, arbusculated cells have highly ramified cell membranes, which may be difficult to recover after enzymatic digestion due to their increased surface area. In both scRNA-seq and snRNA-seq, the spatial context of gene expression is lost upon dissociation of cells from the tissue. Spatial transcriptomics allows for sequencing of cell transcriptomes within the tissue context, adding a novel dimension to the data[184].

This study applied single-nuclei and spatial transcriptomics to the interaction between the model legume *Medicago truncatula* and the AM fungus *Rhizophagus irregularis* to create a 2-dimensional integrated map of plant and fungal transcriptomes during symbiosis. We provide an unbiased spatial and single nuclei transcriptomics dataset that profiled a multi-kingdom interaction. The spatially resolved transcriptome provides insight into coordinated gene expression occurring between the two partners across all major *M. truncatula* root cell types. This transcriptomic map represents a novel resource for AM fungi research and demonstrates the value of novel multi-omics approaches in answering biological questions.

3.3 Results

3.3.1 Nuclear RNA profiling identifies *M. truncatula* cell types

To gain a comprehensive transcriptional profile of the plant/AM fungal interaction, we performed snRNA-seq and spatial RNA-seq on *M. truncatula* roots which were mock-inoculated

or inoculated with the AM fungus *R. irregularis.* We isolated and purified nuclei from *M. truncatula* roots by flow sorting (FANS, Fig. 3-1a) before loading the suspension onto a microfluidic chip for snRNA-seq profiling[185]. Quality filtering and unsupervised clustering resulted in a dataset of 16,890 nuclei grouped in 16 distinct cell clusters (Methods). We assigned cluster identities using cell type-specific gene expression profiles derived from *A. thaliana* root single cell datasets[123,148–151] as well as a rhizobia-colonized *M. truncatula* single nuclei dataset[186] (Table S1, Extended Data Fig. 1). Nine clusters (11,298 cells) exhibited characteristics of cortex cell identity, with one additional cluster (174 cells) composed of cortex cells colonized by *R. irregularis* (Fig. 1b). We also identified all other major *M. truncatula* root cell types and generated marker gene sets for each (Table S1).

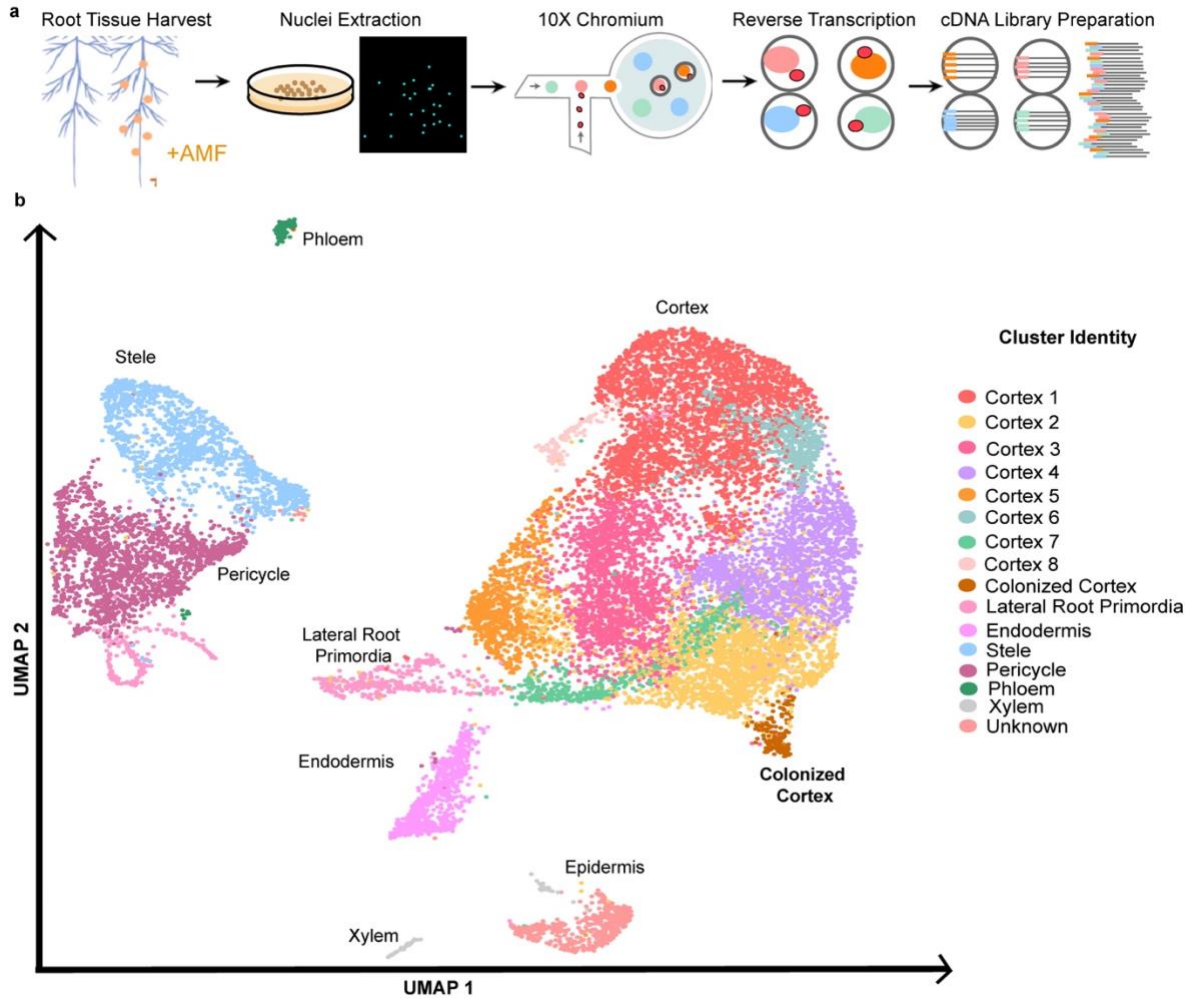

Figure 3-1. Single nuclei RNA profiling in *M. truncatula* roots colonized by *R. irregularis*.

a, Overview of approach. *M. truncatula* root tissue is flash frozen for nuclei extraction and subsequent snRNA-seq using the 10X Genomics Chromium platform. Intact single nuclei are emulsified with gel beads containing barcoded oligonucleotides within a microfluidic chamber, resulting in a barcoded cDNA library after reverse transcription. **b,** UMAP coordinates of 16,890 *M. truncatula* nuclei from three AM-colonized root harvest timepoints clustered by

similarity in transcriptional profiles. The identities of 16 unique clusters are represented by different colors.

3.3.2 Simultaneous spatial capture of plant and fungal transcripts

To investigate gene expression from both symbiotic partners, we performed spatial transcriptomic profiling on inoculated and mock-inoculated *M. truncatula* roots at 28 dpi (Fig. 3-2a, 3-2b, Table S2). An example capture area from an inoculated plant displays numerous root cross sections fixed and stained on the glass surface (Fig. 3-2c panel I). On average, inoculated capture areas resulted in 20,333 and 5,084 transcripts mapping to the *M. truncatula*[37] and *R. irregularis*[115] genomes respectively, while mock-inoculated capture areas resulted in an average of 21,987 (*M. truncatula*) and 23 (*R. irregularis*) transcripts. Spatial UMI (Fig. 3-2c, panel II) and feature (Fig. 3-2c, panel III) distributions indicate a uniform capture of transcripts across the expected areas of each cryosection, with few hotspots of fungal colonization associated with increased transcript counts from *R. irregularis* (Fig.2c panel IV) and increased expression of *MtPT4* (PHOSPHATE TRANSPORTER 4), an marker gene for arbusculated cells[187] (Fig.3-2d, panel V). The spatial technology relies on polyadenylated transcript capture via oligo(dT) primer sequences which enabled unbiased capture of *R. irregularis* and *M. truncatula* transcripts simultaneously. Analyzing the distribution of all *M. truncatula* transcripts within each inoculated capture area (Fig. 3-3a, panel I) and comparing it to that of all *R. irregularis* transcripts (Fig. 3-3a, panel II), distinct patterns of mRNA capture and expression between the two species are evident, indicating the successful spatially-resolved capture of transcriptomes during symbiosis.

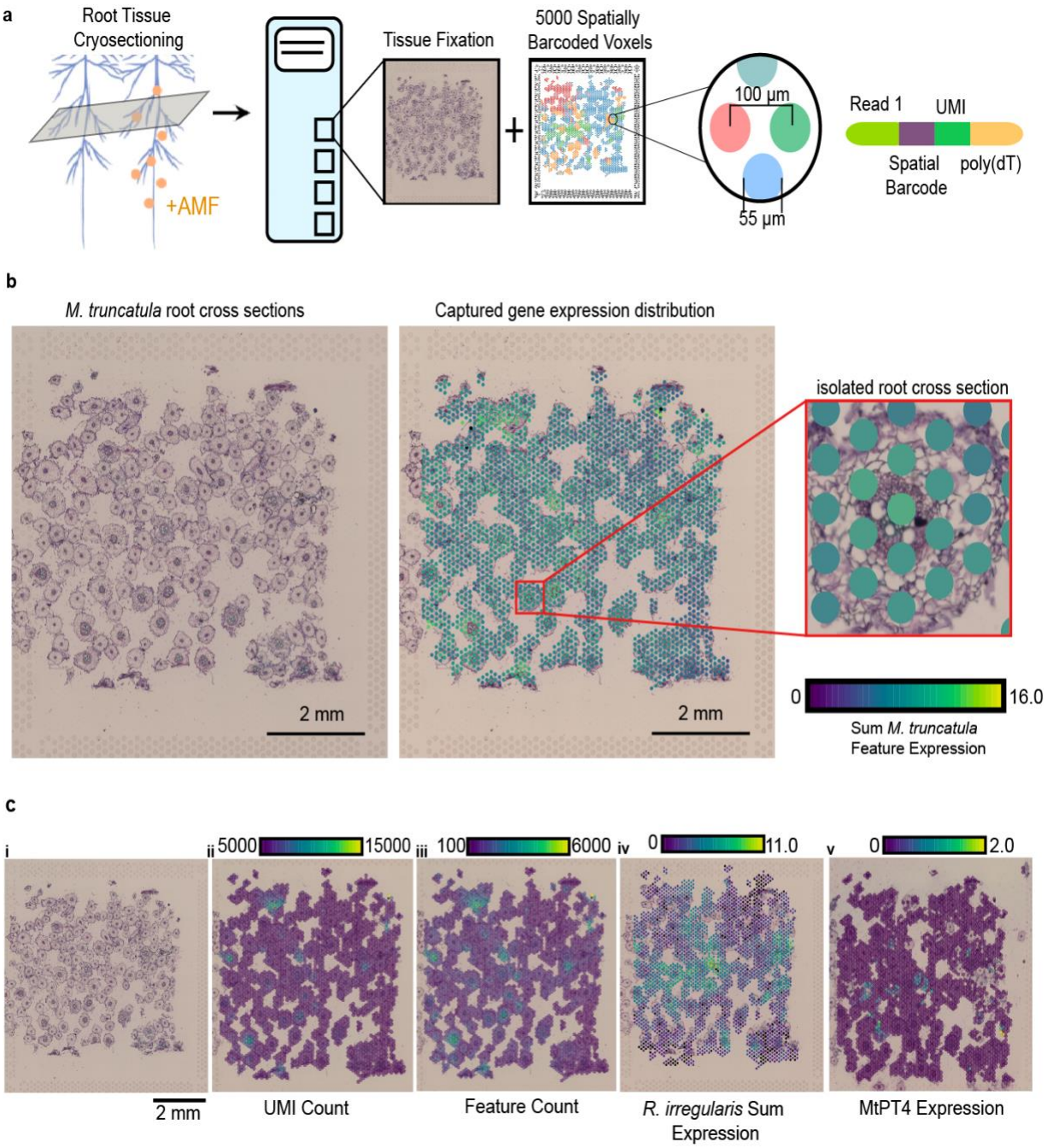

Figure 3-2. Spatial transcriptomics enables simultaneous capture of *M. truncatula* and *R. irregularis* transcripts.

A, *M. truncatula* root tissue is flash frozen to create 16 µm thick cryosections, each containing numerous root cross-sections. Cryosections are fixed to capture areas, each of which is equipped with ~5000 spatially-barcoded voxels at a resolution of 55 µm. **b,** Side-by-side images of brightfield tissue image and underlying spatial capture voxels, with a close-up view of a single root cross-section within the capture area (1 representative capture area out of 9 mycorrhizal capture areas analyzed) highlighting voxel size in relation to the tissue. **c,** Capture area containing cross sections from *M. truncatula* roots infected with *R. irregularis* at 28 dpi (1

representative capture area out of 9 mycorrhizal capture areas analyzed). i, Image of root cross sections within capture area. UMI count (ii) and feature count (iii) overlaid onto spots underlying tissue. iv, Expression pattern of all *R. irregularis* transcripts captured (scale = log2 of UMI counts). v, Expression pattern of the arbuscule marker gene post-imputation, *MtPT4* (*PHOSPHATE TRANSPORTER 4*), exhibiting overlap in spots with the highest expression of fungal transcripts (scale = log2(UMI counts)). Visualization done in Loupe Browser.

3.3.3 Overlapping, symbiosis-responsive transcriptomes

To identify genes associated with AMF colonization within our spatial datasets, we performed dimensionality reduction and clustering of all voxel transcriptome profiles from both AMF- and mock-inoculated spatial capture areas (Extended Data Fig. 2). Due to the relatively low resolution of the Visium platform, (each 55-µm voxel could contain 1 to 5 cells), we refrained from assigning cell identities to spatial dataset clusters (referred to as 'spatial clusters'), as voxels likely represent heterogeneous cell groups. Instead, we identified voxel clusters within the mycorrhizal dataset that could represent sites of AM colonization. To do so, we compiled a list of established AM-responsive marker *M. truncatula* and *R. irregularis* genes (Table S3) functioning in various stages of AM colonization and analyzed their expression across the 13 spatial clusters in reference to a stably-expressed housekeeping gene, *MtEF1α* (ELONGATION FACTOR 1-ALPHA)[188]. Spatial clusters 3 and 12 showed high specific expression of the markers from both species and thus were deemed "AM-responsive" (Fig. 3-3b), with spatial cluster 12 showing higher expression of early markers and spatial cluster 3 showing higher expression of late-stage markers. We detected a few AM symbiosis marker genes within the snRNA-seq dataset that were missing or lowly expressed within the spatial datasets. This may be due to lower detection efficiency of unbiased transcriptomic methods as compared to probe-based capture[189]. To estimate spatial expression of these genes, we integrated nuclear and spatial datasets together and imputed expression values across modalities. Using this approach, we associated the expression of two marker genes, *MtDMI1* (DOES NOT MAKE INFECTION 1) [27] and *MtSKl1* (SICKLE 1)[190], with mycorrhizal capture areas, despite their absence from the spatial dataset (Fig. 3-3c).

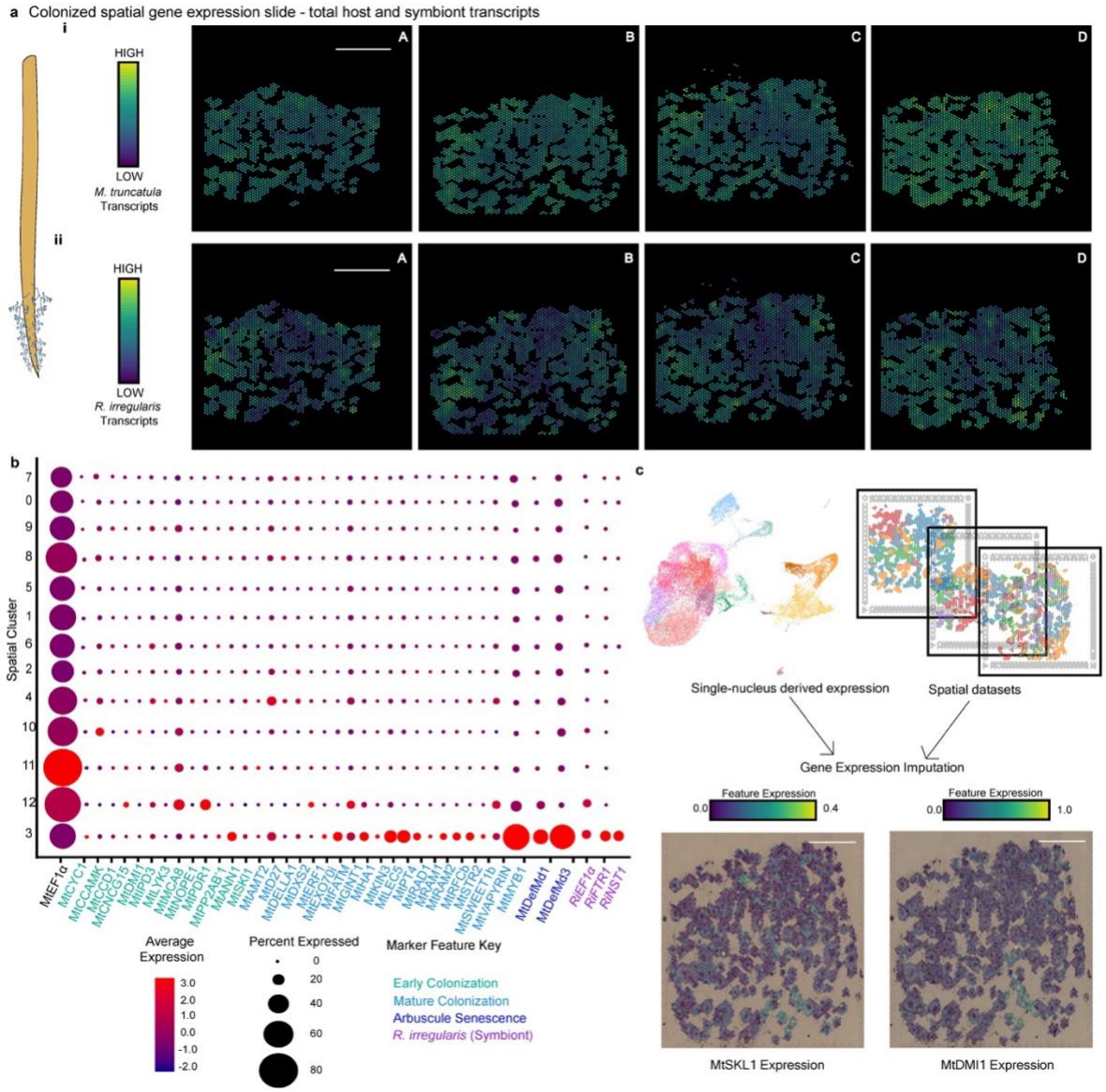

Figure 3-3. Transcriptomic profiling reveals coordinated gene expression between the symbiotic partners.

a, Spatial distributions of host and symbiont transcript expression from 4 unique capture areas containing lateral root cross-sections from *M. truncatula* plants at 28 dpi (scale bar = 1 mm, scale = log2(UMI counts)). i, 4 unique inoculated capture areas exhibiting the spatial distribution of all *M. truncatula* transcripts within the roots. ii, The same 4 capture areas exhibiting the spatial distribution of all *R. irregularis* transcripts within the roots. **b,** Dot-plot of *M. truncatula* and *R. irregularis* housekeeping genes along with genes known to be involved in different stages of the symbiosis utilizing hierarchical clustering within the integrated mycorrhizal spatial object. **c,** Visualization of gene expression imputation from snRNA-seq mycorrhizal integrated dataset for two lowly expressed genes, MtSKL1 and MtDMI, within a single representative Visium Spatial Gene Expression capture area out of 9 mycorrhizal-treated capture areas analyzed (scale bar = 1 mm).

3.3.4 Colonization stage-specific *M. truncatula* gene expression

We used stage-specific markers to determine the distribution of cells across arbuscule development within the snRNA-seq datasets. Low phosphate availability stimulates the interaction between plant and AM fungus, resulting in secretion of strigolactones from cortex cells[191]. *MtABCG59* (ABCG TRANSPORTER 59) is upregulated during phosphate starvation and upon mycorrhizal exposure[192]. We observed enrichment of *MtABCG59* in cells throughout the cortex clusters (Fig. 3-4a), representing cells that are responding to phosphate starvation. Cluster 14, which specifically expressed *MtDXS2* (1-DEOXY-D-XYLULOSE 5-PHOSPHATE SYNTHASE) transcripts, likely represents cells undergoing active AM symbiosis, as *MtDXS2* is required for the methyl D-erythritol phosphate pathway-based isoprenoid production to sustain AM colonization (Fig. 3-4a)[193]. To determine whether we captured a developmental gradient, we first defined an expression module of AM symbiosis marker genes expressed in the AM symbiosis cluster (cluster 14), then computed an AM module score for all cells (Methods). We selected cells in the 98th percentile for this AM module score and re-clustered them into five sub-clusters (Fig. 3-4b). Based on the enrichment of marker genes observed, sub-clusters a, b, and e likely represent earlier stages, as these cells are enriched for *MtABCG59* transcripts. Clusters c and d may represent later stages of colonization based on the enrichment of *MtDXS2* transcripts, and the cells at the edge of cluster d are likely at the most advanced stage of colonization, as they are the only cells in the single cell datasets that contain high levels of *MtPT4* mRNA (Fig. 3-4b).

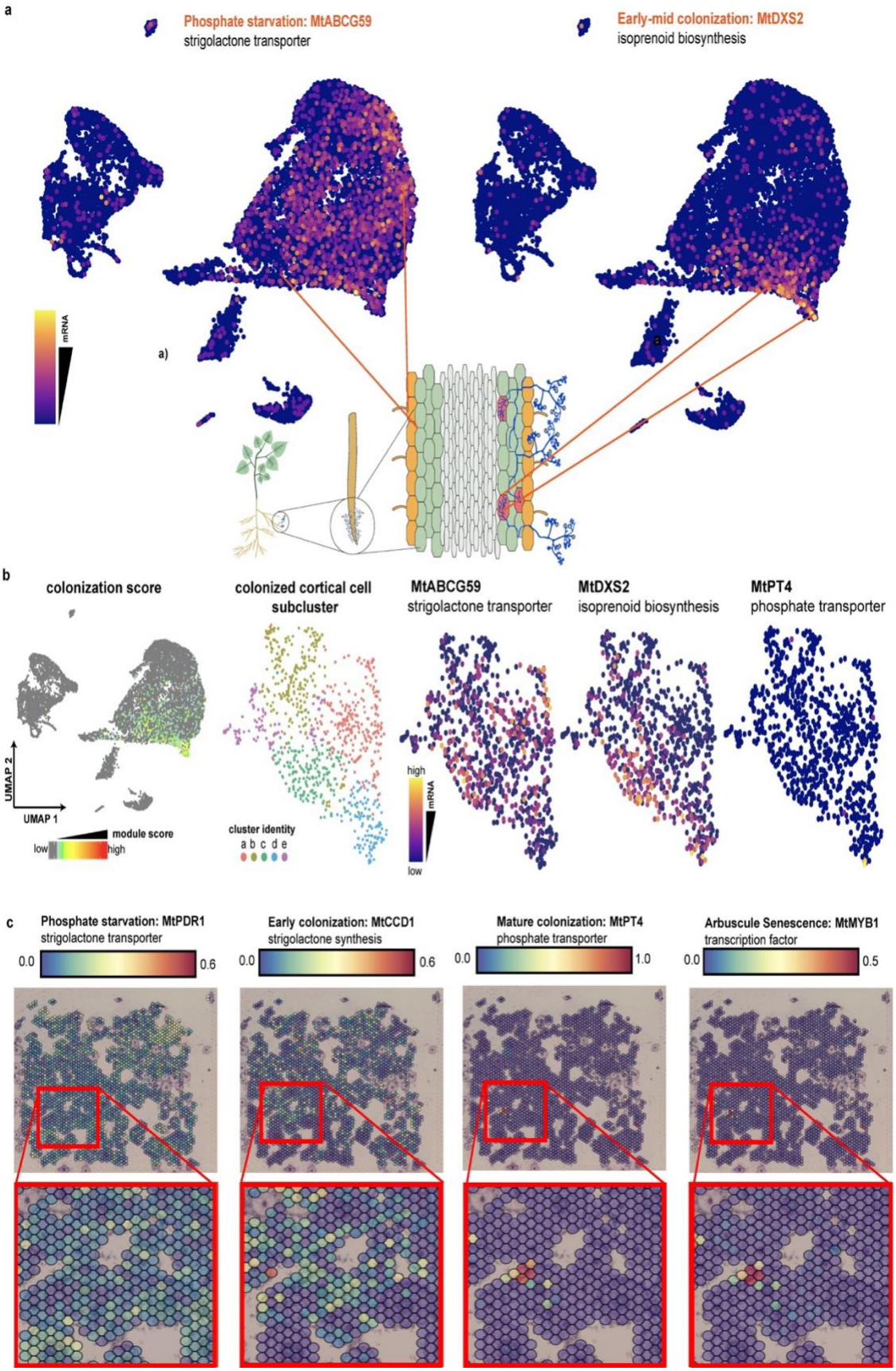
a
Phosphate starvation: MtABCG59
strigolactone transporter
Early-mid colonization: MtDXS2
isoprenoid biosynthesis
mRNA
a)
b
colonization score
colonized cortical cell subcluster
MtABCG59
strigolactone transporter
MtDXS2
isoprenoid biosynthesis
MtPT4
phosphate transporter
UMAP 2
UMAP 1
module score
low
high
cluster identity
a b c d e
high
mRNA
low
c
Phosphate starvation: MtPDR1
strigolactone transporter
0.0
0.6
Early colonization: MtCCD1
strigolactone synthesis
0.0
0.6
Mature colonization: MtPT4
phosphate transporter
0.0
1.0
Arbuscule Senescence: MtMYB1
transcription factor
0.0
0.5

Figure 3-4. Analyzing colonization stage-specific gene expression

a, Expression of canonical pre-and post-AM marker genes shown in a UMAP plot of single nuclei dataset, colored by normalized mRNA counts. (scale = log(UMI counts + 1)).**b,** Module scores based on average expression level of a list of known AM marker genes; cells with module scores in the 98th percentile were selected as 'colonized cortex cells' and clustering was performed on this subset. Three AM marker genes known to be expressed at different colonization stages are expressed in different subclusters of the colonized cluster. **c,** Spatial feature plots of four AM marker genes known to be expressed at different colonization stages: *MtPDR1*, *MtCCD1*, *MtPT4*, and *MtMYB1*. Zoom-panels focus on voxels that switch expression profiles.

We also visualized the spatial dynamics of colonization by tracking the distribution of stage-specific AM symbiosis marker genes. By analyzing expression of *MtABCG59*, *MtCCD1* (CAROTENOID CLEAVAGE DIOXYGENASE 1)[194] , *MtPT4*, and *MtMYB1* (MYB-LIKE TRANSCRIPTION FACTOR 1)[195] we classified voxels within distinct stages of colonization (Fig. 3-4c). We repeated this stage-specific analysis with the snRNA-seq data to show the developmental trajectory of AM colonization starting with the phosphate stress response gene *MtPDR1*(PLEIOTROPIC DRUG RESISTANCE 1*)*[96], which is enriched throughout the cortex cluster. *MtCCaMK* (CALCIUM AND CA2+/CALMODULIN-DEPENDENT PROTEIN KINASE*)*[196] is involved in host-symbiont signaling in early stages, and is enriched in the cells closer to the colonized cluster. *MtPT4* is enriched in a subset of cells at the furthest edge of the colonized cluster and *MtMYB1* is also enriched in these distal cells (Fig. 3-5c, upper panel).

Performing differential gene expression (DEG) analysis we found 258 genes enriched in the AM symbiosis cluster 14 (log FC> 0.25, adjusted $p < 0.01$, Table S4) compared to all other cortex clusters combined. Among these, we recovered known marker genes for AM symbiosis, along with many genes not previously associated with AM signaling as well as genes with no annotated function. These included a gene encoding a monosaccharide transporting ATPase (Medtr8g006790/MtrunA17_Chr8g0335291), which we speculate the plant uses to provide sugars to the fungus, several genes with LRR-domains (Medtr6g037750/ MtrunA17_Chr6g0464631, Medtr3g058840/MtrunA17_Chr3g0102261) which could mediate host-symbiont signaling, and *MtABC19*, which encodes a xenobiotic-transporting ATPase (Medtr3g093430/ MtrunA17_Chr3g0128391) (Fig. 3-5c, lower panel). Lastly, we observed high expression of several lipid transfer *M. truncatula* genes within this cluster (Extended Data Fig. 3).

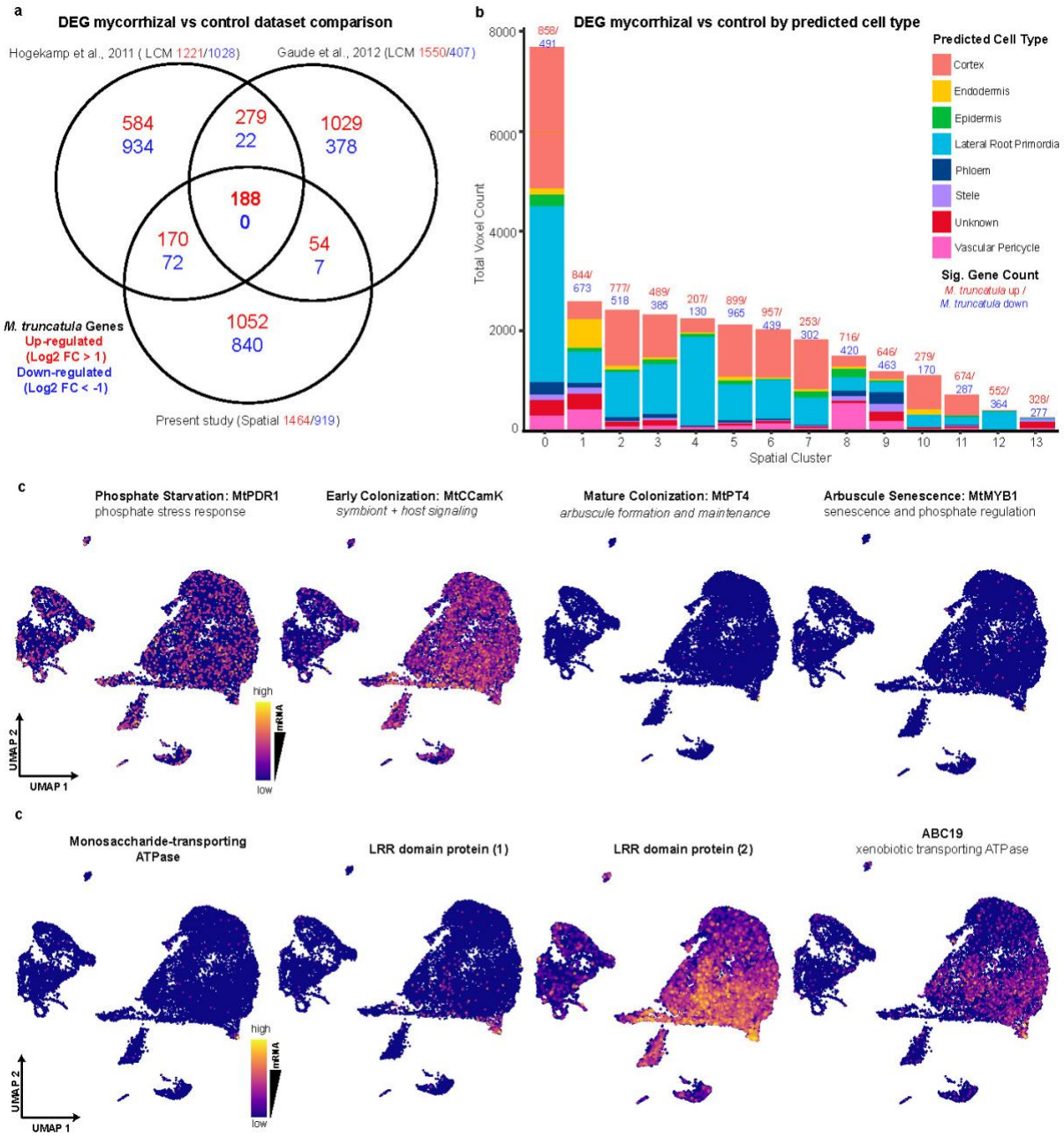

Figure 3-5. Existing and novel transcriptomic studies reveal a robust set of differentially expressed *M. truncatula* genes during the AM symbiosis

a, Venn diagram shows overlap in symbiosis-responsive *M. truncatula* genes with a log-fold change > or < 1 between the spatial dataset rom this study and the two previously published laser-capture microdissection RNA-seq studies from Gaude et al. 2012[15] and Hogekamp et al. 2013[14]. **b,** Breakdown of predicted cell types represented in each cluster within the integrated spatial dataset in terms of number of voxels. Differentially expressed genes between mycorrhizal and control treatments are shown above each bar for each cluster, with *M. truncatula* up regulated counts in red and downregulated counts in blue. **c,** (upper) Expression of four canonical pre-and post-AM symbiosis marker genes shown in a UMAP plot of single nuclei dataset. (lower) Expression of four genes enriched in the colonized cortex cell cluster of this

dataset which have yet unknown roles in AMF colonization, shown in a UMAP plot of single nuclei dataset. UMAP plots colored by normalized mRNA counts (scale = log(UMI counts + 1)) depending on the marker gene, thus reflecting the colonization stage.

3.3.5 A robust set of symbiosis-responsive *M. truncatul*a genes

DEGs between mycorrhizal and control spatial capture areas revealed 2,383 AM-responsive *M. truncatula* transcripts (Fig. 3-5a). Of these, 1464 were upregulated (log2 FC > 1.0) and 919 were downregulated (log2 FC < 1.0) in the mycorrhizal treatment (Table S5). Two LCM-based transcriptomic analyses revealed similar numbers of DEGs in response to mycorrhizal treatment[94,95], with 188 genes significantly upregulated across all three datasets which we refer to as "robust" AM-responsive genes (Fig. 3-5a, Table S5). No genes were found to be significantly downregulated in all three datasets. This set of robust AM-responsive genes includes characterized AM symbiosis marker genes, such as *MtMYB1*, *MtPT4*, and *MtRAD1(*a positive GRAS transcription regulator of the symbiosis)[197]. One of the upregulated transcripts *MtCYC1* (CYCLIN-LIKE 1) encodes a putative Cyclin-like F-box protein and is a known marker for cell division[198], suggesting induction of cortical cell division as a response to AM colonization. However, many of the 188 genes remain to be investigated for their role in AM symbiosis.

The 55-µm resolution of the Visium Spatial Gene Expression platform results in blending of several adjacent cells together into a single profile (i.e., it cannot resolve transcripts of single cells). However, we utilized our annotated snRNAseq and spatial datasets to predict the proportions of each cell type represented in each spatial cluster (Fig. 3-5b). Differences were observed in the proportion of cell types between spatial clusters. We saw a relatively high proportion of voxels identifying as lateral root primordia, which we hypothesize as resulting from the high amount of mRNA captured from meristematic root tissue on the capture area. We also observed large differences in the amount of DEGs between the individual spatial clusters, indicating the method can discern between cell populations experiencing different degrees of AM colonization.

3.3.6 Functional enrichment depicts a marked symbiotic response

We performed functional enrichment analysis for Gene Ontology terms, including Biological Process (Extended Data Fig. 4a), Molecular Function (Extended Data Fig. 4b), and Cellular Component (Extended Data Fig. 4c) among significantly upregulated *M. truncatula* genes (panels I, Tables S6 and S7) and the robust gene set (panels ii, Tables S8 and S7). As expected, we saw a >20-fold enrichment for the "arbuscular mycorrhizal association" biological process term overall, and >80-fold enrichment for this term within the robust set. We also observed a high enrichment (>100 fold) of the "response to symbiotic bacterium" term within the robust set, indicative of genes common to both fungal and bacterial (rhizobial) symbioses. During rhizobial symbiosis, legumes allow controlled infection by rhizobia, leading to the development of root nodules in which rhizobia directly fix and transfer nitrogen to their hosts. The rhizobial symbiosis co-opted numerous components of the ancestral AM symbiosis signaling mechanism[199] and this "common symbiotic signaling pathway" is represented within our robust

dataset by the differential expression of two co-expressed interacting genes, *MtVPY* (MtVAPYRIN)[200] and *MtEXO70i* (MtEXOCYST70)[201]. These genes function during the intracellular phases of endosymbiosis in both AM and rhizobial symbioses, with *MtVPY* genetic mutants impaired in arbuscule and infection thread development, respectively[202]. In the AM symbiosis, *MtVPY* interacts with *MtEXO70i* which is critical to PAM development and arbuscule branching[203]. Another robust gene, *MtCP3* (CYSTEINE PROTEASE 3), likely plays a role in arbuscule degeneration, functioning to degrade the PAM[195] and also contributes to nodule senescence[204], indicating a common functionality. Interestingly, the biological process "proline catabolic process to glutamate" and the molecular function "proline dehydrogenase" showed a >20-fold enrichment (Extended Data Fig. 4a and b). Several studies noted altered proline levels under drought stress in AM-treated plants[205,206], and hypothesized that proline confers protection from changes in water availability. As we did not apply drought stress to plants in our survey, we believe proline metabolism may contribute to a different protective mechanism.

AM fungi convert soil inorganic phosphate (Pi) into inorganic polyphosphate (polyP) and can rapidly accumulate and translocate polyP within hyphae[207]. AM fungi also depolymerize polyP via fungal endopolyphosphatases and transfer this phosphorus into host plant cells across the PAM[208], although the mechanism for this export remains unclear. Some evidence suggests that the majority of this export occurs via the transport of Pi across the apoplastic space and subsequent uptake by the plant via Pi transporters[208]. However, a growing amount of evidence suggests polyP may be directly exported to the apoplastic space and then hydrolyzed by the plant itself[207]. Nguyen and Saito provided evidence that fungal-derived polyP and plant-derived phosphatases had opposing localizations in mature arbuscules, indicating that plant phosphatase activity could account for assimilation of fungal-derived polyP[209]. Surprisingly, "exopolyphosphatase activity" exhibited the highest enrichment of all molecular functions, (>30 fold) in our dataset. This adds support to the hypothesis that polyphosphatase activity by the plant plays a larger role in phosphorus export than previously anticipated.

Lastly, we expected that cellular components enriched in our datasets would include those involved in AM symbiosis, such as the PAM and the plant plasma membrane. The robust dataset showed a >100-fold enrichment for the "PAM" category and captured 100% of the *M. truncatula* genes assigned to that functional category within the genome (Extended Data Fig. 4c). Overall, functional enrichment analysis confirmed a strong symbiotic signature within our mycorrhizal dataset.

3.3.7 Novel symbiosis-responsive *R. irregularis* gene expression

Bulk[103–107] and LCM-based single-cell[94,95] RNA-seq studies conducted on *M. truncatula* in symbiosis with *R. irregularis* utilized a broad spectrum of cell isolation and transcriptomic techniques. In addition, considerable progress has recently been made[107,110,112,113,210,211] to build our knowledge of the genetic landscape of AM fungi and fungal gene expression occurring within this interaction. However, simultaneous capture of plant and fungal mRNA during symbiosis remains challenging. Our approach built upon existing research by providing the first spatially-resolved dataset of simultaneously captured plant and fungal transcriptomes during the AM symbiosis. We detected expression of 12,104 unique fungal transcripts across nine mycorrhizal capture areas (Table S9). Fungal gene expression distribution across the capture areas overlaps arbuscules in the tissue (Fig. 3-6a). Voxels spanning root cross-sections that

display a high degree of arbusculation also exhibit high expression of total *R. irregularis* transcripts. AM fungi provide their hosts with hard-to-access soil nutrients through the actions of transporters across the PAM[212] and benefit from the continuous transfer of lipids and sugars from host plant to fungus[92]. We observed the localized expression of five phosphate transporters (*PT1[RIR_1575600/g11592], PT2[RIR_1235500/g7615], PT4[RIR_0355700/g31083], PT5[RIR_3213400/g18438],* and *PT7[RIR_2900800/g19437]*), three ammonium transporters (*AMT1[RIR_0149600/g16666], AMT2[RIR_0697800/g1222],* and *AMT3[RIR_0390200/g18142]*), and two sugar transporters (*ST2[RIR_2811400/g24501]* and *ST4[RIR_0496600/g26862]*) to spatial cluster #3, the cluster identified as symbiosis-responsive via localization of *M. truncatula* AM symbiosis markers. We observed lower expression of transporter transcripts relative to that of *RiEF1α*, although we did find significant expression of *RiPT1, RiPT4, RiAMT1*, *RiAMT2*, and *RiST2*. Spatial cluster #3 showed localized expression of *M. truncatula* transporters, such as *MtPT4*, *MtAMT2*, and *MtSWEET1b*[213] (Fig. 3-3b), indicative of active nutrient transport occurring in both partners in these voxels.

The same analysis was performed for eight fungal effectors (Fig. 3-6c), including *RiSP7* (SECRETED PROTEIN 7 - RIR_3212100/g18424*)*, an effector protein involved in biotrophic response to AM colonization[214], *RiSLM* (SECRETED LYSIN MOTIF - RIR_1359320), an effector which reduces chitin-triggered immune responses during symbiosis[215], *RiSIS1*(SL-INDUCED PUTATIVE SECRETED PROTEIN 1 - RIR_2427800/g2579*)*, a secreted protein induced in both AM pre-symbiotic and symbiotic phases[210], and *RiNLE1* (NUCLEUS LOCALIZED EFFECTOR 1 - RIR_2535800/g7021), an effector upregulated in arbuscules involved in the suppression of defense responses[216], as well as four members of the MycFOLD effector family (*RiMycFOLD2* - RIR_3103500/g17566, *RiMycFOLD9* -RIR_2782800/g17548 , *RiMycFOLD11* -RIR_098400/g17317 , and *RiMycFOLD16* -RIR_1383400/g25859)[217]. Most effectors exhibited specific expression in spatial cluster #3, though relative to *RiEF1α*, the expression of one of these effectors, *RiNLE1*, was extremely high (Fig. 3-6c). In fact, *RiNLE1* represented the fifth most highly expressed fungal transcript. Evidence suggests that *RiNLE1* translocates to the plant nucleus of arbusculated cells and interacts with the Histone H2B protein to suppress defense responses via epigenetic modification of *MtH2B (*Medtr4g064020/MtrunA17_Chr4g0031671)[216]. Altogether, the high level of expression and high proportion of cells (60%) that *RiNLE1* is expressed in within spatial cluster #3 further supports that this spatial cluster represents arbusculated cells and that other marker genes that specify this cluster are likely involved in AM symbiosis. Table S10 describes all plant and fungal transcripts found to be expressed in spatial cluster #3.

Lastly, we identified at least one Gene Ontology classification for 8,559 out of the 12,104 expressed transcripts (Table S11). The top biological processes represented include “signaling”, “transmembrane transport”, and “lipid metabolism” consistent with processes carried out during AM symbiosis (Fig. 3-6d, panel i). Similarly, “transferase activity”, “transporter activity”, and “lipid binding” rank highly among molecular function terms (Fig. 3-6d, panel ii). “Membrane “and “nucleus” were well represented among cellular components, with >1,000 and >800 transcripts classified to each, respectively (Fig. 3-6d, panel iii). This dataset of >12,000 symbiosis-responsive spatially-resolved *R. irregularis* genes and corresponding tissue images is the first of its kind and holds immense potential for in-depth characterization.

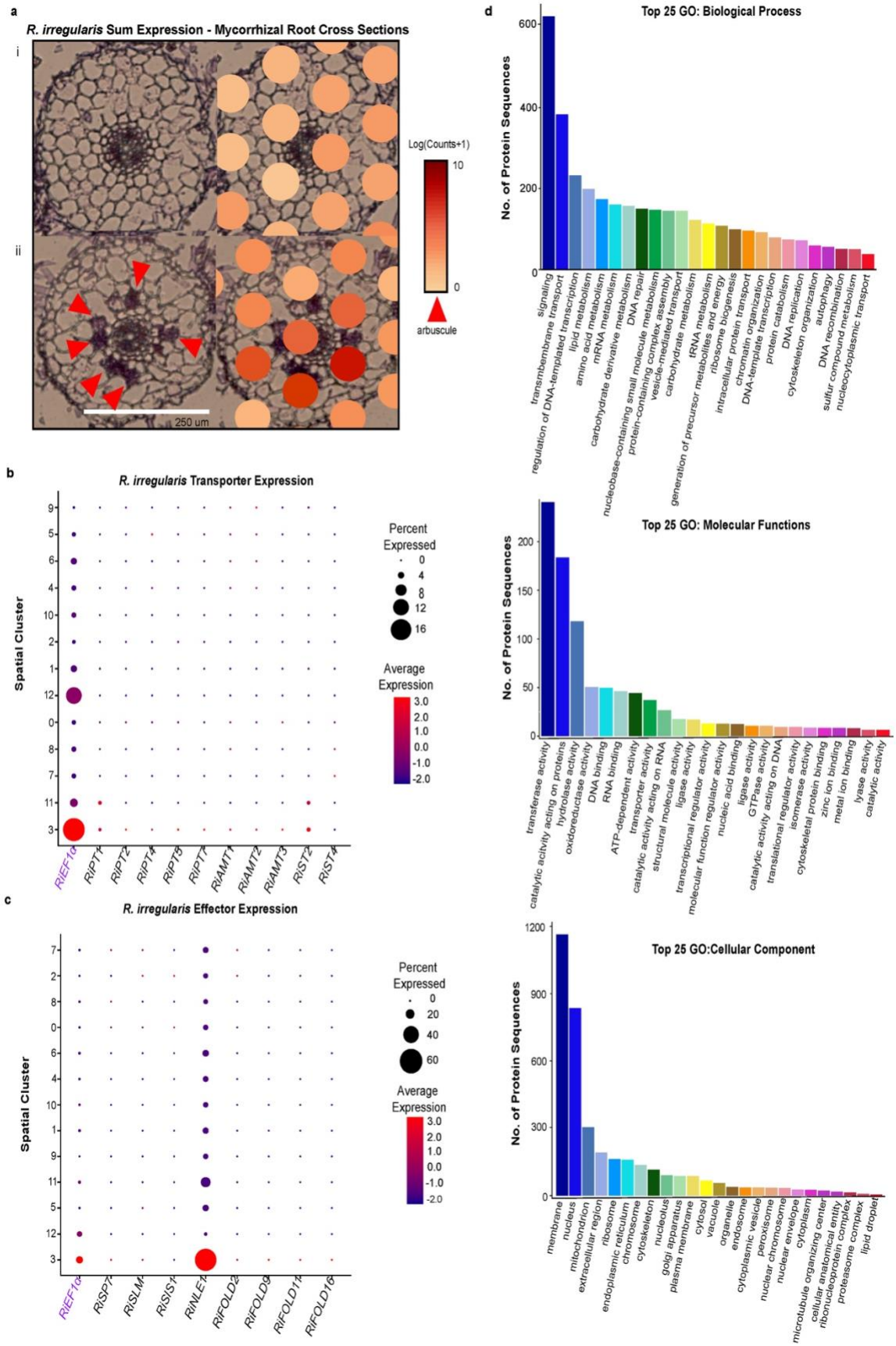
a
R. irregularis Sum Expression - Mycorrhizal Root Cross Sections
i
ii
250 um
Log(Counts+1)
10
0
arbuscule
b
R. irregularis Transporter Expression
Spatial Cluster
RiEF1α
RiPT1
RiPT2
RiPT4
RiPT5
RiPT7
RiAMT1
RiAMT2
RiAMT3
RiST2
RiST4
Percent Expressed
0
4
8
12
16
Average Expression
3.0
2.0
1.0
0.0
-1.0
-2.0
c
R. irregularis Effector Expression
Spatial Cluster
RiEF1α
RiSP7
RiSLM
RiSIS1
RiNLE1
RiFOLD2
RiFOLD9
RiFOLD11
RiFOLD16
Percent Expressed
0
20
40
60
Average Expression
3.0
2.0
1.0
0.0
-1.0
-2.0
d
Top 25 GO: Biological Process
No. of Protein Sequences
signaling
transmembrane transport
regulation of DNA-templated transcription
lipid metabolism
amino acid metabolism
mRNA metabolism
carbohydrate derivative metabolism
DNA repair
nucleobase-containing small molecule metabolism
protein-containing complex assembly
vesicle-mediated transport
carbohydrate metabolism
generation of precursor metabolites and energy
tRNA metabolism
ribosome biogenesis
intracellular protein transport
chromatin organization
DNA-template transcription
protein catabolism
DNA replication
cytoskeleton organization
autophagy
DNA recombination
sulfur compound metabolism
nucleocytoplasmic transport
Top 25 GO: Molecular Functions
No. of Protein Sequences
transferase activity
catalytic acitvity acting on proteins
hydrolase activity
oxidoreductase activity
DNA binding
RNA binding
ATP-dependent activity
transporter activity
catalytic activity acting on RNA
structural molecule activity
ligase activity
transcriptional regulator activity
molecular function regulator activity
nucleic acid binding
ligase activity
GTPase activity
catalytic activity acting on DNA
translational regulator activity
isomerase activity
cytoskeletal protein binding
zinc ion binding
metal ion binding
lyase activity
catalytic activity
Top 25 GO:Cellular Component
No. of Protein Sequences
membrane
nucleus
mitochondrion
extracellular region
ribosome
endoplasmic reticulum
chromosome
cytoskeleton
nucleolus
golgi apparatus
plasma membrane
cytosol
vacuole
organelle
endosome
cytoplasmic vesicle
peroxisome
nuclear chromosome
nuclear envelope
cytoplasm
microtubule organizing center
cellular anatomical entity
ribonucleoprotein complex
proteasome complex
lipid droplet

Figure 3-6. Spatially-resolved *R. irregularis* transcripts reveal novel AM-specific gene expression patterns

a, Single root cross-section within capture area (left) and overlapping distributions of all *R. irregularis* transcript expression (right) visualized in Loupe Browser. i, Representative root cross-section from a mycorrhizal capture area lacking recognizable fungal structures shows low expression of *R. irregularis* transcripts. ii, Representative root cross-section from a mycorrhizal capture area that contains visible arbuscules (red arrows) shows high expression of *R. irregularis* transcripts, particularly around arbuscules (scale bar = 250 um, scale = log(UMI counts + 1)). ~50 root cross sections across 9 mycorrhizal-treated capture areas analyzed. **b,** Dotplot of RiEF1α and various transporters utilizing hierarchical clustering within integrated mycorrhizal spatial object. c, Dotplot of RiEF1α and various effector proteins utilizing hierarchical clustering within the integrated mycorrhizal spatial object. d, barplot depicting top 25 GO categories for all expressed *R. irregularis* transcripts (biological process (panel i), molecular function (panel ii), and cellular component (panel iii)).

3.4 Discussion

Advances in single-cell transcriptomics transformed molecular genetics by allowing cell-type specific analysis and, more recently, conservation of the tissue context[218]. Here, we combined single-nucleus and spatial RNA-seq to construct the first high resolution spatially-resolved integrated map of a multi-kingdom symbiotic interaction. We successfully adapted the spatial transcriptomics platform for use with plant roots and utilized transcriptome-wide mRNA capture from two species simultaneously. In addition, we identified cell type-specific responses to the AM symbiosis and integrated data from both approaches to discover novel AM-responsive transcripts.

snRNA-seq increases resolution and throughput for the identification of cell-state responses to external treatments and eliminates the hurdle of protoplasting cells[219]. snRNA-seq provides a potential advantage over scRNA-seq in conceptually allowing profiling of plant and fungal nuclei in the same assay. However, even in batches of nuclei not subjected to gated flow-sorting, we failed to recover a significant number of fungal transcripts and obtained no defined fungal nuclei, possibly because fungal nuclei were not captured or were destroyed by our plant nuclei extraction protocol. AM fungi consist of multinucleate hyphae in a large syncytium but differ from other multinucleated fungi due to the unusually high number of nuclei (up to 35,000) that exist within their cells[164]. This aspect of their biology may complicate interpretation of snRNA-seq data when compared to spatial or bulk RNA-seq.

Spatial transcriptomics allows for a side-by-side comparison of gene expression and tissue features and further enabled the capture of fungal transcripts. Yet limitations exist for this technology as well, notably a super-cellular resolution (large inter-voxel distances that miss many cells and large voxel sizes that blend adjacent cells together). Probe-based capture technologies significantly improve the resolution of spatial transcriptomics, but this limits analysis to a set of pre-defined genes, and may also lead to lower capture efficiency due to fewer primers[220]. There is a clear need for a high-resolution spatial technology that allows for unbiased mRNA capture from intact tissue.

We found 258 *M. truncatula* genes that were significantly upregulated in the colonized cortex cells (CCC) versus all other cortex cells of mycorrhizal-treated snRNA-seq datasets. These genes were enriched for GO terms related to fungal symbiosis, terpene synthesis pathways, and transport proteins. We also found 17 different cytochrome P450-like proteins, whose roles in plant-microbe interactions include hydroxylation of fatty acids and terpene synthesis[221], and 19 leucine-rich repeat (LRR) domain-containing proteins which are typically associated with pathogenesis but have been shown to also be upregulated in AM symbiosis[221,222]. Several xenobiotic, sugar, and amino acid transporters were also significantly upregulated in CCC. The identification of known and novel transcripts within the CCC cluster, along with the 188 genes upregulated among three distinct RNA-seq studies in the same symbiotic system, present a community resource for characterization of novel AM-associated genes.

R. irregularis forms symbioses with many diverse plant species in natural and agricultural ecosystems[223] and serves as a model species for the AM symbiosis. Despite the biological importance of this fungus, functional annotation and characterization of its genes has been slow due to the difficulty in its genetic manipulation[36]. Recent advances in CRISPR-Cas9[224] gene editing and continued efforts in creating pure cultures of AM fungi[177,178] will hopefully bring forth a new chapter of AM symbiotic research that focuses on the fungal partner. Recent efforts in improving AM fungal genome assemblies[111,163] and functional characterization of *R. irregularis* genes involved in symbiosis[210,214–216,225,226] lay the groundwork for this shift. We identified spatial cluster #3 as AM-responsive based on the expression of both *M. truncatula* and *R. irregularis* marker genes for the AM symbiosis. The transcripts expressed within this cluster, as well as the thousands of *R. irregularis* genes expressed within the mycorrhizal capture areas in this study, represent excellent targets for functional characterization studies in both partners and it is our hope that the AM community can use these datasets as a resource to uncover new functionalities.

3.5 Methods

3.5.1 Plant growth and inoculation

Seeds of *Medicago truncatula* Gaertn, cv Jemalong A17 (Noble Foundation) were scarified in concentrated sulfuric acid for 5-10 min and rinsed with distilled water, sterilized in 3.75% sodium hypochlorite solution, then rinsed five times with sterile distilled water and placed on 1⁄2 Murashige and Skoog medium, 1% agar plates at 4C or RT for 48h. Sand cones were prepared as follows: 8.25 inch cone-tainers (Stuewe and Sons) with 1 cm^3 rock wool at base, filled up to 12.7 cm with autoclaved calcined clay (Turface Athletics MVP 50), followed by 2.5 cm of autoclaved horticultural sand (American Soil and Stone) and topped with 2.5 cm fine play sand (SAKRETE). To inoculate seedlings with *Rhizophagus irregularis* (Błaszk., Wubet, Renker and Buscot) C. Walker and A. Schüßler: 50 mL Agtiv Field Crops liquid mycorrhizal inoculant (PremierTech, Rivière-du-Loup, Québec, Canada) spores were captured on a 40 µm filter, rinsed with distilled water and resuspended in 50 mL distilled water. 1 mL of resuspended spores was applied to the horticultural sand layer and an additional 300 µL applied to the fine play sand layer. Germinated seedlings were transplanted to the top fine sand layer of inoculated and non-inoculated sand cones. Plants were grown in 22-24 ˚C 16 h day/ 8 h night, with 300 µmol m^{-2} s^{-1}

light intensity, and 60% relative humidity. Plants were watered daily and fertilized twice a week with 1/2X Hoagland's medium modified with 20 µM phosphate to stimulate AM colonization.

3.5.2 Colonization assessment

AM colonization in WT roots at 21, 28, or 38 dpi was visualized via staining of AM chitin using 2.5 µg/mL wheat germ agglutinin (WGA) Alexa Fluor 488 (Thermo Fisher Scientific) in 1X Phosphate-Buffered Saline solution (pH 7.0). Briefly, roots collected from the fine sand layer were rinsed, fixed in 50% ethanol for 30 minutes, and cleared in 10% KOH at 65 ºC for 48 h. Cleared roots were neutralized with 0.1 M HCl and stained with WGA-488 in 1X PBS at 4 ˚C for 24 h prior to imaging. Colonization was quantified using the Trouvelot method[227] on a Leica DM6B fluorescence microscope using five biological replicates for each treatment (Extended Data Fig. 5a, Table S12).

3.5.3 Quantitative real-time PCR of target genes

To quantify expression of target genes, 100 mg of roots from the fine sand layer were flash frozen in liquid nitrogen. Total RNA was extracted using the RNeasy Plant Mini Kit (Qiagen) and corresponding DNase. cDNA synthesis was conducted using the SuperScript™ IV Reverse Transcriptase (Thermo Fisher Scientific) from 500 ng of total RNA and qPCR was conducted from cDNA diluted 1:5 using the PowerUp SYBR Green Master Mix (Thermo Fisher Scientific). A 200 nM primer concentration and the following protocol was used for qPCR for all targets: 2 min at 50 °C and 2 min at 95°C, followed by 39 repeats of 15 s at 95 °C, 15 s at 60 °C and 1 min at 72 °C, and ending with 5 s at 95°C. A melting curve (55–95 °C; at increments of 0.5 °C) was generated to verify the specificity of primer amplification. Five biological replicates and three technical replicates of all targets (*MtPT4* and *RiTUB*) were quantified for gene expression levels relative to the housekeeping gene *MtEF1α* using the ΔΔCT method (Extended Data Fig. 5b). All primer sequences used for qPCR can be found in Table S13, raw ΔΔCT values used for statistical analysis can be found in Table S14.

3.5.4 Nuclei and bulk root tissue RNA profiling

M. truncatula roots from three plants from each treatment were harvested at 21-, 28-, and 38-days post inoculation; 150 mg of roots grown in the inoculated fine sand layer were either flash frozen in liquid nitrogen, or nuclei extraction was performed up to the 20 µm filtration step, and then flash frozen. RNA was extracted using the RNeasy Plant Mini Kit (Qiagen). Library preparation and sequencing were performed at the QB3 UC Berkeley Genomics Core Sequencing Facility.

3.5.5 Nuclei extraction and sequencing

M. truncatula roots from three plants per condition were harvested at 21-, 28-, or 38-dpi. 150 mg of roots growing in inoculated fine sand layer was weighed out and placed in the lid of a petri dish and chopped rapidly with a razor blade for three minutes in 600µL NIBAM: 1x NIB (Sigma CELLYTPN1-1KT), 4% BSA, 1 mM DTT, 0.4 U/µL Superase RNAse inhibitor (Sigma), 1:100 Protease Inhibitor Cocktail for plant tissues (Sigma). NIBAM-root slurry was strained through 40 µm and 20 µm filters (CellTrics). SYBR Green (1:10000) was used to visualize nuclei during purification on the Influx Flow Cytometer. 20,000 nuclei were sorted into 19 µL of 'landing buffer' (phosphate buffered saline with 0.4U/µL Superase RNAse inhibitor) with a final volume

of 43 µL. DAPI was applied to 2 µL of nuclei suspension to evaluate the quality of nuclei on a Leica AxioObserver at 20x magnification. The remaining 41 µL was mixed with 10x Genomics Chromium RT Master Mix with no additional water added and loaded onto a Chromium Chip G, and thereafter the standard manufacturer's protocol was followed (V3.1 Dual Index). Twelve cycles were used for cDNA amplification, and the completed cDNA library was quantified using an Agilent Bioanalyzer. Sequencing was performed at the QB3 UC Berkeley Genomics Core Sequencing Facility on a single NovaSeq SP lane with the sequencing parameters: 28 bp (read 1 length), 10 bp (index 1 length), 10 bp (index 2 length), 90 bp (read 2 length), or at Novogene (Sacramento, CA) using the sequencing parameters: 150bp (read 1 length), 10 bp (index 1), 10 bp (index2) and 150 bp (read 2 length).

3.5.6 Tissue preparation for spatial transcriptomics

Spatial transcriptomics was performed with the Visium Spatial Gene Expression platform from 10X Genomics. Harvested plant roots were rinsed with deionized H_2O and cryopreserved in OCT (Optimal Cutting Temperature compound) via submerging of OCT-embedded molds into a dewar of isopentane chilled liquid nitrogen for even freezing. Cryomolds of roots were stored at -80 °C until cryosectioning. Cryosectioning was performed on an Epredia™ CryoStar™ NX70 Cryostat with a blade temperature of 14 °C and a sample head temperature of –12 °C with a section thickness of 16 ϩ. Cryosections were placed onto the surface of the chilled Visium Spatial Gene Expression slide and adhered to the slide using heat from the sectioner's finger placed on the back surface of the capture area. Prepared slides were stored at 80 °C prior to processing for 10x Visium spatial transcriptome sequencing according to the manufacturer's instructions with the following modifications: First, cryosections were stained using an incubation of 0.05% Toluidine Blue-O in 1X PBS for 1 min and rinsed 3X with 1X PBS. Second, A pre-permeabilization step was added as suggested by Giacomello et al.[228] The pre-permeabilization mix for each slide (48 µl Exonuclease I, 4.5 µl of Bovine Serum Albumin, and 428 µl of 2% PVP 40) was then prepared, and 70 µl was pipetted into each well. Pre-permeabilization occurred for 30 min at 37 °C after which the manufacturer's protocol for tissue permeabilization was followed. Permeabilization Enzyme (70 µl) was added to each capture area and incubation at 37 °C occurred for 12 min based on the results of the manufacturer's Tissue Optimization protocol (Extended Data Fig. 6).

3.5.7 Data processing and analysis

Cellranger and Spaceranger software (10X Genomics, Pleasanton, CA) were used to preprocess single nuclei and spatial transcriptomic sequencing libraries respectively. A formatted reference genome was generated using Cellranger or Spaceranger's "mkref" function using the *Medicago truncatula* MedtrA17_4.0[37] whole genome sequence and annotation and the *Rhizophagus irregularis* Rir_HGAP_ii_V2 (DAOM 181602, DAOM 197198)[115] whole genome sequence and annotation using default parameters. Single-nuclei and spatial reads were aligned to the genome references using the "count" function in Cellranger 7.0 and Spaceranger 1.3 software packages (10x Genomics, Pleasanton, CA), respectively. Brightfield tissue images were aligned to the spatial capture area fiducial frame and voxels corresponding to overlaying tissue were manually selected for all capture areas in Loupe Browser (10X Genomics). Data analysis for both the single nuclei and spatial data was performed using the Seurat[22] 4.3.0 package in R 4.2.1 available at: https://www.R-project.org.

3.5.8 Filtering and normalization

For both single nuclei and spatial datasets, normalization and scaling were performed using the SCTransform R function in Seurat prior to clustering. Metrics used for filtering of the data during quality control steps can be found in Table S2.

3.5.9 Principal components analysis and K-means clustering

Principal components analysis was performed on both snRNA-seq and spatial RNA-seq datasets using the RunPCA function in Seurat with the "SCT" assay specified. The FindNeighbors function was applied to construct a Shared Nearest Neighbor (SNN) graph for the data using the first 30 principal components. Clustering was performed using the FindClusters function which utilizes the SNN graph from the previous step. Finally, the RunUMAP function was utilized to construct the Uniform Manifold Approximation and Projection dimensionality reduction and visualize the dataset in two dimensions. Of the seven snRNA-seq datasets generated (Extended Data Fig. 7, Table S2), we selected five for further characterization, resulting in a final dataset of 16,890 nuclei with an average of 1,120 mRNA molecules per cell after quality filtering. The remaining two datasets were not included due to poor apparent colonization by *R. irregularis*. All spatial datasets were analyzed.

3.5.10 Integration of replicate datasets

Replicate capture areas or samples from each treatment (mycorrhizal or mockinoculated) were integrated into two sets of Seurat objects (snRNA-seq, spatial) using the data integration pipeline in Seurat[229]. First, we applied the PrepSCTIntegration function using all transcripts for integration. We then identified a set of integration anchors with the FindIntegrationAnchors function. Finally, we applied the IntegrateData function. Principal component analysis and dimensionality reduction was performed on the integrated objects in the same manner as the individual objects with the following adjustments: 1) number of PCs = 30, 2) metric = cosine, and 3) resolution was set to 0.5 for clustering. UMAP plots for all datasets were created using the DimPlot() function and are displayed in Extended Data Fig. 7 (snRNA-seq) and Extended Data Fig. 2 (spatial).

3.5.11 Cluster Identification for snRNA-seq

We determined that clusters 0, 1, 2, 4, 6, 8, 9, 14, and 16 are cortical cells based on enrichment of *ISOFLAVONE SYNTHASE1* (*MtIFS1*, Medtr4g088195) and *ISOFLAVONE SYNTHASE3 (MtIFS3*, Medtr4g088160)[230], as well as *ATP-BINDING CASSETTE TRANSPORTER59* (*MtABCG59*, Medtr3g107870)[192], which encodes a strigolactone transporter which is expressed in cortical cells under phosphate-depleted conditions. Cluster 14 represents cortical cells which are colonized by AM fungi, based on a range of known marker genes, including *ATP-BINDING CASSETTE TRANSPORTER* (*MtNOPE1*, Medtr3g093270)[231], two isoforms of *ABCB FOR MYCORRHIZATION AND NODULATION* (*MtAMN2*, Medtr4g081190 and *MtAMN3*, Medtr8g022270)[232], *1-deoxy-D-xylulose 5-phosphate synthase* (*MtDXS2*, Medtr8g068265)[193], and *REDUCED ARBUSCULAR MYCORRHIZA1 (MtRAM1*, Medtr7g027190)[195], and *VAPYRIN* (*MtVPY*, Medtr1g089180)[23]. We specifically focused on more mature roots, excluding meristematic or developing cells for most cell types as arbuscules do not form in these cell types. As a result, we did not observe evidence for developmental variation (trajectories) that are typically

captured in single-cell studies of embryonic or meristematic tissues. Marker genes for quiescent center and lateral root primordia, however, were used to identify cluster 12 as meristematic cells, including four homologs of *PLETHORA* (*MtPLT1-4*, Medtr2g098180, Medtr4g065370, Medtr5g031880, and Medtr7g080460) [233] and *YUCCA (MtYUC8*, Medtr7g099330). *MtYUC8*[234] and *MtPLT* genes tend to be associated with nodule formation, as well, but other genes which are upregulated by nodulation, such as NODULE INCEPTION (*MtNIN*, Medtr5g099060)[235], were either absent from our dataset or expressed at low levels and not specific to any cluster. RESPIRATORY BURST OXIDASE HOMOLOGS (*MtRboHF*, Medtr7g060540)[236], which is specifically expressed in root hairs, defined a small cluster adjacent to the LRP cluster as root hairs. The presence of *SCARECROW* (*MtSCR*, Medtr7g074650)[237] indicated that cluster 7 represents endodermal cells. Clusters 3, 5, and 11 were predicted to be vascular tissue, with several stele-specific *A. thaliana* homologs such as three homologs of transcription factor MYB DOMAIN PROTEIN (MtMYB0*71*, Medtr5g014990, *MtMYB113* Medtr2g096380, and *MtMYB112*, Medtr4g063100)TEMP, as well as functionally characterized *M. truncatula* marker genes enriched in these clusters: three PHOSPHATE TRANSPORTER homologs: (*MtPHO1.1-1.3*, Medt1g041695, Medtr1g075640, Medtr8g069955)[24,195] and *SUGAR TRANSPORT PROTEIN13* (*MtSTP13*, Medtr1g104780)[94]. Based on homologs from Arabidopsis marker genes such as PEROXIDASE13 (*MtPrx13*, Medtr1g101830)[186] and LOB-DOMAIN PROTEIN (*MtLBD18*, Medtr8g036085)[186], cluster 17 represents xylem cells. *FE/ALTERED PHLOEM DEVELOPMENT* (*MtFe*, Medtr6g444980) and Arabidopsis PHLOEM EARLY DOF1 homologs (*PEAR1*, Medtr3g077750 and Medtr4g461080) were enriched in cluster 13, suggesting that these are phloem cells[238]. We defined cluster 15 as representing companion cells, as it is enriched for Arabidopsis phloem marker homolog SUPER NUMERIC NODULES (*MtSUNN*, Medtr4g070970)[239] and homologs of Arabidopsis companion cell markers Arabidopsis *SUCROSE PROTON SYMPORTER2* (*AtSUC2*, Medtr1g096910) and Arabidopsis *FT INTERACTING PROTEIN1 (AtFTIP1*, Medtr0291s0010)[240]. Clusters 5 and 11 were enriched for *MtPHO1.1-1.3* (Medtr1g041695, Medtr1g075640, and Medtr8g069955)[24], suggesting that these are central cylinder/pericycle cells. Marker genes for all snRNA-seq clusters can be found in Table S13 and a dot-plot showing expression of markers for each cluster can be found in Extended Data Fig. 1.

3.5.12 Differential gene expression

Differentially expressed genes (upregulated and downregulated) between the mycorrhizal and control integrated datasets for all clusters were identified using the Likelihood Ratio Test from the DESeq2[241] package with an adjusted p-value of <0.05 and a log2 foldchange threshold of -1.0 or 1.0.

3.5.13 Module score analysis

To determine which cells represented colonized cortex cells, we generated a list of genes (Table S3) which are known to be involved in colonization, and used these as input to assign a module score to each cell using the Seurat AddModuleScore function. Cells with a score above the threshold of 98th percentile were selected as 'colonized' cells, and subsetted to a new object for further sub-clustering analysis.

3.5.14 Gene expression imputation

Using the annotated snRNA-seq integrated object as a reference and the spatial integrated object as a query, we performed a data transfer using the UMI counts from the RNA assay within the single nuclei object as the reference data and stored the new data under a new assay called "imputation". We then were able to predict gene expression within the spatial dataset using the expression values from the snRNA-seq dataset by specifying the assay to "imputation" during the analysis.

3.5.15 Voxel cell type proportion prediction in spatial RNA-seq

Using the annotated snRNA-seq integrated object as a reference and the spatial integrated object as a query, we performed a label transfer using the cell type annotations as the reference data. The query dataset is then projected onto the PCA of the reference dataset and the labels are predicted.

3.5.16 Comparison to previous datasets

We compared our dataset to two prior studies (Gaude et al. 2012 and Hogekamp et al., 2013)[94,95] that significantly improved our understanding of gene expression changes during the mycorrhizal symbiosis between *M. truncatula* and *R. irregularis*. We wanted to include these datasets in our analysis to identify a core set of DEGs between the three different RNA-seq techniques and be able to compare and contrast the various methods in spatial transcriptomics. One major hurdle to this comparison resulted from the use of the Affymetrix Medicago GeneChip array by these two studies leading to a difference in feature IDs. We constructed an ID converter (Table S14) to convert between the Affymetrix GeneChip, MedtrA17_4.0, and the *M. truncatula* A17 r5.0 gene IDs for a certain locus in bulk fashion using data available at https://medicago.toulouse.inra.fr/MtrunA17r5.0-ANR[242]. Genes identified as common between datasets can be found in Table S5.

3.5.17 Gene Ontology and functional enrichment analysis

For *M. truncatula*, we conducted gene ontology and functional enrichment analyses utilizing the PANTHER Classification system (www.pantherdb.org)[243]. For *R. irregularis*, we conducted gene ontology analysis with the Blast2Go software[244] (Blast2Go, https://www.biobam.com/blast2go)/.

3.6 Data Availability

Raw feature and UMI counts for all datasets are displayed in File S1. Data availability on NCBI GEO (Gene Expression Omnibus) is available at https://www.ncbi.nlm.nih.gov/geo/query/acc.cgi?acc=GSE240107. Genome assemblies for MedtrA17_4.0[37] and the *Rhizophagus irregularis* Rir_HGAP_ii_V2 (DAOM 181602, DAOM 197198)[115] were accessed at https://www.ebi.ac.uk/ena/browser/view/GCA_000219495.2 and https://www.ebi.ac.uk/ena/browser/view/GCA_002897155.1, respectively.

3.7 Code Availability

All scripts used for data analysis are available on GitHub at https://github.com/kserrano109/Medicago_Rhizophagus_RNAseq. Information on all Seurat objects used within the data analysis for all datasets can be found in Table S15.

3.8 Acknowledgments

We would like to acknowledge Christopher Gee, Lorenzo Washington, Victoria Vera, Jutta Dalton, Maria Harrison, Trevor Tivey, Bruno Guillotin, and Rihanna Hunter for their advice, expertise, and technical help. We also would like to thank the QB3 UC Berkeley Genomics Core Sequencing Facility (*QB3 Genomics, UC Berkeley, Berkeley, CA, RRID:SCR_022170)* for their help in cryosectioning and sequencing. This study was performed at the DOE Joint BioEnergy Institute (http://www.jbei.org) and the DOE Joint Genome Institute (https://ror.org/04xm1d337) supported by the U. S. Department of Energy, Office of Science, Office of Biological and Environmental Research, through contract DE-AC02-05CH11231 between Lawrence Berkeley National Laboratory and the U.S. Department of Energy. This study was supported by a Laboratory Directed Research and Development award to B.C. at Lawrence Berkeley National Laboratory, and by an Early Career Research Program award to B.C. to H.V.S.

3.9 Author Contributions

K.S, M.B, H.V.S. and B.C. planned experiments; K.S., M.B., T.D., and D.G performed experiments; R.O., R.M., and A.V. provided consultation; K.S., M.B., and B.C. analyzed the data; K.S., M.B., H.V.S., and B.C. wrote the manuscript.

3.10 Competing Interests

The authors declare no competing interests.

3.11 Significance Statement

This study significantly advanced our current understanding of communication during beneficial plant-microbe interactions by employing cutting-edge transcriptomic technologies to analyze the AM symbiosis between *M. truncatula and R. irregularis.* Through the creation of a 2-dimensional integrated map of plant and fungal transcriptomes during symbiosis, we were able to analyze groups of cells and identify specific cell types with a marked symbiosis-specific transcriptomic signature. Such spatially-resolved transcriptomic data are unprecedented in the field of AM symbiosis research, allowing for a deeper understanding of the molecular dialogue between the two organisms. By identifying the colonized cortical cell cluster in the single-nuclei datasets and spatial cluster #3 from the spatial datasets as symbiosis-specific, we were able to identify thousands of genes from both the plant and the fungus that are great candidates for further functional characterization. Moreover, the thousands of *R. irregularis* genes expressed within the mycorrhizal capture areas provide a wealth of information for understanding the fungal response to symbiosis at the molecular level. Laying the groundwork for deeper exploration into the AM fungal genes involved in symbiosis, this research overcomes barriers that have previously hindered such analyses. Overall, the integration of single-nuclei and spatial transcriptomics allowed for the identification of plant and fungal gene clusters involved in

symbiosis-specific functionalities, and the datasets generated by this study serve as a valuable resource for the AM research community, fostering further investigations into the molecular mechanisms driving this important mutualistic interaction. The next chapter will cover two research studies conducted to investigate the effect of two different genetic engineering strategies in transgenic *Sorghum bicolor* and *Oryza sativa* on their symbiotic capabilities when infected with the AM fungus, *R. irregularis*.

Chapter 4. Effects of Plant Host Genetic Modification on the Arbuscular Mycorrhizal Colonization Capacity of *Rhizophagus irregularis* on *Oryza sativa* and *Sorghum bicolor*

4.1 Abstract

The AM symbiosis requires sustained cross-kingdom communication and immense plant cell restructuring throughout the entire root tissue. Plant cell walls (PCWs) function to maintain cell structural integrity and mediate plant-microbial interactions. Small peptides can serve as crucial signaling molecules in plant-microbe interactions. In this study, I investigate the effects of PCW modifications, specifically the overexpression of *OsAT10* (encoding a BAHD acyltransferase) in *S. bicolor* for improved biofuel feedstock properties and the effects of overexpressing a gene encoding a small PSY family peptide, *OsPSY1,* in *O. sativa* associated with enhanced root growth on their ability to be colonized by *R. irregularis*. Transgenic *S. bicolor* and *O. sativa* lines overexpressing *OsAT10* and *OsPSY1*, respectively, demonstrated enhanced symbiotic capacity with arbuscular mycorrhizal fungi, offering potential avenues for future sustainable crop improvement in biofuel feedstocks and food crops.

4.2 Introduction

4.2.1 Plant cell wall structure and function

The plant cell wall (PCW) is a diverse and complex structure which is responsible for a myriad of functions throughout all developmental stages and across distinct tissue types. Surrounding the plasma membrane, the PCW maintains the cell's structural integrity and shapes the plant cell while also providing the necessary flexibility to withstand large tensile forces and allow for processes such as cell division and differentiation[245]. PCWs also mediate plant-microbial interactions by acting as a physical barrier for entry into the cell, producing microbial-influencing compounds, detecting PCW degradation products, and serving as a source of carbon during plant-microbe symbiosis[246]. The structure and composition of the PCW varies greatly among unique plant species, developmental stages, and tissue types, and this diversity is seen not only in the major polysaccharide components of the PCW but also in the wide range of receptors, pores, and channels present throughout the PCW[247]. For example, young plant cells require greater porosity in the PCW to allow for free diffusion of water and nutrients between cells, whereas the PCW must be impermeable in specialized vascular tissues[247]. Generally, the 'primary' cell wall refers to the PCW established in young cells during cell division and expansion which provides basic support and mediates interactions between cells, while the 'secondary' cell wall is a thicker and more durable structure that is deposited between the primary cell wall and the plasma membrane at a later stage when cell expansion is finished[245,247].

The PCW can be represented as a complex, dynamic matrix in which cellulose microfibrils (complexes of hydrogen-bonded, unbranched (1,4)-β-D-glucan chains) act as the support beams and are the major component of PCWs while the rest of the space is filled with hemicellulosic and pectic polysaccharides[248]. Hemi-cellulosic polysaccharides such as xyloglucans, glucomannans, xylans, and mixed-linkage glucans, function to strengthen the plant cell wall via their interaction with cellulose and, in some tissues, lignin[249]. Pectic polysaccharides, such as homogalacturonan, rhamnogalacturonan I, and rhamnogalacturonan II, are extremely diverse and play important roles in cell wall expansion, strength, and intercellular signaling[250]. In addition,

PCWs also contain a wide variety of proteins and glycoproteins[251]. In contrast to cellulose microfibrils, the hemicellulosic and pectic polysaccharide components of the PCW are extremely structurally complex and can be distinguished further by sugar substitutions and side chains which influence their interactions with other components in the PCW[247,249].

In vascular plants, secondary cell wall formation is associated with lignification. Lignin is hydrophobic phenolic polymer that is created through radical coupling of three monolignols synthesized via the phenylpropanoid pathway: coniferyl alcohol, sinapyl alcohol, and p-coumaroyl alcohol. These monolignols then constitute the guaiacyl (G), sinapyl (S), and hydroxyl-coumaroyl (H) units of the lignin polymer, respectively[252]. Different plant species and tissues will vary in their lignin composition. For example, gymnosperms will be rich in G units, while dicots will have higher representation of both G and S units[252]. Lignin is the second most abundant biopolymer, accounting for almost 30% of the global organic carbon content[253]. It serves to reinforce PCWs, enhancing the rigidity of the PCW and increasing resistance to external forces. It also further restricts the passage of small molecules and microbes, and plays further roles in abiotic and biotic stress[254]. Because of their high abundance in PCWs, lignocellulosics represent a renewable resource for the production of biofuels. However, once produced, lignin remains anchored in the cell wall as plants do not contain the mechanisms necessary to recycle the lignin polymer. Therefore, lignocellulosics are recalcitrant and require complex and expensive biorefinery processing for conversion of polysaccharides into usable monosaccharides[255]. There are two main hurdles that preclude the feasibility of such biorefinery and must be addressed: 1) developing suitable biofuel feedstocks with optimal agronomic traits and biomass yields that withstand environmental stress and 2) reducing recalcitrance to degradation or optimizing PCW composition for fermentation during the biorefinery process[256]. Metabolic engineering of plant species commonly used as feedstocks, monocots in particular, to modify natural lignin structure and composition has been the main strategy in recent years to achieve these goals.

4.2.2 Overexpression of *Oryza sativa* BAHD acyltransferase AT10 affects plant cell wall properties in diverse plant species

In grasses and other monocots, PCWs can consist of up to 40% dry weight of glucuronoarabinoxylan (GAX) which is comprised of β-1,4-linked xylan residues[257]. The substitutions of GAX in monocots is unique. Arabinofuranose residues are the most common substitution at O3 of xylose, and hydroxycinnamic acid ferulic acid (FA) substitutions occur relatively frequently at O5 of arabinofuranose residues[257]. Cross-linking of adjacent xylans occurs through the formation of dehydrodimers of ferulate and linkage between ferulate and monolignols can facilitate lignin polymerization[257]. *para*-coumaric acid (*p*-CA) is another hydroxycinnamic acid that can be ester linked to grass PCW components. *p*-CA substituents rapidly pass radicals to sinapyl alcohols, facilitating lignin polymerization[257]. Cell wall-associated FA blocks biomass digestibility and FA as well as *p-CA* have been shown to deter fungal pathogens and insect pests[258]. BAHD acyltransferases play a role in the incorporation of FA into PCWs and mediate lignin biosynthesis as several members use hydroxycinnamoyl-CoAs as substrates[259]. In 2012, OsAT4 was characterized and shown to possess *p*-coumarate monolignol acyltransferase activity in vitro[260]. In 2013, OsAT10 emerged as a front-runner for altered PCW hydroxycinnamate content when Bartley et al. provided evidence that OsAT10

overexpression in *O. sativa* increased matrix polysaccharide-associated ester-linked *p*-CA and decreased matrix polysaccharide-associated FA, significantly altering the ratio of ester-linked FA:*p*-CA in leaf tissue[257]. This change was associated with increased *in vitro* saccharification, but had no effect on lignin content. Similarly, in 2018, Li *et al.* demonstrated that overexpression of *OsAT10* in switchgrass decreased cell wall-bound FA and increased cell wall-bound *p*-CA in leaf tissues, associated with a 40% increase in saccharification[261].

In 2021, Tian *et al.* generated *Sorghum bicolor* transgenic lines that overexpressed the *OsAT10* codon-optimized sequence under the control of the *S. bicolor* polyubiquitin gene (*pSbUbi:AT10*) via *Agrobacterium*-mediated transformation in an attempt to reduce biomass recalcitrance[262]. *pSbUbi:AT10* lines exhibited a 23-42-fold increase of *p*CA-Ara, while FA-Ara was significantly reduced on average[262]. Furthermore, *pSbUbi:AT10* lines did not seem to be significantly altered in cellulose or xylan content. However, all transgenic lines showed small reductions of lignin content (6-16%), and analysis of lignin monomeric composition revealed reductions in the S/G ratio for 6 transgenic lines compared to WT[262]. Lastly, all *pSbUbi:AT10* lines resulted in a higher sugar titer after pre-treatment with the ionic liquid cholinium phosphate compared to the wild-type control, indicating the modifications to the PCW of these transgenic lines allowed for more efficient saccharification[262]. In contrast to the previously mentioned study conducted by Bartley *et al.* in *O. sativa*[257], this increased saccharification was attributed to the reduction in lignin content rather than the change in FA:*p*-CA ratio, suggesting a connection between xylan-bound p-CA and lignification.

As mentioned previously, the PCW plays a role in mediating plant-microbial interactions as it represents the first interface for interaction between species. Whether pathogenic or mutualistic, microbial infection of plant cells requires PCW loosening or degradation. Microbes have developed a wide range of PCW-degrading proteins and hydrolases and plants have, in turn, developed methods by which to recognize these compounds and modify the composition and distribution of cell wall polysaccharides and associated enzymes to protect the PCW[263]. The response by the plant is determined by the type of infection, but can include programmed cell death, secretion of anti-microbial compounds, pathogenesis-related protein, and structural modifications to the PCW[264]. Upon microbial infection, plant cells can polymerize lignin and deposit suberin, a hydrophobic lipid-based polymer, to reinforce the PCW and add an additional layer of control[264]. Lignin biosynthesis is upregulated upon pathogen infection, as the plant attempts to thicken the cell wall[246]. For roots in particular, a specialized feature of the PCW is the Casparian strip, a hydrophobic band between cells of the endodermis which acts as a barrier to block diffusion of external substances into the vasculature and prevent nutrient leakage[265].

In the case of the AM symbiosis, the PCW represents not only the first point of contact between species, but is involved throughout the entirety of the interaction, as this relationship consists of sustained wall-to-wall contact between the plant and fungus. AM fungi penetrate the epidermal cell layer and travel inter- and intra-cellularly to the endodermis at which point the plant cell accommodates the growing arbuscule within the cortex cell. Then, the two species must transfer molecules through their plasma membranes and cell walls, across the symbiotic interface. Expansins, extracellular proteins involved in cell wall-loosening, have been implicated as playing a role in accommodating the fungus through the root and inside the cortical cells and are upregulated in AM roots[46,266]. However, the mechanism by which AM fungi suppress defense

responses and navigate across plant cell walls without a suite of PCW degrading enzymes is still unknown, but the limited amount of CAZymes found in AM fungi indicates that the plant host is largely modulating fungal colonization depending on its nutritional needs[267]. Furthermore, it is now evident that the peri-arbuscular membrane (PAM) formed within the plant cell to surround the developing arbuscule, although structurally unique, is plant-derived and many studies have shown traditional PCW polysaccharides such as β-1,4-glucans, non-esterified homogalacturonans and xyloglucans at the symbiotic interface and PAM[46,266]. In our own research utilizing spatial transcriptomics in *M. truncatula*, we observed upregulation of *MtCESA6 (CELLULOSE SYNTHASE 6)* and *MtPME1* (*PECTIN METHYLESTERASE 1)* to be upregulated in *R. irregularis*-colonized roots as compared to mock-inoculated roots[46]. Recently, scientists have begun to explore the effects of AM fungal colonization on the PCW and it has been observed that the mycorrhizal symbiosis alters the cellulose and hemicellulose content of certain grasses[268,269]. Furthermore, a transcriptomics study conducted in 2018 on *Helianthus annuus* mock-inoculated and AM-inoculated roots colonized by the AM fungus *Rhizoglomus irregulare* detected the up-regulation of several BADH acyltransferases in mycorrhizal roots[270]. Given the importance of the PCW and plant-derived PCW polysaccharides in mediating and maintaining the AM symbiosis as well as the significant alterations to PCW composition in *pSbUbi:AT10* transgenic *S. bicolor* lines observed by Tian et al., we hypothesized that this PCW modification may impact the symbiotic capacity of *S. bicolor*. In the present study, I investigate three unique *pSbUbi:AT10* transgenic lines on their symbiotic capacity upon infection with *R. irregularis* in comparison to a wild-type control.

4.2.3 PLANT PEPTIDE CONTAINING SULFATED TYROSINE (PSY) family peptides

Cell-to-cell signaling governs various cellular functions within plants. Plant peptides can act as signals during plant development, growth, defense, and symbiosis. Generally, peptides can be divided into four major structural groups based on whether they get secreted or non-secreted and whether they function extracellularly or intracellularly[271]. Tyrosine sulfation is a post-translational modification that can occur in secreted proteins in plants. The PSY (PLANT PEPTIDE CONTAINING SULFATED TYROSINE) family peptides represent one category of small secreted proteins that have undergone tyrosine sulfation via the actions of *TYROSYLPROTEIN SULFOTRANSFERASE* (*TPST*) and play significant roles in regulating root growth[271]. PSY family peptides function as extracellular signals and bind to leucine-rich repeat receptor-like kinases (LRR-RLKs) to trigger downstream signaling pathways[272]. In *A. thaliana*, there are nine-members within the PSY family and PSY1 is the most-studied, having been one of the first plant tyrosine sulfonated secreted proteins identified in 2007[273]. It has been shown that PSY peptides bind to three LRR-RLKs known or *ROOT ELONGATION RECEPTOR KINASES (REKs)1/2/3* (synonymous with *PSYR1/2/3, PSY RECEPTOR*) which negatively regulate root growth[274]. Additionally, the application of synthetic PSY peptide enhances root growth[275].

PSYR signaling has also been demonstrated to be involved in stress regulation. Triple *psyr1,2,3,* mutants were exposed to high salinity, high temperature, and pathogen exposure (*Pseudomonas syringae* pv. tomato (*Pst*) DC3000) and exhibited more severe growth defects and higher susceptibility to infection than the wild-type[272]. Furthermore, *tpst1* mutants in which PSYR signaling is constitutively active demonstrated higher tolerance to temperature stress while treatment of plants with PSY5 impaired salt tolerance[272]. In a separate study, PSY1,2,5,6, and 8

were significantly upregulated in response to abscisic acid (ABA) treatment which is involved in a variety of abiotic and biotic stress response, while PSY3 and PSY4 were downregulated[276]. Taken together, these data suggest that the PSY family peptides and PSYR receptors play a role in stress tolerance, with PSY peptides promoting root elongation and growth while inhibiting stress response mediated by PSYR LRR-RLKs. This is consistent with the discovery in recent years of several microbial mimics of PSY peptides. In 2017, Pruitt et al. discovered that the biotrophic pathogen *Xanthomonas oryzae pv. oryzae (Xoo)* releases a sulfated peptide RaxX that is structurally similar to PSY family peptides to facilitate *Xoo* infection[277]. A receptor for RaxX, *XA21*, is present in some Xoo-resistant rice varieties and recognizes RaxX, but is unable to recognize *AtPSY1,* indicating XA21 is specific to this bacterial mimic. RaxX was found to also mimic the growth promoting activities of PSY peptides, and treating *psyr1* mutants with RaxX or PSY1 enhanced root growth in a similar manner, indicating there may be another receptor that recognizes both of these peptides[275]. Further experiments revealed that sulfated RaxX enhances root growth in *O. sativa* as well[277]. In 2023, it was discovered that root-knot nematodes (*Meloidogyne spp.)* encode PSY-like peptides (MigPSYs) that share sequence similarity to RaxX and the plant PSYs[278]. These MigPSYs also stimulate root growth in *A. thaliana* and their expression peaks at the earliest points of the infection cycle, suggesting they may act to bind and repress host defense/stress response activated by PSYRs[278].

4.2.4 Peptide hormones as regulators of symbiosis establishment

As demonstrated by the microbial mimics of PSY peptides, peptides allow for cross-kingdom communication. In both the rhizobial and AM symbiosis, the microbes can produce effectors, including small secreted peptides to enhance their infectivity. One of the most well-characterized small signaling peptides produced by the AM fungus *R. irregularis, RiSIS1* (*SL-induced SECRETED PROTEIN*) responds to strigolactone secretion by the plant host and, in turn, positively regulates root colonization and was found to be upregulated in mycorrhizal roots[279,280]. As is the case for fungal pathogens, AM fungi also produce molecular mimics of plant peptides. Plant CLE (*CLAVATA3/ESR)* peptides are known to interact with LRR-RLK receptors and function in multiple plant developmental, metabolic, and environmental processes, including symbiosis establishment[281]. In the rhizobial symbiosis, CLE peptides function as long-distance signals. Following rhizobial infection, a transcription factor *NIN* (*NODULE INCEPTION*) is induced and activates the expression of two peptides in the root, *CLE-RS1* and *CLE-RS2*, which are able to travel to the shoot to activate downstream responses[282]. This signaling in the shoot negatively regulates nodule formation, thus completing a long-distance negative feedback loop. Interestingly, this negative regulation is thought to occur to balance carbon expenditure and nitrogen acquisition, as the plant will activate CLE peptide signaling upon sufficient nitrogen status. Similarly, CLE peptides function to regulate the AM symbiosis by modulating root strigolactone production through a negative feedback loop requiring the LRR-RLK SUNN[283]. A model has been proposed in which subtractive or additive peptides function to balance nutrient acquisition and symbiosis over time, allowing the plant to dynamically respond to stimuli by regulating peptide concentration, rather than their presence or absence[284]. The AM fungal species *R. irregularis* and *Gigaspora rosea* both encode CLE-like peptides (*RiCLE1* and *GrCLE1)* which are induced only in colonized roots of *M. truncatula* and not in asymbiotic fungal structures[285]. RiCLE1 is homologous to MtCLE5, which is induced by low phosphate status. Both RiCLE1 and MtCLE5 can stimulate the production of lateral roots and synthetic RiCLE1

can increase AM colonization[286]. Thus, the CLE peptide mimics may function to enhance AM colonization of plant roots by stimulating lateral root growth and creating more fungal entry points.

There are many other examples of the involvement of plant peptides in establishing or maintaining endosymbiosis. *M. truncatula* has nearly 800 genes encoding NCR (*NODULE-CYSTEINE-RICH)* peptides, which have anti-microbial properties and cause rhizobia within nodules to cease to divide and become non-motile[287]. NCRs also mediate bacterial selection by the plant host, as *NFS1 and NFS2 (NITROGEN FIXATION SPECIFICITY*) are genes that can actively terminate inefficient symbionts allowing the plant to select high N-fixation strains[288]. One of the most famous small secreted peptides families involved in the AM symbiosis is the cysteine-rich defensin-like peptide *MtDefMd1,2* and *3.* These peptides are upregulated in mycorrhizal roots, specifically in cortex cells during the late stages of arbusculation[289]. Based on its homology to NCR peptides, *MtDefMd1/2/3* are thought to play a role in arbuscule senescence, controlling the lifespan of arbuscules and thus mediating symbiotic capacity[290]. More research on peptide control of symbiosis and nutrient acquisition is necessary to fully understand these processes, but it is evident that small peptides from both the plant and microbe are functioning as signals during the symbiosis and play important roles in the interaction. Given the root growth enhancing effects of the PSY family peptides on *O. sativa,* we hypothesized that overexpression of *PSY1* may impact symbiotic colonization of *O. sativa* by *R. irregularis.* In the present study, I investigate three unique *OsPSY1* over-expression transgenic lines on their symbiotic capacity upon infection with *R. irregularis* in comparison to a wild-type control.

4.3 Results

4.3.1 Expression of *pSbUbi:AT10* in *S. bicolor* increases expression of arbusculated cell marker gene *SbPT11* and significantly increases fungal biomass in the roots during the AM symbiosis

Three distinct transgenic *pSbUbi:AT10* S. *bicolor* (JBEI0615, JBEI0634, and JBEI0647) and their wild-type lines were grown in phosphate-depleted sand cone-tainer which stimulate the AM symbiosis. Upon germination, plants in the mycorrhizal treatment were inoculated with sterile *R. irregularis* spores in a specific layer of sand within the cone-tainer, while the control treatment received a mock-inoculation of sterile distilled water. At 21 days post-inoculation (21-dpi), roots were harvested for colonization assessment by either the Trouvelot fungal root scoring method[227] or through RT-qPCR of two marker genes the AM symbiosis: 1) *SbPT11* (*PHOSPHATE TRANSPORTER 11)* and 2) *RiTUB (B-TUBULIN)*. *SbPT11* is an AM-inducible inorganic orthophosphate (Pi) transporter in the *Pht1* family[291], while *RiTUB* is commonly used a proxy to assess fungal biomass within the root system[46,292,293]. Expression of *SbPT11* and *RiTUB* was normalized to that of a housekeeping gene, *SbEF1a,* which is reported to be stably expressed during the AM symbiosis[294].

As shown in Fig. 4-1, a comparison of inoculated and mock-inoculated plants from each line revealed a significantly stronger response to *R. irregularis* colonization by the *pSbUbi:AT10* transgenic lines than the WT. In the case of *SbPT11,* only one line (JBEI0634) showed significantly higher expression in the mycorrhizal treatment as compared to the control (ANOVA; $p=0.034$). The WT and all other transgenic *S. bicolor* lines did not show significant differences in

SbPT11 between the mycorrhizal and control treatments (Fig. 4-1). In a previous study which analyzed the expression of *SbPT11* across various diverse *S. bicolor* accessions at 42-dpi, there was high variability in the expression of *SbPT11* in response to AM treatment[294], which may explain this weak response and supports their observation that unique *S. bicolor* genotypes may vary in *SbPT11*expression. However, all transgenic *pSbUbi:AT10* lines displayed a significantly higher expression of *RiTUB* in response to AM-treatment (Fig. 4-1). While the difference between the expression of *RiTUB* in the mycorrhizal-treated and control WT plants was not significant ANOVA; p=0.133), expression of *RiTUB* is nevertheless notably higher in the mycorrhizal treatment. Overall, these results suggest that the transgenic *pSbUbi:AT10* lines were experiencing a stronger level of AM colonization than the WT at the 21-dpi mark.

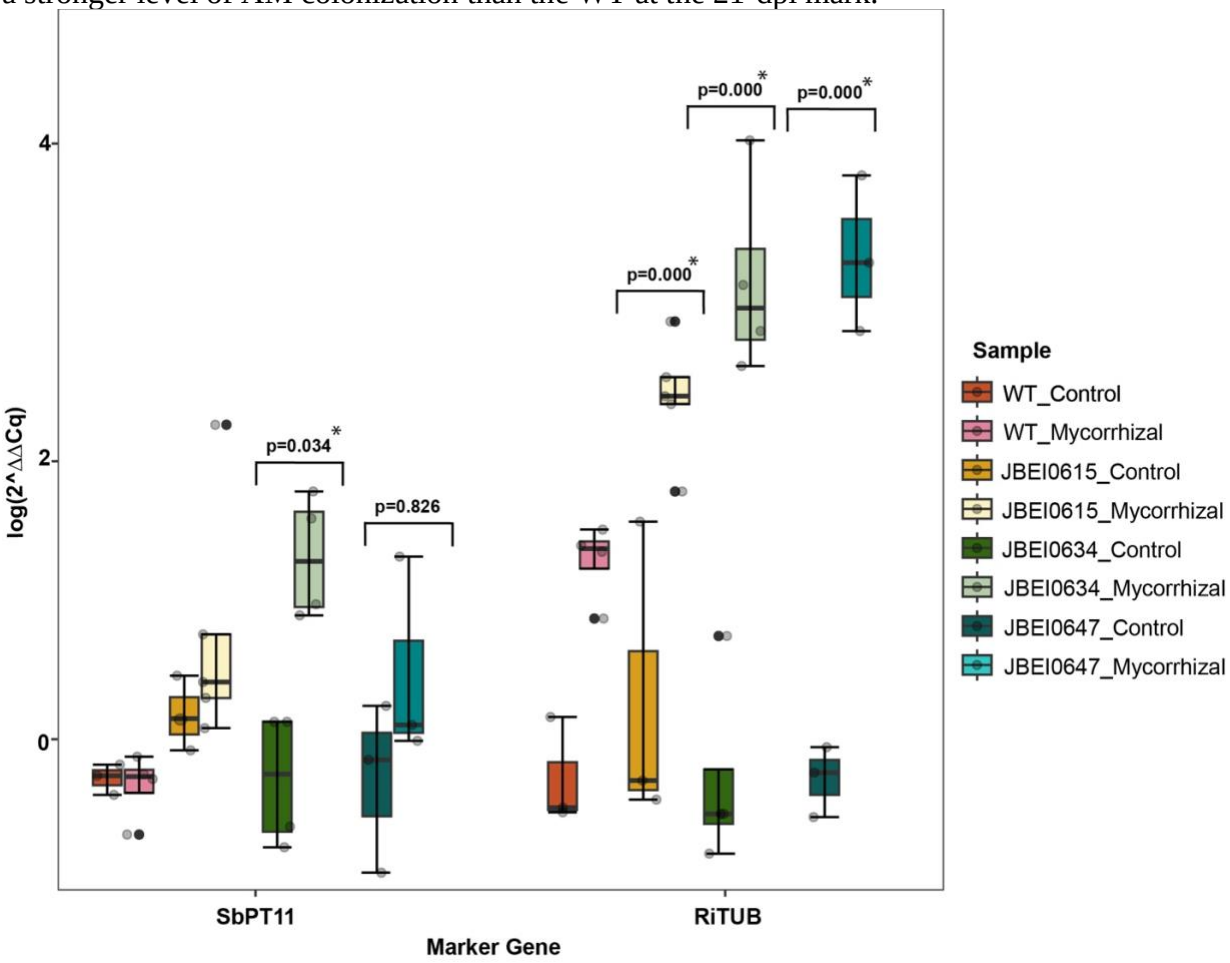

Figure 4-1. AM colonization of WT and transgenic *pSbUbi:AT10* S. bicolor lines results in upregulation of *SbPT11* and *RiTUB*.

Expression of SbPT11 and RiTUB relative to *SbEF1α* measured by qRT-PCR; Data are presented as mean values +/- SEM (n = 3-5). The box plots indicate the median (line inside the box), the lower and upper quartiles (box), margined by the smallest and largest data within the interval of 1.5x the interquartile range from the box (whiskers); outliers are shown (data points outside of box). P-values were determined using the student's T-test between AM inoculated and mock-inoculated samples of the same transgenic background (*indicates significant p-value <0.05).

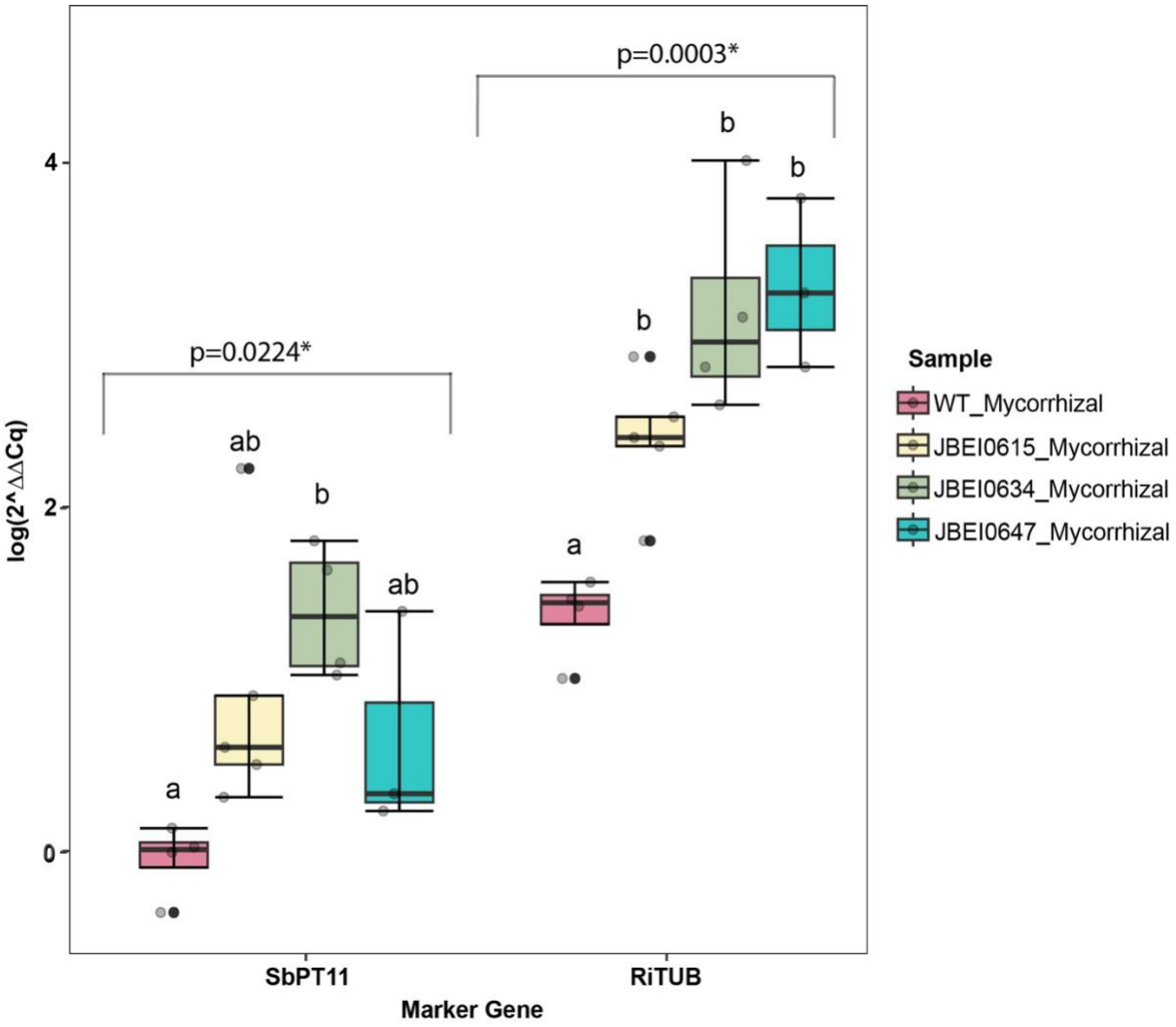

Figure 4-*2*. PCW alterations in transgenic *pSbUbi:AT10* S. *bicolor* lines results in upregulation of symbiosis-responsive genes from both host and symbiont.

Expression of SbPT11 and RiTUB relative to *SbEF1α* measured by qRT-PCR; Data are presented as mean values +/- SEM (n = 3-5). The box plots indicate the median (line inside the box), the lower and upper quartiles (box), margined by the smallest and largest data within the interval of 1.5x the interquartile range from the box (whiskers); outliers are shown (data points outside of box). P values were determined using one-way analysis of variance (ANOVA, *indicates significant p-value <0.05). Means not sharing any letter are significantly different by the Tukey-test at the 5% level of significance.

Comparing only mycorrhizal-treated samples, it became evident that the transgenic *pSbUbi:AT10* lines harbored a higher level of AM fungal biomass within their roots than the WT, as confirmed by the significantly higher expression of *RiTUB* in all three transgenic lines than the WT (Fig. 4-2, ANOVA; p=0.0003). A similar expression pattern was observed for *SbPT11*, with the *pSbUbi:AT10* lines line displaying higher *SbPT11* expression than the WT, which was significant in the case of JBEI0634 (Fig. 4-2, ANOVA; p=0.0224). Taken together,

these results indicate that the PCW modifications in the transgenic *pSbUbi:AT10* lines may be enhancing their symbiotic capacity.

4.3.2 Expression of *pSbUbi:AT10* in *S. bicolor* results in significantly altered vesicle abundance in the root system and mycorrhized root fragments

Does this enhancement in symbiotic capacity correlate with any specific AM fungal symbiotic phenotype? The results of the modified Trouvelot scoring method during the colonization assessment did not reveal any differences between the frequency or intensity of mycorrhizal colonization in the root system of transgenic *pSbUbi:AT10* lines compared to WT, though the intensity of mycorrhization (M) was almost significantly higher in the JBEI0615 line than the others (Fig. 4-3, ANOVA; p=0.059). Furthermore, no significant differences were observed for the abundance of arbuscules (A/a) and intraradical hyphae (H/h). However, there were significant differences in the abundance of vesicles in both the root system (V%) and across mycorrhizal root fragments (v%) (Fig. 4-3, ANOVA; p=0.024 (V) and p=0.019 (v)). In particular, line JBEI0647 demonstrated a significantly higher abundance of vesicles. Vesicles are lipid-filled structures within mycorrhizal roots that are thought to function as carbon storage for the fungus[295]. A higher abundance of vesicles within JBEI0647 may be indicative of increased lipid transfer from the plant to the AM fungus, but the same trend was not seen across all transgenic lines, thus it cannot explain the higher AM fungal biomass in transgenic roots compared to WT. More research is necessary to fully understand the enhanced mycorrhizal capacity observed in *pSbUbi:AT10* lines compared to WT *S. bicolor*.

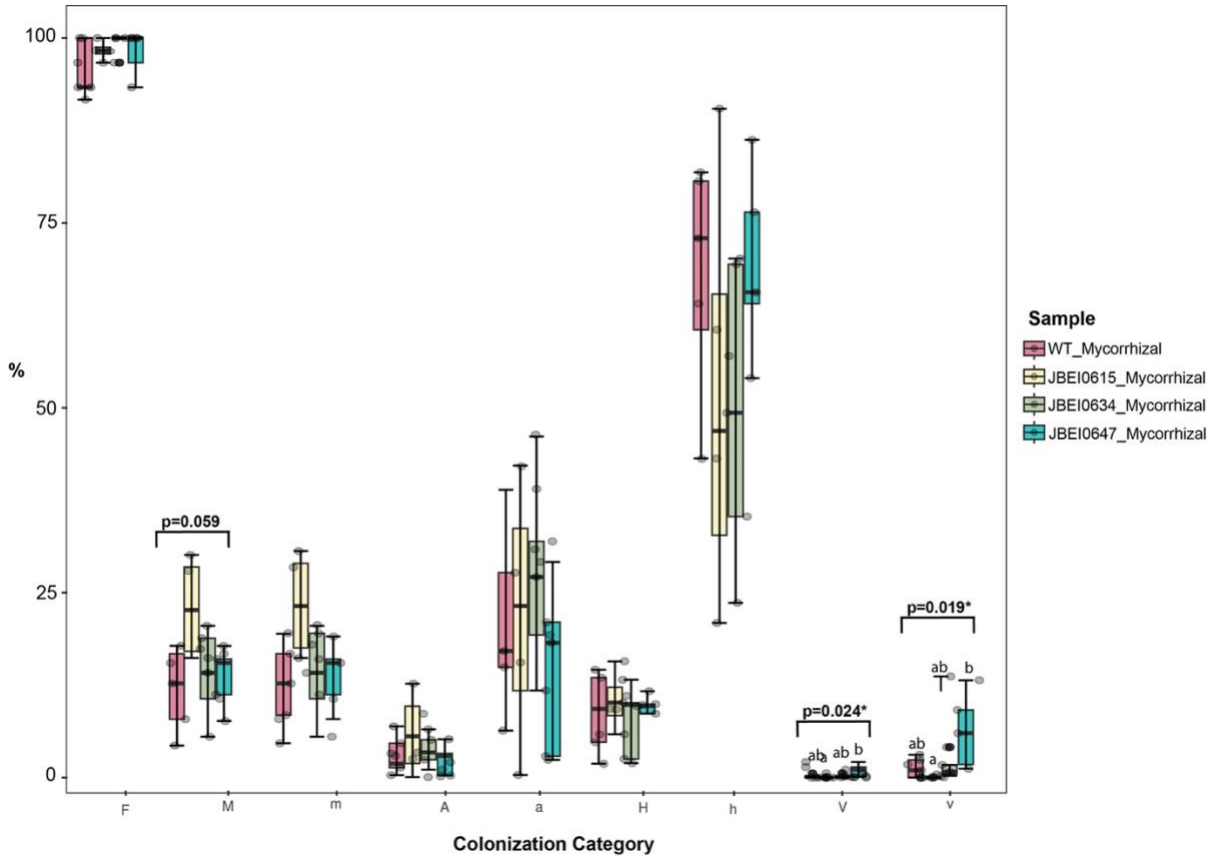

Figure 4-3. Colonization scoring of *pSbUbi:AT10 transgenic S. bicolor* reveals differences in vesicle abundance throughout the mycorrhizal root system.

AM colonization quantified by the Trouvelot method at 21 dpi with *R. irregularis* in roots; Data are presented as mean values +/- SEM (n = 5). F%, frequency of infection; M%, total mycorrhization, m%, mycorrhization in root fragments; A%, total arbuscule abundance; a%, arbuscule abundance in root fragments; H%, total intraradical hyphae abundance; h%, intraradical hyphal abundance in root fragments; V%, total vesicle abundance; v%, vesicle abundance in root fragments. P values were determined using one-way analysis of variance (ANOVA) (* indicates significant p-value <0.05). Means not sharing any letter are significantly different by the Tukey-test at the 5% level of significance.

4.3.3 Over-expression of *OsPSY1* in *O. sativa* increases expression of arbusculated cell marker gene *OsPT11* and increases fungal biomass in the roots during symbiosis

Three distinct transgenic *OsPSY1 O. sativa* (*OsPSY1-9*, *OsPSY1-17*, and *OsPSY1-32*) and their corresponding WT segregant lines were grown and treated as described above for *S. bicolor*. At 21-dpi, roots were harvested for colonization assessment by either the Trouvelot fungal root scoring method or through RT-qPCR of two marker genes the AM symbiosis: 1) *OsPT11* (*PHOSPHATE TRANSPORTER 11)* and 2) *RiTUB (B-TUBULIN)*. *OsPT11* is an AM-inducible phosphate transporter that is highly specific to AM colonization[296]. Expression of *OsPT11* and *RiTUB* was normalized to that of a housekeeping gene, *OsUBQ*, which is reported to be stably expressed during the AM symbiosis[297].

As shown in Fig. 4-4, a comparison of inoculated and mock-inoculated plants from each line revealed a marked response to *R. irregularis* colonization by all WT and transgenic lines. In the case of *OsPT11*, only one line (*OsPSY1-9)* did not show significantly higher expression of *OsPT11* in the mycorrhizal treatment compared to the control treatment, though this difference was nearly significant (ANOVA; p=0.0897). Similarly, all lines displayed a significantly higher expression of *RiTUB* in response to AM-treatment (Fig. 4-4). Overall, these results confirm that all *O. sativa* lines were experiencing significantly high levels of AM colonization at 21-dpi and exhibiting marked plant host response to symbiosis.

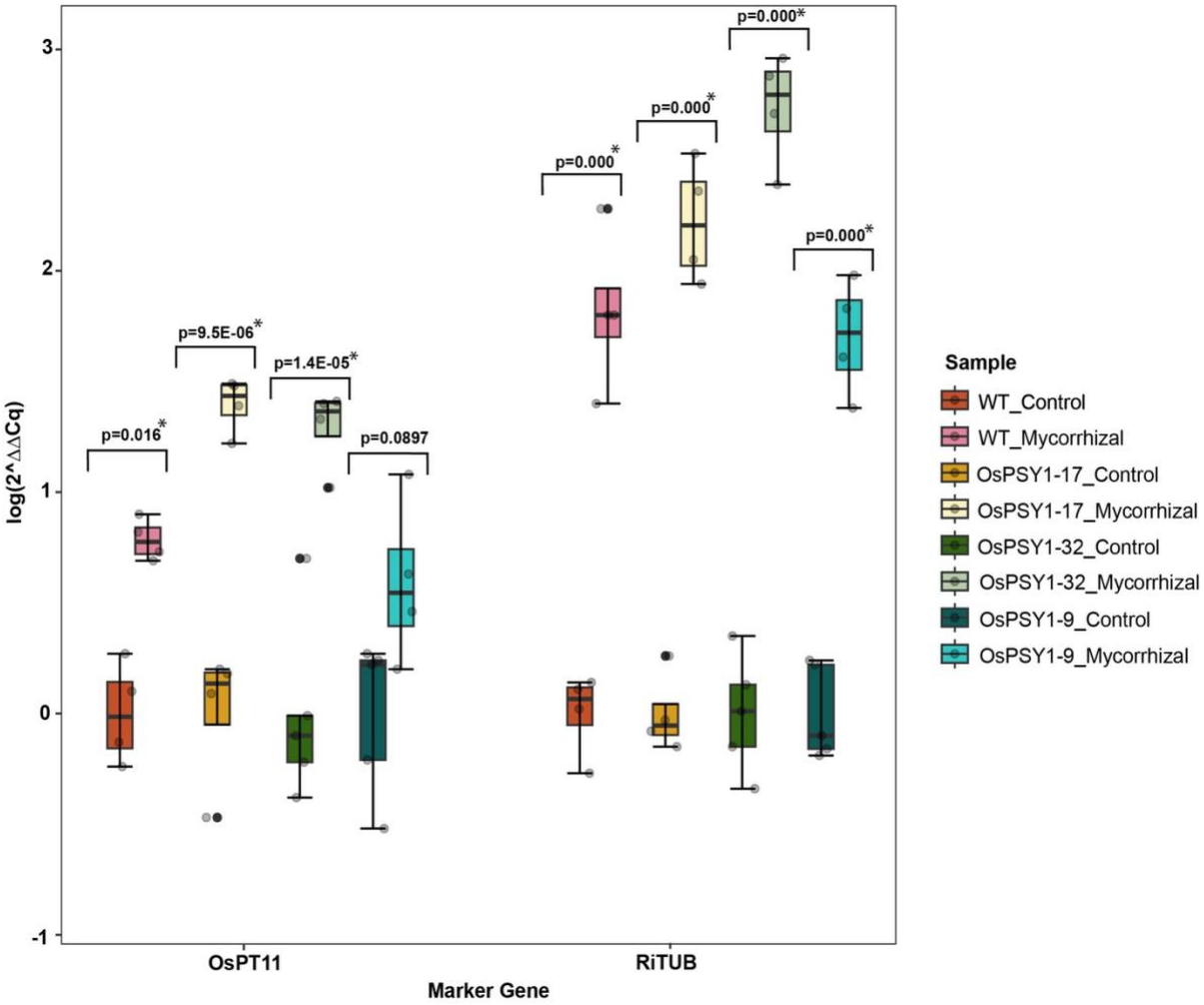

Figure 4-4. AM fungal colonization of WT transgenic *O. sativa* lines results in upregulation of *OsPT11* and *RiTUB*.

Expression of *OsPT11* and *RiTUB* relative to *OsUBQ* measured by qRT-PCR; Data are presented as mean values +/- SEM (n = 3-5). The box plots indicate the median (line inside the box), the lower and upper quartiles (box), margined by the smallest and largest data within the interval of 1.5x the interquartile range from the box (whiskers); outliers are shown (data points outside of box). P-values were determined using the student's T-test between AM inoculated and mock-inoculated samples of the same transgenic background (*indicates significant p-value <0.05).

Comparing only mycorrhizal-treated samples, two of the three *OE-OsPSY1* lines (OsPSY1-17 and OsPSY1-32) displayed significantly higher expression of *OsPT11 (*ANOVA; p=.0006) and *RiTUB* (ANOVA; p=.0012) compared to the WT (Fig. 4-5). *OE-OsPSY1-9* line did not display any significant difference in *OsPT11* or *RiTUB* expression in response to AM colonization than the WT. However, this line also does not experience the same level of root growth enhancement as the other two transgenic lines in root growth experiments, indicating that the expression of *OsPSY1* may be lower in this transgenic line than the others (Flor Ercoli and Pamela Ronald, personal communication). Taken together, these results suggest that overexpressing *OsPSY1* in *O. sativa* increase fungal biomass in the root system, increase plant host response to AM colonization, and may enhance symbiotic capacity.

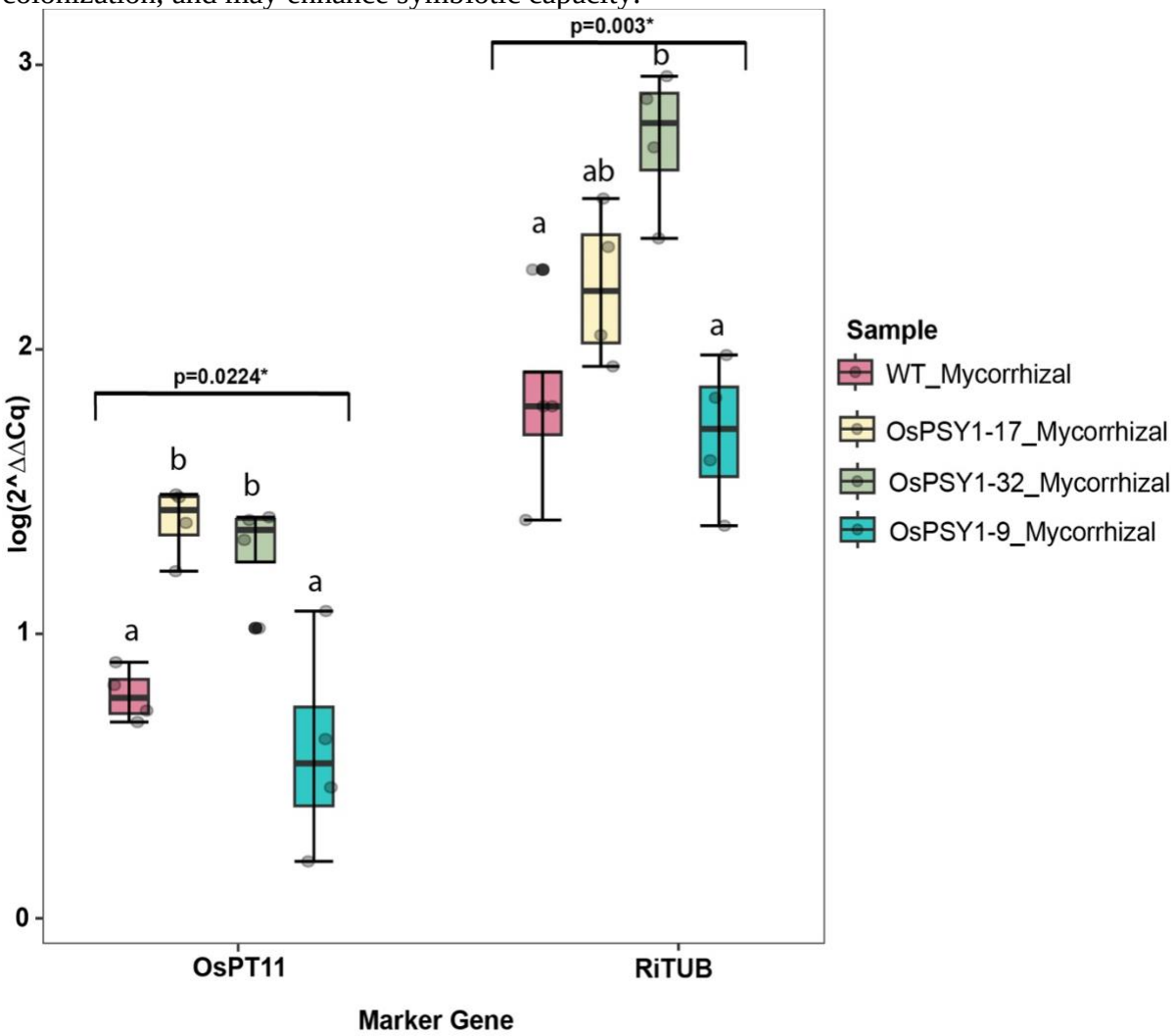

Figure 4-5.13Overexpression of *OsPSY1* small secreted peptide in transgenic *O. sativa* lines results in upregulation of symbiosis-responsive genes from both host and symbiont.

Expression of *OsPT11* and *RiTUB* relative to *OsUBQ* measured by qRT-PCR; Data are presented as mean values +/- SEM (n = 3-5). The box plots indicate the median (line inside the box), the lower and upper quartiles (box), margined by the smallest and largest data within the interval of 1.5x the interquartile range from the box (whiskers); outliers are shown (data points outside of box). P values were determined using one-way analysis of variance

(ANOVA)(*indicates significant p-value <0.05). Means not sharing any letter are significantly different by the Tukey-test at the 5% level of significance.

4.3.4 Over-expression of OsPSY in *O. sativa* significantly affects arbuscule, hyphal, and vesicle abundance in the root system during symbiosis.

Does this enhancement in symbiotic capacity correlate with any specific AM fungal symbiotic phenotype? The results of the modified Trouvelot scoring method during the colonization assessment revealed interesting differences across various AM phenotypic categories between transgenic *OE-OsPSY1* and WT lines (Fig. 4-6). Intensity of mycorrhization in root fragments (m) was significantly lower in the *OE-OsPSY1-17* line than the WT (ANOVA; p=0.016), though this difference was not seen in the overall root system (M). All *OE-OsPSY1* lines showed a significantly higher abundance of arbuscules within root fragments (a) analyzed (Fig. 4-6, ANOVA; p=0.018) than the WT which is consistent with the observed increase in expression of *OsPT11*. Conversely, the WT showed a significantly higher abundance of intraradical hyphae in all root fragments and throughout the root system (H/h) than the transgenic lines (Fig. 4-6, ANOVA; p=0.002 and p=1.68E-05). Lastly, the *OE-OsPSY1-9* line showed a significantly higher abundance of vesicles in the root fragments and throughout the root system (V/v) than all other lines (Fig. 4-6, ANOVA; p=0.002 and p=0.0003). In most cases, the *OE-OsPSY1-9* demonstrated a more similar phenotype to WT than the other transgenic lines, consistent with the RT-qPCR results. Overall, the trade-off between increased arbuscule abundance and decreased intraradical hyphae abundance in the transgenic *OE-OsPSY1 O. sativa* lines compared to the WT could point to a role for the PSY1 peptide in arbuscule development or maintenance.

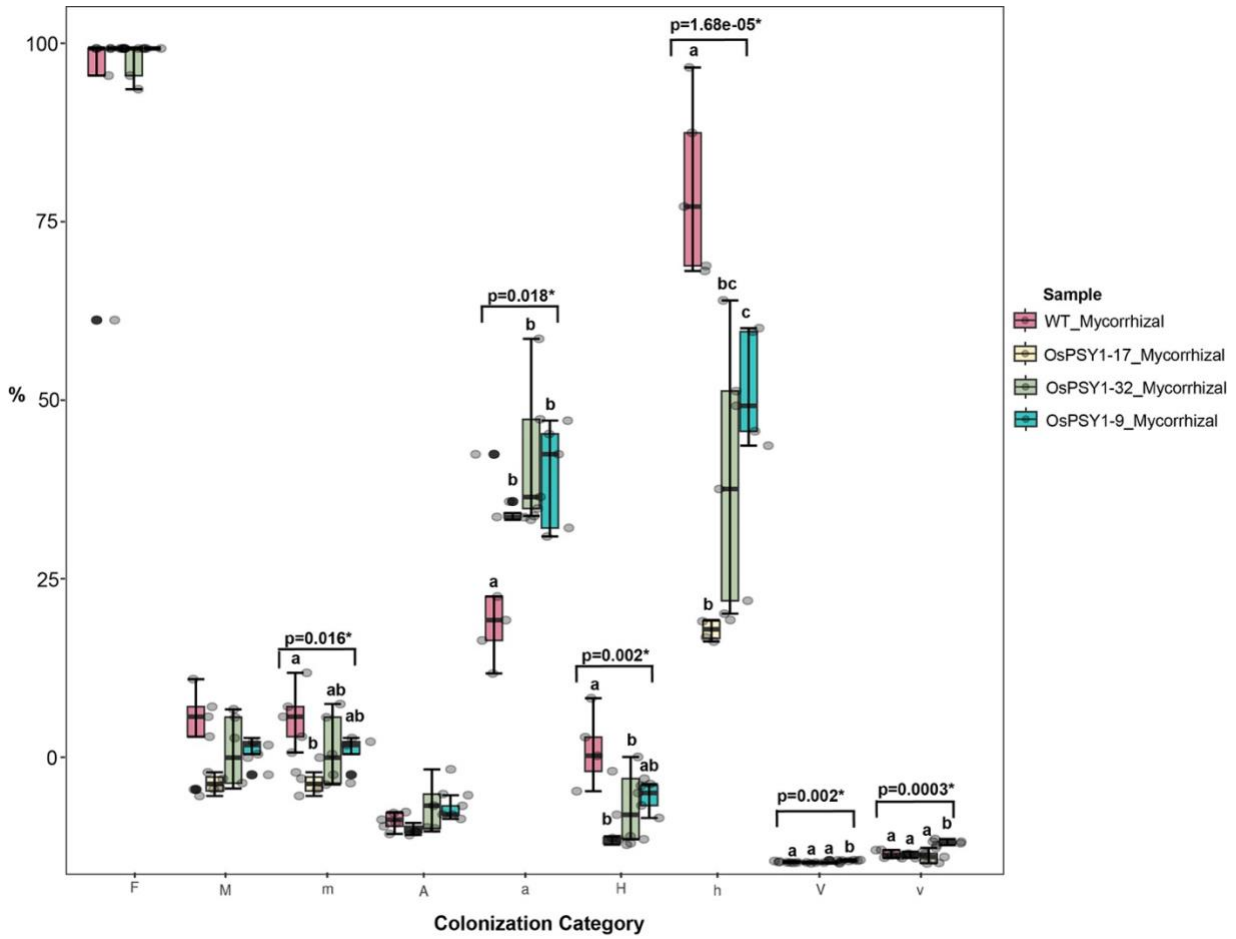

Figure 4-6. Overexpression of *OsPSY1* small secreted peptide in transgenic *O. sativa* lines significantly alters symbiotic root fungal phenotypes.

AM colonization quantified by the Trouvelot method at 21 dpi with *R. irregularis* in roots; Data are presented as mean values +/- SEM (n = 5). F%, frequency of infection; M%, total mycorrhization, m%, mycorrhization in root fragments; A%, total arbuscule abundance; a%, arbuscule abundance in root fragments; H%, total intraradical hyphae abundance; h%, intraradical hyphal abundance in root fragments; V%, total vesicle abundance; v%, vesicle abundance in root fragments. P-values were determined using one-way analysis of variance (ANOVA) (* indicates significant p-value <0.05). Means not sharing any letter are significantly different by the Tukey-test at the 5% level of significance.

4.4 Methods

4.4.1 Plant growth and inoculation

S. bicolor seeds were sterilized in 50% sodium hypochlorite solution and shaken for 5 minutes, then rinsed five times with sterile distilled water and incubated at 30˚C for 24 hours at which time they were placed directly into sand cone-tainers. *O. sativa* seeds were sterilized in 20% sodium hypochlorite solution and shaken for 30 minutes, then rinsed five times with sterile distilled water and placed in 0.3% agar plates at 28˚C for 6 days. Sand cones were prepared as follows: 8.25-inch cone-tainers (Stuewe and Sons) with 1 cm^3 rock wool at base, filled up to

12.7 cm with autoclaved calcined clay (Turface Athletics MVP 50), followed by 2.5 cm of autoclaved horticultural sand (American Soil and Stone) and topped with 2.5 cm fine play sand (SAKRETE). To inoculate seedlings with *Rhizophagus irregularis* (Błaszk., Wubet, Renker and Buscot) C. Walker and A. Schüßler: 50 mL Agtiv Field Crops liquid mycorrhizal inoculant (PremierTech, Rivière-du-Loup, Québec, Canada) spores were captured on a 40 µm filter, rinsed with distilled water and resuspended in 50 mL distilled water. 1 mL of resuspended spores was applied to the horticultural sand layer and an additional 300 µL applied to the fine play sand layer. Germinated seedlings were transplanted to the top fine sand layer of inoculated and non-inoculated sand cones. *S. bicolor* plants were grown in 30˚C 16h day/8 h night, with 250 µmol m^{-2} s^{-1} light intensity, and 60% relative humidity. *O. sativa* plants were grown in 28˚C 14h day/10 h night, with 300 µmol m^{-2} s^{-1} light intensity, and 60% relative humidity. All plants were watered daily and fertilized twice a week with 1/2X Hoagland's medium modified with 20 µM phosphate to stimulate AM colonization.

4.4.2 Colonization assessment

R. irregularis colonization of *S. bicolor* and *O. sativa* roots at 21 dpi was visualized via staining of AM chitin using 3.5 µg/mL wheat germ agglutinin (WGA) Alexa Fluor 488 (Thermo Fisher Scientific) in 1X Phosphate-Buffered Saline solution (pH 7.0). Roots were rinsed, fixed in 50% ethanol for 30 minutes, and cleared in 10% KOH at 65 ºC for 72 h. Cleared roots were neutralized with 0.1 M HCl and stained with WGA-488 in 1X PBS at 4 ˚C for 24 h prior to imaging. Colonization was quantified using the Trouvelot method[227] on a Leica DM6B fluorescence microscope using 3-5 biological replicates for each treatment.

4.4.3 Quantitative real-time PCR of target genes

To quantify expression of target genes, 100 mg of roots from the fine sand layer were flash frozen in liquid nitrogen. Total RNA was extracted using the Nucleospin Plant and Fungal RNA Kit (Thermo Fisher Scientific) and corresponding DNase. cDNA synthesis was conducted using the SuperScript™ III Reverse Transcriptase (Thermo Fisher Scientific) from 500 ng of total RNA and qPCR was conducted from cDNA diluted 1:5 using the PowerUp SYBR Green Master Mix (Thermo Fisher Scientific). A 200 nM primer concentration and the following protocol was used for qPCR for all targets: 2 min at 50 °C and 2 min at 95°C, followed by 39 repeats of 15 s at 95 °C, 15 s at 60 °C and 1 min at 72 °C, and ending with 5 s at 95°C. A melting curve (55–95 °C; at increments of 0.5 °C) was generated to verify the specificity of primer amplification. Five biological replicates and three technical replicates of all targets (*SbPT11, OsPT11,* and *RiTUB*) were quantified for gene expression levels relative to the housekeeping genes, *SbEF1a* and *OsUBQ for S. bicolor* and *O. sativa* respectively, using the ΔΔCT method. Primer sequences can be found in Table 4-1.

Target Name	Primer Sequence	Reference
OsUBQ F	CATATCCCAGATGAGCGTATCATG	/10.1105/tpc.112.104901[297]
OsUBQ R	GAGAAGTTCCCTGCTTCAAGCA	/10.1105/tpc.112.104901[297]
OsPT11 F	CATGGAGCTGCTGCTGTTCTAG	/10.1105/tpc.112.104901[297]
OsPT11 R	CAGACAACCATAGCTCCATTGG	/10.1105/tpc.112.104901[297]
SbEF1α F	TGCTGTCAAGTTTGCTGAGC	/10.1111/pce.13509[294]

SbEF1α R	ATTTGGGCTCCTTCTCAAGC	/10.1111/pce.13509[294]
SbPT11 F	GGAAATTAAGGGACACGAATAA	/10.1111/pce.13509[294]
SbPT11 R	ACTCAAACTTTATGGAACACTC	/10.1111/pce.13509[294]
RiTUB F	ATACCGTGGCGATGTCGTTC	/10.1016/j.cub.2021.03.067[298]
RiTUB R	GACAACGGTTGGGGGTTGATAG	/10.1016/j.cub.2021.03.067[298]

Table 4-1. Primer Sequences

4.5 Discussion

S. bicolor and *O. sativa* are agriculturally-relevant crops that are widely targeted for generation of varieties with optimized biofuel-related and nutritional traits, as well as tolerance to abiotic and biotic stress. For both of these species, AM symbiosis has been shown to improve biomass, grain yield, plant nutrition, and tolerance to various biotic and abiotic stresses[299–302]. Here, I observed enhanced AM colonization by *R. irregularis* as a result of genetic engineering of *S. bicolor* transgenic lines that overexpressed the *OsAT10* BAHD acyltransferase (*pSbUbi:AT10)* and in transgenic lines that overexpressed the *OsPSY1* small family peptide in *O. sativa (OE-OsPSY1).*

pSbUbi:AT10 transgenics previously demonstrated improved saccharification efficiency and reduced PCW lignin content compared to the WT[262], both desirable qualities for biofuel production. As biofuel and other bioproduct feedstocks are often grown on marginal or sub-optimal land, another desirable quality for feedstock genetic engineering is tolerance to abiotic stress. In this study, *pSbUbi:AT10* transgenics displayed a stronger response to AM colonization than the WT and accumulated significantly higher levels of fungal biomass as measured by the expression levels of *RiTUB* in the roots compared to WT plants. Lastly, two lines of both *pSbUbi:AT10* transgenics showed significantly higher vesicle abundance in mycorrhizal roots from the WT. Fungal vesicles are lipid storage organs and a colonization phenotype in which vesicle abundance is altered could be indicative of changes to symbiotic nutrient exchange and homeostasis[303]. Vesicles represent the completion of the symbiotic life cycle and signify that the plant and fungal symbiont are assimilating the exchanged nutrients[304]. An increase in vesicle abundance could be another sign of increased metabolic exchange between the host and symbiont. Conversely, it could signify increased arbuscule turnover. Interpretation of changes in vesicle abundance can therefore provide insight into the health and functionality of the AM symbiosis.

There are several possibilities to why these transgenics demonstrate higher symbiotic capacity. The first is that lignin biosynthesis is upregulated upon pathogen infection and while AM fungi have been shown to suppress defense responses in the host[305], the reduction of lignin content and other modifications to the PCW in *pSbUbi:AT10* transgenics may be further enabling AM fungal infection as the PCW is less cross-linked and thus could be easier to penetrate. Alternatively, the reduction in lignin may lead to increased leakage of various metabolites, including sugars, out of the root through the apoplast[306], which would make them more available to hyphae during infection. Another possibility is that there is a specific role for BAHD acyltransferases in the AM symbiosis, which would be consistent with the results of a previous study finding BAHD acyltransferases to be upregulated during the AM symbiosis[270]. BAHD acyltransferases are involved in a variety of plant functions such as signal transduction, stress response, and metabolism, as they acylate primary and secondary metabolites in plants[259]. *OsAT10* in particular

has been shown to be involved in cell growth and cold stress response[307]. Other functions of BAHD acyltransferases include pathogen immunity, insect defense, and membrane biosynthesis[308]. Further research is necessary to fully investigate the effects of *AT10* on the AM symbiosis and the underlying mechanisms that enable increased mycorrhization.

OE-OsPSY1 transgenic lines also demonstrated enhanced symbiotic capacity in the present study upon colonization by *R. irregularis*. Two of three transgenic lines demonstrated higher expression of the arbusculated cell marker gene, *OsPT11*, and *RiTUB*, a proxy for fungal biomass in the root system, than the WT. This increase in expression of symbiosis-responsive marker genes was also accompanied by an increase in arbuscule abundance upon colonization scoring of mycorrhizal roots, indicating that these transgenics are better able to form or maintain arbuscules, which are the critical sites for metabolite exchange between the two species[93]. In contrast, intraradical hyphal abundance was lower in all transgenics than in the WT, which adds further complexity to this analysis. Since arbuscule formation follows intraradical hyphal passage throughout the root, further research should include colonization assessments at multiple colonization timepoints to better disentangle these phenotypes. Overexpression of *PSY1* and synthetic applications of other PSY family peptides is associated with root elongation and growth[275]. It is well established that a host plant's root architecture can influence its ability to interact and benefit from AM symbiosis[309,310]. It is possible that *OE-OsPSY1* transgenics demonstrate higher mycorrhization due to increased root length as compared to WT plants and the increased root surface area for AM colonization such as is the case for lateral root growth associated with CLE peptides[283]. Another possibility is that *OsPSY1* has a more direct functionality in the symbiosis. The significantly higher abundance of arbuscules in *OE-OsPSY1* lines and higher expression of the arbusculated cell marker *OsPT11* are key signs that there may be a functional role for *OsPSY1* in arbuscule formation. Follow-up experiments at various time-points as well as structural arbuscule phenotyping with *OE-OsPSY1* and *OsPSY1* knock-out mutants could better inform this initial hypothesis and provide more insight into the specific arbusculation stage that *OsPSY1* is affecting. Further research, including field trials, into the role of *PSY1* and other small peptides which can be synthetically applied or genetically engineered in crop varieties in the AM symbiosis has the potential to inform future biotechnological agricultural developments.

4.6 Significance Statement

This study explored the effects of genetic engineering *S. bicolor* and *O. sativa* plants for desirable agricultural and bioenergy traits on their ability to interact with AM fungi. Mycorrhizal colonization represents a sustainable manner in which to enhance plant nutrition, abiotic and biotic stress tolerance, and crop yield in marginal lands. Therefore, it would be desirable for genetic engineering of feedstock and food crops for desirable traits to additionally improve their symbiotic capacity. This research identified a potential role for both *OsAT10* and *OsPSY1* in the AM symbiosis and provides the basis for future research that could determine possible mechanisms by which these two genes lead to increased mycorrhization. Starting in the first chapter of this thesis, I present novel approaches by which scientists are beginning to target plant-microbe interactions for genetic engineering of crops for improved human nutrition. In the second and third chapters, I present the rhizobial and mycorrhizal endosymbioses as a resource for such genetic engineering. Finally, this final chapter underscores how interconnected

pathways and metabolic processes can function in plants, illustrating how genetic engineering targeted for characteristics can inadvertently impact plant-microbe interactions.

Literature Cited

1. Brader, G. *et al.* Ecology and Genomic Insights into Plant-Pathogenic and Plant-Nonpathogenic Endophytes. *Annu. Rev. Phytopathol.* **55**, 61–83 (2017).
2. Yu, Y. *et al.* Induced Systemic Resistance for Improving Plant Immunity by Beneficial Microbes. *Plants* **11**, 386 (2022).
3. Meena, K. K. *et al.* Abiotic Stress Responses and Microbe-Mediated Mitigation in Plants: The Omics Strategies. *Front. Plant Sci.* **8**, (2017).
4. Rho, H. & Kim, S.-H. Endophyte Effects on Photosynthesis and Water Use of Plant Hosts: A Meta-Analysis. in *Functional Importance of the Plant Microbiome* (ed. Doty, S. L.) 43–69 (Springer International Publishing, Cham, 2017). doi:10.1007/978-3-319-65897-1_4.
5. Lange, M. *et al.* Plant diversity increases soil microbial activity and soil carbon storage. *Nat. Commun.* **6**, 6707 (2015).
6. Liang, C., Schimel, J. P. & Jastrow, J. D. The importance of anabolism in microbial control over soil carbon storage. *Nat. Microbiol.* **2**, 17105 (2017).
7. Gougoulias, C., Clark, J. M. & Shaw, L. J. The role of soil microbes in the global carbon cycle: tracking the below-ground microbial processing of plant-derived carbon for manipulating carbon dynamics in agricultural systems. *J. Sci. Food Agric.* **94**, 2362–2371 (2014).
8. Archibald, J. M. Endosymbiosis and Eukaryotic Cell Evolution. *Curr. Biol.* **25**, R911–R921 (2015).
9. *Mycorrhiza: State of the Art, Genetics and Molecular Biology, Eco-Function, Biotechnology, Eco-Physiology, Structure and Systematics*. (Springer Berlin Heidelberg, Berlin, Heidelberg, 2008). doi:10.1007/978-3-540-78826-3.
10. Gutjahr, C. & Parniske, M. Cell and Developmental Biology of Arbuscular Mycorrhiza Symbiosis. *Annu. Rev. Cell Dev. Biol.* **29**, 593–617 (2013).
11. Luginbuehl, L. H. & Oldroyd, G. E. D. Understanding the Arbuscule at the Heart of Endomycorrhizal Symbioses in Plants. *Curr. Biol.* **27**, R952–R963 (2017).
12. Oldroyd, G. E. D. Speak, friend, and enter: signalling systems that promote beneficial symbiotic associations in plants. *Nat. Rev. Microbiol.* **11**, 252–263 (2013).
13. Genre, A. & Russo, G. Does a Common Pathway Transduce Symbiotic Signals in Plant–Microbe Interactions? *Front. Plant Sci.* **7**, (2016).
14. Kidaj, D. *et al.* Biological activity of Nod factors. *Acta Biochim. Pol.* (2020) doi:10.18388/abp.2020_5353.
15. Coba De La Peña, T., Fedorova, E., Pueyo, J. J. & Lucas, M. M. The Symbiosome: Legume and Rhizobia Co-evolution toward a Nitrogen-Fixing Organelle? *Front. Plant Sci.* **8**, 2229 (2018).
16. Gresshoff, P. M. *Molecular Biology Of Symbiotic Nitrogen Fixation*. (CRC Press, Milton, 2018).
17. Fellbaum, C. R. *et al.* Carbon availability triggers fungal nitrogen uptake and transport in arbuscular mycorrhizal symbiosis. *Proc. Natl. Acad. Sci.* **109**, 2666–2671 (2012).
18. Udvardi, M. & Poole, P. S. Transport and Metabolism in Legume-Rhizobia Symbioses. *Annu. Rev. Plant Biol.* **64**, 781–805 (2013).
19. Salmeron-Santiago, I. A. *et al.* An Updated Review on the Modulation of Carbon Partitioning and Allocation in Arbuscular Mycorrhizal Plants. *Microorganisms* **10**, 75 (2021).

20. Nouri, E. *et al.* Phosphate Suppression of Arbuscular Mycorrhizal Symbiosis Involves Gibberellic Acid Signaling. *Plant Cell Physiol.* **62**, 959–970 (2021).
21. Werner, G. & Kiers, T. E. Partner selection in the mycorrhizal mutualism. *New Phytol.* **205**, 1437–1442 (2015).
22. Libault, M. The Carbon-Nitrogen Balance of the Nodule and Its Regulation under Elevated Carbon Dioxide Concentration. *BioMed Res. Int.* **2014**, 1–7 (2014).
23. Murray, J. D. *et al.* Vapyrin, a gene essential for intracellular progression of arbuscular mycorrhizal symbiosis, is also essential for infection by rhizobia in the nodule symbiosis of Medicago truncatula. *Plant J. Cell Mol. Biol.* **65**, 244–252 (2011).
24. Nguyen, N. N. T. *et al.* PHO1 family members transport phosphate from infected nodule cells to bacteroids in Medicago truncatula. *Plant Physiol.* **185**, 196–209 (2021).
25. Wang, E. *et al.* A H+-ATPase That Energizes Nutrient Uptake during Mycorrhizal Symbioses in Rice and *Medicago truncatula*. *Plant Cell* **26**, 1818–1830 (2014).
26. Arrighi, J.-F. *et al.* The RPG gene of Medicago truncatula controls Rhizobium-directed polar growth during infection. *Proc. Natl. Acad. Sci.* **105**, 9817–9822 (2008).
27. Ané, J.-M. *et al. Medicago truncatula DMI1* Required for Bacterial and Fungal Symbioses in Legumes. *Science* **303**, 1364–1367 (2004).
28. Hartmann, R. M. *et al.* Insights into the complex role of GRAS transcription factors in the arbuscular mycorrhiza symbiosis. *Sci. Rep.* **9**, 3360 (2019).
29. Irving, T. B. *et al. KIN3* impacts arbuscular mycorrhizal symbiosis and promotes fungal colonisation in *Medicago truncatula*. *Plant J.* **110**, 513–528 (2022).
30. Genre, A. & Russo, G. Does a Common Pathway Transduce Symbiotic Signals in Plant–Microbe Interactions? *Front. Plant Sci.* **7**, (2016).
31. Roy, S. *et al.* Celebrating 20 Years of Genetic Discoveries in Legume Nodulation and Symbiotic Nitrogen Fixation. *Plant Cell* **32**, 15–41 (2020).
32. Gaude, N., Bortfeld, S., Duensing, N., Lohse, M. & Krajinski, F. Arbuscule-containing and non-colonized cortical cells of mycorrhizal roots undergo extensive and specific reprogramming during arbuscular mycorrhizal development. *Plant J.* **69**, 510–528 (2012).
33. Hogekamp, C. & Küster, H. A roadmap of cell-type specific gene expression during sequential stages of the arbuscular mycorrhiza symbiosis. *BMC Genomics* **14**, 306 (2013).
34. Cervantes-Gámez, R. G. *et al.* Arbuscular Mycorrhizal Symbiosis-Induced Expression Changes in Solanum lycopersicum Leaves Revealed by RNA-seq Analysis. *Plant Mol. Biol. Report.* **34**, 89–102 (2016).
35. Keller-Pearson, M. *et al.* A dual transcriptomic approach reveals contrasting patterns of differential gene expression during drought in arbuscular mycorrhizal fungus and carrot. *Mol. Plant-Microbe Interactions*® MPMI-04-23-0038-R (2023) doi:10.1094/MPMI-04-23-0038-R.
36. Manley, B. F. *et al.* A highly contiguous genome assembly reveals sources of genomic novelty in the symbiotic fungus *Rhizophagus irregularis*. *G3 GenesGenomesGenetics* jkad077 (2023) doi:10.1093/g3journal/jkad077.
37. Tang, H. *et al.* An improved genome release (version Mt4.0) for the model legume Medicago truncatula. *BMC Genomics* **15**, 312 (2014).
38. Diwan, D., Rashid, Md. M. & Vaishnav, A. Current understanding of plant-microbe interaction through the lenses of multi-omics approaches and their benefits in sustainable agriculture. *Microbiol. Res.* **265**, 127180 (2022).

39. Ye, Q. *et al.* Differentiation trajectories and biofunctions of symbiotic and un-symbiotic fate cells in root nodules of Medicago truncatula. *Mol. Plant* **15**, 1852–1867 (2022).
40. Kelly, S., Mun, T., Stougaard, J., Ben, C. & Andersen, S. U. Distinct Lotus japonicus Transcriptomic Responses to a Spectrum of Bacteria Ranging From Symbiotic to Pathogenic. *Front. Plant Sci.* **9**, 1218 (2018).
41. Mateus, I. D. *et al.* Dual RNA-seq reveals large-scale non-conserved genotype × genotype-specific genetic reprograming and molecular crosstalk in the mycorrhizal symbiosis. *ISME J.* **13**, 1226–1238 (2019).
42. Zouari, I. *et al.* From root to fruit: RNA-Seq analysis shows that arbuscular mycorrhizal symbiosis may affect tomato fruit metabolism. *BMC Genomics* **15**, 221 (2014).
43. Liu, Z. *et al.* Integrated single-nucleus and spatial transcriptomics captures transitional states in soybean nodule maturation. *Nat. Plants* **9**, 515–524 (2023).
44. Liu, Z. *et al.* Single-nucleus transcriptomes reveal spatiotemporal symbiotic perception and early response in Medicago. *Nat. Plants* **9**, 1734–1748 (2023).
45. Serrano, K. & Bezrutcyzk, M. Genome to gut: crop engineering for human microbiomes. *Nat. Rev. Microbiol.* (2023) doi:10.1038/s41579-022-00850-6.
46. Serrano, K. *et al.* Spatial co-transcriptomics reveals discrete stages of the arbuscular mycorrhizal symbiosis. *Nat. Plants* (2024) doi:10.1038/s41477-024-01666-3.
47. Bar-On, Y. M., Phillips, R. & Milo, R. The biomass distribution on Earth. *Proc. Natl. Acad. Sci.* **115**, 6506–6511 (2018).
48. Mackenzie, J. S. & Jeggo, M. The One Health Approach—Why Is It So Important? *Trop. Med. Infect. Dis.* **4**, 88 (2019).
49. Berendsen, R. L., Pieterse, C. M. J. & Bakker, P. A. H. M. The rhizosphere microbiome and plant health. *Trends Plant Sci.* **17**, 478–486 (2012).
50. Grice, E. A. & Segre, J. A. The Human Microbiome: Our Second Genome. *Annu. Rev. Genomics Hum. Genet.* **13**, 151–170 (2012).
51. Banerjee, S. & Van Der Heijden, M. G. A. Soil microbiomes and one health. *Nat. Rev. Microbiol.* **21**, 6–20 (2023).
52. Thursby, E. & Juge, N. Introduction to the human gut microbiota. *Biochem. J.* **474**, 1823–1836 (2017).
53. Bull, M. J. & Plummer, N. T. Part 1: The Human Gut Microbiome in Health and Disease. *Integr. Med. Encinitas Calif* **13**, 17–22 (2014).
54. Horrocks, V., King, O. G., Yip, A. Y. G., Marques, I. M. & McDonald, J. A. K. Role of the gut microbiota in nutrient competition and protection against intestinal pathogen colonization. *Microbiology* **169**, (2023).
55. Hou, Q., Huang, J., Ayansola, H., Masatoshi, H. & Zhang, B. Intestinal Stem Cells and Immune Cell Relationships: Potential Therapeutic Targets for Inflammatory Bowel Diseases. *Front. Immunol.* **11**, 623691 (2021).
56. Wiertsema, S. P., Van Bergenhenegouwen, J., Garssen, J. & Knippels, L. M. J. The Interplay between the Gut Microbiome and the Immune System in the Context of Infectious Diseases throughout Life and the Role of Nutrition in Optimizing Treatment Strategies. *Nutrients* **13**, 886 (2021).
57. LeBlanc, J. G. *et al.* Bacteria as vitamin suppliers to their host: a gut microbiota perspective. *Curr. Opin. Biotechnol.* **24**, 160–168 (2013).
58. Gomaa, E. Z. Human gut microbiota/microbiome in health and diseases: a review. *Antonie Van Leeuwenhoek* **113**, 2019–2040 (2020).

59. Durack, J. & Lynch, S. V. The gut microbiome: Relationships with disease and opportunities for therapy. *J. Exp. Med.* **216**, 20–40 (2019).
60. McBurney, M. I. *et al.* Establishing What Constitutes a Healthy Human Gut Microbiome: State of the Science, Regulatory Considerations, and Future Directions. *J. Nutr.* **149**, 1882–1895 (2019).
61. Vliex, L. M. M., Penders, J., Nauta, A., Zoetendal, E. G. & Blaak, E. E. The individual response to antibiotics and diet — insights into gut microbial resilience and host metabolism. *Nat. Rev. Endocrinol.* (2024) doi:10.1038/s41574-024-00966-0.
62. King, C. H. *et al.* Baseline human gut microbiota profile in healthy people and standard reporting template. *PLOS ONE* **14**, e0206484 (2019).
63. Rinninella, E. *et al.* What is the Healthy Gut Microbiota Composition? A Changing Ecosystem across Age, Environment, Diet, and Diseases. *Microorganisms* **7**, 14 (2019).
64. Rothschild, D. *et al.* Environment dominates over host genetics in shaping human gut microbiota. *Nature* **555**, 210–215 (2018).
65. Kurilshikov, A. *et al.* Large-scale association analyses identify host factors influencing human gut microbiome composition. *Nat. Genet.* **53**, 156–165 (2021).
66. Bokulich, N. A. *et al.* Antibiotics, birth mode, and diet shape microbiome maturation during early life. *Sci. Transl. Med.* **8**, (2016).
67. Cotillard, A. *et al.* Dietary intervention impact on gut microbial gene richness. *Nature* **500**, 585–588 (2013).
68. Wilson, A. S. *et al.* Diet and the Human Gut Microbiome: An International Review. *Dig. Dis. Sci.* **65**, 723–740 (2020).
69. David, L. A. *et al.* Diet rapidly and reproducibly alters the human gut microbiome. *Nature* **505**, 559–563 (2014).
70. Losasso, C. *et al.* Assessing the Influence of Vegan, Vegetarian and Omnivore Oriented Westernized Dietary Styles on Human Gut Microbiota: A Cross Sectional Study. *Front. Microbiol.* **9**, 317 (2018).
71. Wong, M.-W. *et al.* Impact of vegan diets on gut microbiota: An update on the clinical implications. *Tzu Chi Med. J.* **30**, 200 (2018).
72. Tomova, A. *et al.* The Effects of Vegetarian and Vegan Diets on Gut Microbiota. *Front. Nutr.* **6**, 47 (2019).
73. Berg, G., Erlacher, A. & Grube, M. The Edible Plant Microbiome: Importance and Health Issues. in *Principles of Plant-Microbe Interactions* (ed. Lugtenberg, B.) 419–426 (Springer International Publishing, Cham, 2015). doi:10.1007/978-3-319-08575-3_44.
74. Leff, J. W. & Fierer, N. Bacterial Communities Associated with the Surfaces of Fresh Fruits and Vegetables. *PLoS ONE* **8**, e59310 (2013).
75. Maffei, D. F., Batalha, E. Y., Landgraf, M., Schaffner, D. W. & Franco, B. D. G. M. Microbiology of organic and conventionally grown fresh produce. *Braz. J. Microbiol.* **47**, 99–105 (2016).
76. Wicaksono, W. A. *et al.* The edible plant microbiome: evidence for the occurrence of fruit and vegetable bacteria in the human gut. *Gut Microbes* **15**, 2258565 (2023).
77. Yang, Q. *et al.* Genetic analysis of seed traits in Sorghum bicolor that affect the human gut microbiome. *Nat. Commun.* **13**, 5641 (2022).
78. Berg, G., Erlacher, A. & Grube, M. The Edible Plant Microbiome: Importance and Health Issues. in *Principles of Plant-Microbe Interactions: Microbes for Sustainable Agriculture*

(ed. Lugtenberg, B.) 419–426 (Springer International Publishing, Cham, 2015). doi:10.1007/978-3-319-08575-3_44.
79. Wassermann, B., Rybakova, D., Müller, C. & Berg, G. Harnessing the microbiomes of Brassica vegetables for health issues. *Sci. Rep.* **7**, 17649 (2017).
80. Soto-Giron, M. J. *et al.* The Edible Plant Microbiome represents a diverse genetic reservoir with functional potential in the human host. *Sci. Rep.* **11**, 24017 (2021).
81. Probiotics Market. *Global Probiotics Market Size & Forecast*. https://www.marketsandmarkets.com/Market-Reports/probiotics-market-69.html (2024).
82. Bloomberg Intelligence. *Plant-Based Foods Poised for Explosive Growth*. https://www.bloomberg.com/professional/bi-research/?dyn=plant-based-food (2021).
83. Seyfferth, C. *et al.* Advances and Opportunities in Single-Cell Transcriptomics for Plant Research. *Annu. Rev. Plant Biol.* **72**, 847–866 (2021).
84. Cervantes-Pérez, S. A., Thibivillliers, S., Tennant, S. & Libault, M. Review: Challenges and perspectives in applying single nuclei RNA-seq technology in plant biology. *Plant Sci.* **325**, 111486 (2022).
85. Denyer, T. & Timmermans, M. C. P. Crafting a blueprint for single-cell RNA sequencing. *Trends Plant Sci.* **27**, 92–103 (2022).
86. Mo, Y. & Jiao, Y. Advances and applications of single-cell omics technologies in plant research. *Plant J.* **110**, 1551–1563 (2022).
87. Zhu, J., Moreno-Pérez, A. & Coaker, G. Understanding plant pathogen interactions using spatial and single-cell technologies. *Commun. Biol.* **6**, 814 (2023).
88. Yin, R., Xia, K. & Xu, X. Spatial transcriptomics drives a new era in plant research. *Plant J.* tpj.16437 (2023) doi:10.1111/tpj.16437.
89. Oldroyd, G. E. D. Speak, friend, and enter: signalling systems that promote beneficial symbiotic associations in plants. *Nat. Rev. Microbiol.* **11**, 252–263 (2013).
90. Lin, J., Frank, M. & Reid, D. No Home without Hormones: How Plant Hormones Control Legume Nodule Organogenesis. *Plant Commun.* **1**, 100104 (2020).
91. Breakspear, A. *et al.* The Root Hair "Infectome" of *Medicago truncatula* Uncovers Changes in Cell Cycle Genes and Reveals a Requirement for Auxin Signaling in Rhizobial Infection. *Plant Cell* **26**, 4680–4701 (2014).
92. Wang, W. *et al.* Nutrient Exchange and Regulation in Arbuscular Mycorrhizal Symbiosis. *Mol. Plant* **10**, 1147–1158 (2017).
93. MacLean, A. M., Bravo, A. & Harrison, M. J. Plant Signaling and Metabolic Pathways Enabling Arbuscular Mycorrhizal Symbiosis. *Plant Cell* **29**, 2319–2335 (2017).
94. Gaude, N., Bortfeld, S., Duensing, N., Lohse, M. & Krajinski, F. Arbuscule-containing and non-colonized cortical cells of mycorrhizal roots undergo extensive and specific reprogramming during arbuscular mycorrhizal development. *Plant J.* **69**, 510–528 (2012).
95. Hogekamp, C. & Küster, H. A roadmap of cell-type specific gene expression during sequential stages of the arbuscular mycorrhiza symbiosis. *BMC Genomics* **14**, 306 (2013).
96. Kretzschmar, T. *et al.* A petunia ABC protein controls strigolactone-dependent symbiotic signalling and branching. *Nature* **483**, 341–344 (2012).
97. Waters, M. T., Gutjahr, C., Bennett, T. & Nelson, D. C. Strigolactone Signaling and Evolution. *Annu. Rev. Plant Biol.* **68**, 291–322 (2017).
98. Pimprikar, P. & Gutjahr, C. Transcriptional Regulation of Arbuscular Mycorrhiza Development. *Plant Cell Physiol.* **59**, 678–695 (2018).

99. Luginbuehl, L. H. & Oldroyd, G. E. D. Understanding the Arbuscule at the Heart of Endomycorrhizal Symbioses in Plants. *Curr. Biol.* **27**, R952–R963 (2017).
100. Bapaume, L. & Reinhardt, D. How membranes shape plant symbioses: signaling and transport in nodulation and arbuscular mycorrhiza. *Front. Plant Sci.* **3**, (2012).
101. Pumplin, N. & Harrison, M. J. Live-Cell Imaging Reveals Periarbuscular Membrane Domains and Organelle Location in *Medicago truncatula* Roots during Arbuscular Mycorrhizal Symbiosis. *Plant Physiol.* **151**, 809–819 (2009).
102. Kobae, Y. & Fujiwara, T. Earliest Colonization Events of Rhizophagus irregularis in Rice Roots Occur Preferentially in Previously Uncolonized Cells. *Plant Cell Physiol.* **55**, 1497–1510 (2014).
103. Camps, C. *et al.* Combined genetic and transcriptomic analysis reveals three major signalling pathways activated by Myc- LCO s in *Medicago truncatula*. *New Phytol.* **208**, 224–240 (2015).
104. Bonneau, L., Huguet, S., Wipf, D., Pauly, N. & Truong, H. Combined phosphate and nitrogen limitation generates a nutrient stress transcriptome favorable for arbuscular mycorrhizal symbiosis in *M edicago truncatula* . *New Phytol.* **199**, 188–202 (2013).
105. Hohnjec, N., Vieweg, M. F., Pühler, A., Becker, A. & Küster, H. Overlaps in the Transcriptional Profiles of *Medicago truncatula* Roots Inoculated with Two Different Glomus Fungi Provide Insights into the Genetic Program Activated during Arbuscular Mycorrhiza. *Plant Physiol.* **137**, 1283–1301 (2005).
106. Cope, K. R. *et al.* Physiological and transcriptomic response of Medicago truncatula to colonization by high- or low-benefit arbuscular mycorrhizal fungi. *Mycorrhiza* **32**, 281–303 (2022).
107. Apelt, F. *et al.* Shoot and root single cell sequencing reveals tissue- and daytime-specific transcriptome profiles. *Plant Physiol.* **188**, 861–878 (2022).
108. Chen, W., Ye, T., Sun, Q., Niu, T. & Zhang, J. Arbuscular Mycorrhizal Fungus Alters Root System Architecture in Camellia sinensis L. as Revealed by RNA-Seq Analysis. *Front. Plant Sci.* **12**, 777357 (2021).
109. Handa, Y. *et al.* RNA-seq Transcriptional Profiling of an Arbuscular Mycorrhiza Provides Insights into Regulated and Coordinated Gene Expression in *Lotus japonicus* and *Rhizophagus irregularis*. *Plant Cell Physiol.* **56**, 1490–1511 (2015).
110. Dallaire, A. *et al.* Transcriptional activity and epigenetic regulation of transposable elements in the symbiotic fungus *Rhizophagus irregularis*. *Genome Res.* **31**, 2290–2302 (2021).
111. Yildirir, G. *et al.* Long reads and Hi-C sequencing illuminate the two-compartment genome of the model arbuscular mycorrhizal symbiont *Rhizophagus irregularis*. *New Phytol.* **233**, 1097–1107 (2022).
112. Beaudet, D. *et al.* Ultra-low input transcriptomics reveal the spore functional content and phylogenetic affiliations of poorly studied arbuscular mycorrhizal fungi. *DNA Res.* **25**, 217–227 (2018).
113. Zeng, T. *et al.* Host- and stage-dependent secretome of the arbuscular mycorrhizal fungus *Rhizophagus irregularis*. *Plant J.* **94**, 411–425 (2018).
114. Chen, E. C. *et al.* Single nucleus sequencing reveals evidence of inter-nucleus recombination in arbuscular mycorrhizal fungi. *eLife* **7**, e39813 (2018).
115. Maeda, T. *et al.* Evidence of non-tandemly repeated rDNAs and their intragenomic heterogeneity in Rhizophagus irregularis. *Commun. Biol.* **1**, 87 (2018).

116. Tisserant, E. *et al.* The transcriptome of the arbuscular mycorrhizal fungus *Glomus intraradices* (DAOM 197198) reveals functional tradeoffs in an obligate symbiont. *New Phytol.* **193**, 755–769 (2012).
117. Lanfranco, L. & Bonfante, P. Lessons from arbuscular mycorrhizal fungal genomes. *Curr. Opin. Microbiol.* **75**, 102357 (2023).
118. Geurts, R. & Vleeshouwers, V. G. A. A. Mycorrhizal Symbiosis: Ancient Signalling Mechanisms Co-opted. *Curr. Biol.* **22**, R997–R999 (2012).
119. Wang, D., Dong, W., Murray, J. & Wang, E. Innovation and appropriation in mycorrhizal and rhizobial Symbioses. *Plant Cell* **34**, 1573–1599 (2022).
120. Jovic, D. *et al.* Single-cell RNA sequencing technologies and applications: A brief overview. *Clin. Transl. Med.* **12**, e694 (2022).
121. Van Den Brink, S. C. *et al.* Single-cell sequencing reveals dissociation-induced gene expression in tissue subpopulations. *Nat. Methods* **14**, 935–936 (2017).
122. Frank, M. *et al.* Single-cell analysis identifies genes facilitating rhizobium infection in Lotus japonicus. *Nat. Commun.* **14**, 7171 (2023).
123. Denyer, T. *et al.* Spatiotemporal Developmental Trajectories in the Arabidopsis Root Revealed Using High-Throughput Single-Cell RNA Sequencing. *Dev. Cell* **48**, 840-852.e5 (2019).
124. Zheng, D. *et al.* Recent progresses in plant single-cell transcriptomics. *Crop Des.* **2**, 100041 (2023).
125. Marx, V. Method of the Year: spatially resolved transcriptomics. *Nat. Methods* **18**, 9–14 (2021).
126. Giacomello, S. A new era for plant science: spatial single-cell transcriptomics. *Curr. Opin. Plant Biol.* **60**, 102041 (2021).
127. Moses, L. & Pachter, L. Museum of spatial transcriptomics. *Nat. Methods* **19**, 534–546 (2022).
128. Chen, C., Ge, Y. & Lu, L. Opportunities and challenges in the application of single-cell and spatial transcriptomics in plants. *Front. Plant Sci.* **14**, 1185377 (2023).
129. Cheng, M. *et al.* Spatially resolved transcriptomics: a comprehensive review of their technological advances, applications, and challenges. *J. Genet. Genomics* **50**, 625–640 (2023).
130. Ståhl, P. L. *et al.* Visualization and analysis of gene expression in tissue sections by spatial transcriptomics. *Science* **353**, 78–82 (2016).
131. Rodriques, S. G. *et al.* Slide-seq: A scalable technology for measuring genome-wide expression at high spatial resolution. *Science* **363**, 1463–1467 (2019).
132. Stickels, R. R. *et al.* Highly sensitive spatial transcriptomics at near-cellular resolution with Slide-seqV2. *Nat. Biotechnol.* **39**, 313–319 (2021).
133. Vickovic, S. *et al.* High-definition spatial transcriptomics for in situ tissue profiling. *Nat. Methods* **16**, 987–990 (2019).
134. Liu, Y. *et al.* High-Spatial-Resolution Multi-Omics Sequencing via Deterministic Barcoding in Tissue. *Cell* **183**, 1665-1681.e18 (2020).
135. Cho, C.-S. *et al.* Microscopic examination of spatial transcriptome using Seq-Scope. *Cell* **184**, 3559-3572.e22 (2021).
136. Chen, A. *et al.* Spatiotemporal transcriptomic atlas of mouse organogenesis using DNA nanoball-patterned arrays. *Cell* **185**, 1777-1792.e21 (2022).

137. Yue, L. *et al.* A guidebook of spatial transcriptomic technologies, data resources and analysis approaches. *Comput. Struct. Biotechnol. J.* **21**, 940–955 (2023).
138. Chen, K. H., Boettiger, A. N., Moffitt, J. R., Wang, S. & Zhuang, X. Spatially resolved, highly multiplexed RNA profiling in single cells. *Science* **348**, aaa6090 (2015).
139. Shah, S., Lubeck, E., Zhou, W. & Cai, L. In Situ Transcription Profiling of Single Cells Reveals Spatial Organization of Cells in the Mouse Hippocampus. *Neuron* **92**, 342–357 (2016).
140. Eng, C.-H. L. *et al.* Transcriptome-scale super-resolved imaging in tissues by RNA seqFISH+. *Nature* **568**, 235–239 (2019).
141. Groiss, S. *et al. Highly Resolved Spatial Transcriptomics for Detection of Rare Events in Cells*. http://biorxiv.org/lookup/doi/10.1101/2021.10.11.463936 (2021) doi:10.1101/2021.10.11.463936.
142. Merritt, C. R. *et al.* Multiplex digital spatial profiling of proteins and RNA in fixed tissue. *Nat. Biotechnol.* **38**, 586–599 (2020).
143. Goh, J. J. L. *et al.* Highly specific multiplexed RNA imaging in tissues with split-FISH. *Nat. Methods* **17**, 689–693 (2020).
144. Borm, L. E. *et al.* Scalable in situ single-cell profiling by electrophoretic capture of mRNA using EEL FISH. *Nat. Biotechnol.* (2022) doi:10.1038/s41587-022-01455-3.
145. Nobori, T., Oliva, M., Lister, R. & Ecker, J. R. Multiplexed single-cell 3D spatial gene expression analysis in plant tissue using PHYTOMap. *Nat. Plants* **9**, 1026–1033 (2023).
146. Femino, A. M., Fay, F. S., Fogarty, K. & Singer, R. H. Visualization of Single RNA Transcripts in Situ. *Science* **280**, 585–590 (1998).
147. Jean-Baptiste, K. *et al.* Dynamics of Gene Expression in Single Root Cells of *Arabidopsis thaliana*. *Plant Cell* **31**, 993–1011 (2019).
148. Ryu, K. H., Huang, L., Kang, H. M. & Schiefelbein, J. Single-Cell RNA Sequencing Resolves Molecular Relationships Among Individual Plant Cells. *Plant Physiol.* **179**, 1444–1456 (2019).
149. Shulse, C. N. *et al.* High-Throughput Single-Cell Transcriptome Profiling of Plant Cell Types. *Cell Rep.* **27**, 2241-2247.e4 (2019).
150. Zhang, T.-Q., Xu, Z.-G., Shang, G.-D. & Wang, J.-W. A Single-Cell RNA Sequencing Profiles the Developmental Landscape of Arabidopsis Root. *Mol. Plant* **12**, 648–660 (2019).
151. Shahan, R. *et al.* A single-cell Arabidopsis root atlas reveals developmental trajectories in wild-type and cell identity mutants. *Dev. Cell* **57**, 543-560.e9 (2022).
152. Cervantes-Pérez, S. A. *et al.* Cell-specific pathways recruited for symbiotic nodulation in the Medicago truncatula legume. *Mol. Plant* **15**, 1868–1888 (2022).
153. Giolai, M. *et al.* Spatially resolved transcriptomics reveals plant host responses to pathogens. *Plant Methods* **15**, 114 (2019).
154. Saarenpää, S. *et al.* Spatial metatranscriptomics resolves host–bacteria–fungi interactomes. *Nat. Biotechnol.* (2023) doi:10.1038/s41587-023-01979-2.
155. Tang, B., Feng, L., Hulin, M. T., Ding, P. & Ma, W. Cell-type-specific responses to fungal infection in plants revealed by single-cell transcriptomics. *Cell Host Microbe* **31**, 1732-1747.e5 (2023).
156. Fan, Z., Chen, R. & Chen, X. SpatialDB: a database for spatially resolved transcriptomes. *Nucleic Acids Res.* gkz934 (2019) doi:10.1093/nar/gkz934.

157. Plant Cell Atlas Consortium *et al.* Vision, challenges and opportunities for a Plant Cell Atlas. *eLife* **10**, e66877 (2021).
158. Sarkar, N. POLYADENYLATION OF mRNA IN PROKARYOTES. *Annu. Rev. Biochem.* **66**, 173–197 (1997).
159. Nobori, T. *et al.* Transcriptome landscape of a bacterial pathogen under plant immunity. *Proc. Natl. Acad. Sci.* **115**, (2018).
160. Kuchina, A. *et al.* Microbial single-cell RNA sequencing by split-pool barcoding. *Science* **371**, eaba5257 (2021).
161. Blattman, S. B., Jiang, W., Oikonomou, P. & Tavazoie, S. Prokaryotic single-cell RNA sequencing by in situ combinatorial indexing. *Nat. Microbiol.* **5**, 1192–1201 (2020).
162. Serrano, K. *et al. Spatial Co-Transcriptomics Reveals Discrete Stages of the Arbuscular Mycorrhizal Symbiosis*. http://biorxiv.org/lookup/doi/10.1101/2023.08.02.551648 (2023) doi:10.1101/2023.08.02.551648.
163. Sperschneider, J. *et al.* Arbuscular mycorrhizal fungi heterokaryons have two nuclear populations with distinct roles in host–plant interactions. *Nat. Microbiol.* **8**, 2142–2153 (2023).
164. Kokkoris, V., Stefani, F., Dalpé, Y., Dettman, J. & Corradi, N. Nuclear Dynamics in the Arbuscular Mycorrhizal Fungi. *Trends Plant Sci.* **25**, 765–778 (2020).
165. Chen, M., Arato, M., Borghi, L., Nouri, E. & Reinhardt, D. Beneficial Services of Arbuscular Mycorrhizal Fungi – From Ecology to Application. *Front. Plant Sci.* **9**, 1270 (2018).
166. Begum, N. *et al.* Role of Arbuscular Mycorrhizal Fungi in Plant Growth Regulation: Implications in Abiotic Stress Tolerance. *Front. Plant Sci.* **10**, (2019).
167. Jacott, C. N., Murray, J. D. & Ridout, C. J. Trade-Offs in Arbuscular Mycorrhizal Symbiosis: Disease Resistance, Growth Responses and Perspectives for Crop Breeding. *Agronomy* **7**, 75 (2017).
168. Keymer, A. *et al.* Lipid transfer from plants to arbuscular mycorrhiza fungi. *eLife* **6**, e29107 (2017).
169. Lanfranco, L., Bonfante, P. & Genre, A. The Mutualistic Interaction between Plants and Arbuscular Mycorrhizal Fungi. *Microbiol. Spectr.* **4**, 10.1128/microbiolspec.funk-0012–2016 (2016).
170. Harrison, M. J. Molecular and cellular aspects of the arbuscular mycorrhizal symbiosis. *Annu. Rev. Plant Biol.* **50**, 361–389 (1999).
171. Wang, P. *et al.* Medicago SPX1 and SPX3 regulate phosphate homeostasis, mycorrhizal colonization, and arbuscule degradation. *Plant Cell* **33**, 3470–3486 (2021).
172. Lindsay, P. L., Williams, B. N., MacLean, A. & Harrison, M. J. A Phosphate-Dependent Requirement for Transcription Factors IPD3 and IPD3L During Arbuscular Mycorrhizal Symbiosis in *Medicago truncatula*. *Mol. Plant-Microbe Interactions*® **32**, 1277–1290 (2019).
173. Uhe, M., Hogekamp, C., Hartmann, R. M., Hohnjec, N. & Küster, H. The mycorrhiza-dependent defensin MtDefMd1 of Medicago truncatula acts during the late restructuring stages of arbuscule-containing cells. *PLOS ONE* **13**, e0191841 (2018).
174. Gibelin-Viala, C. *et al.* The *Medicago truncatula* LysM receptor-like kinase LYK9 plays a dual role in immunity and the arbuscular mycorrhizal symbiosis. *New Phytol.* **223**, 1516–1529 (2019).

175. Breuillin-Sessoms, F. *et al.* Suppression of Arbuscule Degeneration in *Medicago truncatula phosphate transporter4* Mutants Is Dependent on the Ammonium Transporter 2 Family Protein AMT2;3. *Plant Cell* **27**, 1352–1366 (2015).
176. Jiang, Y. *et al.* Medicago AP2-Domain Transcription Factor WRI5a Is a Master Regulator of Lipid Biosynthesis and Transfer during Mycorrhizal Symbiosis. *Mol. Plant* **11**, 1344–1359 (2018).
177. Kameoka, H. *et al.* Stimulation of asymbiotic sporulation in arbuscular mycorrhizal fungi by fatty acids. *Nat. Microbiol.* **4**, 1654–1660 (2019).
178. Sugiura, Y. *et al.* Myristate can be used as a carbon and energy source for the asymbiotic growth of arbuscular mycorrhizal fungi. *Proc. Natl. Acad. Sci.* **117**, 25779–25788 (2020).
179. Limpens, E. Laser microdissection of arbuscular mycorrhiza. in *The Model Legume Medicago truncatula* 501–512 (John Wiley & Sons, Ltd, 2020). doi:10.1002/9781119409144.ch62.
180. Harrison, M. J. Signaling in the arbuscular mycorrhizal symbiosis. *Annu Rev Microbiol* **59**, 19–42 (2005).
181. Montero, H., Choi, J. & Paszkowski, U. Arbuscular mycorrhizal phenotyping: the dos and don'ts. *New Phytol.* **221**, 1182–1186 (2019).
182. Shaw, R., Tian, X. & Xu, J. Single-Cell Transcriptome Analysis in Plants: Advances and Challenges. *Mol. Plant* **14**, 115–126 (2021).
183. Guillotin, B. *et al.* A pan-grass transcriptome reveals patterns of cellular divergence in crops. *Nature* **617**, 785–791 (2023).
184. Larsson, L., Frisén, J. & Lundeberg, J. Spatially resolved transcriptomics adds a new dimension to genomics. *Nat. Methods* **18**, 15–18 (2021).
185. Thibivilliers, S., Anderson, D. & Libault, M. Isolation of Plant Root Nuclei for Single Cell RNA Sequencing. *Curr. Protoc. Plant Biol.* **5**, e20120 (2020).
186. Cervantes-Pérez, S. A. *et al.* Cell-specific pathways recruited for symbiotic nodulation in the Medicago truncatula legume. *Mol. Plant* **15**, 1868–1888 (2022).
187. Harrison, M. J., Dewbre, G. R. & Liu, J. A Phosphate Transporter from Medicago truncatula Involved in the Acquisition of Phosphate Released by Arbuscular Mycorrhizal Fungi. *Plant Cell* **14**, 2413–2429 (2002).
188. Bravo, A., York, T., Pumplin, N., Mueller, L. A. & Harrison, M. J. Genes conserved for arbuscular mycorrhizal symbiosis identified through phylogenomics. *Nat. Plants* **2**, 15208 (2016).
189. Moses, L. & Pachter, L. Museum of spatial transcriptomics. *Nat. Methods* **19**, 534–546 (2022).
190. Varma Penmetsa, R. *et al.* The *Medicago truncatula* ortholog of Arabidopsis EIN2, *sickle* , is a negative regulator of symbiotic and pathogenic microbial associations. *Plant J.* **55**, 580–595 (2008).
191. Besserer, A. *et al.* Strigolactones Stimulate Arbuscular Mycorrhizal Fungi by Activating Mitochondria. *PLoS Biol.* **4**, e226 (2006).
192. Banasiak, J., Borghi, L., Stec, N., Martinoia, E. & Jasiński, M. The Full-Size ABCG Transporter of Medicago truncatula Is Involved in Strigolactone Secretion, Affecting Arbuscular Mycorrhiza. *Front. Plant Sci.* **11**, 18 (2020).
193. Floss, D. S. *et al.* Knock-down of the MEP pathway isogene 1-deoxy-D-xylulose 5-phosphate synthase 2 inhibits formation of arbuscular mycorrhiza-induced apocarotenoids,

and abolishes normal expression of mycorrhiza-specific plant marker genes. *Plant J. Cell Mol. Biol.* **56**, 86–100 (2008).
194. Floss, D. S., Schliemann, W., Schmidt, J., Strack, D. & Walter, M. H. RNA Interference-Mediated Repression of *MtCCD1* in Mycorrhizal Roots of *Medicago truncatula* Causes Accumulation of C27 Apocarotenoids, Shedding Light on the Functional Role of CCD1. *Plant Physiol.* **148**, 1267–1282 (2008).
195. Floss, D. S. *et al.* A Transcriptional Program for Arbuscule Degeneration during AM Symbiosis Is Regulated by MYB1. *Curr. Biol. CB* **27**, 1206–1212 (2017).
196. Singh, S. & Parniske, M. Activation of calcium- and calmodulin-dependent protein kinase (CCaMK), the central regulator of plant root endosymbiosis. *Curr. Opin. Plant Biol.* **15**, 444–453 (2012).
197. Rey, T. *et al.* The Medicago truncatula GRAS protein RAD1 supports arbuscular mycorrhiza symbiosis and Phytophthora palmivora susceptibility. *J. Exp. Bot.* **68**, 5871–5881 (2017).
198. Russo, G. *et al.* Ectopic activation of cortical cell division during the accommodation of arbuscular mycorrhizal fungi. *New Phytol.* **221**, 1036–1048 (2019).
199. Chen, C. & Zhu, H. Are common symbiosis genes required for endophytic rice-rhizobial interactions? *Plant Signal. Behav.* **8**, e25453 (2013).
200. Pumplin, N. *et al. Medicago truncatula* Vapyrin is a novel protein required for arbuscular mycorrhizal symbiosis. *Plant J.* **61**, 482–494 (2010).
201. Zhang, X., Pumplin, N., Ivanov, S. & Harrison, M. J. EXO70I Is Required for Development of a Sub-domain of the Periarbuscular Membrane during Arbuscular Mycorrhizal Symbiosis. *Curr. Biol.* **25**, 2189–2195 (2015).
202. Lindsay, P. L., Ivanov, S., Pumplin, N., Zhang, X. & Harrison, M. J. Distinct ankyrin repeat subdomains control VAPYRIN locations and intracellular accommodation functions during arbuscular mycorrhizal symbiosis. *Nat. Commun.* **13**, 5228 (2022).
203. Heck, C. *et al.* Symbiotic Fungi Control Plant Root Cortex Development through the Novel GRAS Transcription Factor MIG1. *Curr. Biol.* **26**, 2770–2778 (2016).
204. Van Wyk, S. G., Du Plessis, M., Cullis, C. A., Kunert, K. J. & Vorster, B. J. Cysteine protease and cystatin expression and activity during soybean nodule development and senescence. *BMC Plant Biol.* **14**, 294 (2014).
205. Zou, Y.-N., Wu, Q.-S., Huang, Y.-M., Ni, Q.-D. & He, X.-H. Mycorrhizal-Mediated Lower Proline Accumulation in Poncirus trifoliata under Water Deficit Derives from the Integration of Inhibition of Proline Synthesis with Increase of Proline Degradation. *PLoS ONE* **8**, e80568 (2013).
206. Wu, H.-H., Zou, Y.-N., Rahman, M. M., Ni, Q.-D. & Wu, Q.-S. Mycorrhizas alter sucrose and proline metabolism in trifoliate orange exposed to drought stress. *Sci. Rep.* **7**, 42389 (2017).
207. Ohtomo, R. & Saito, M. Polyphosphate dynamics in mycorrhizal roots during colonization of an arbuscular mycorrhizal fungus. *New Phytol.* **167**, 571–578 (2005).
208. Ezawa, T. & Saito, K. How do arbuscular mycorrhizal fungi handle phosphate? New insight into fine-tuning of phosphate metabolism. *New Phytol.* **220**, 1116–1121 (2018).
209. Nguyen, C. T. & Saito, K. Role of Cell Wall Polyphosphates in Phosphorus Transfer at the Arbuscular Interface in Mycorrhizas. *Front. Plant Sci.* **12**, 725939 (2021).
210. Tsuzuki, S., Handa, Y., Takeda, N. & Kawaguchi, M. Strigolactone-Induced Putative Secreted Protein 1 Is Required for the Establishment of Symbiosis by the Arbuscular

Mycorrhizal Fungus *Rhizophagus irregularis*. *Mol. Plant-Microbe Interactions®* **29**, 277–286 (2016).
211. Kamel, L. *et al.* The Comparison of Expressed Candidate Secreted Proteins from Two Arbuscular Mycorrhizal Fungi Unravels Common and Specific Molecular Tools to Invade Different Host Plants. *Front. Plant Sci.* **8**, 124 (2017).
212. Banasiak, J., Jamruszka, T., Murray, J. D. & Jasiński, M. A roadmap of plant membrane transporters in arbuscular mycorrhizal and legume–rhizobium symbioses. *Plant Physiol.* **187**, 2071–2091 (2021).
213. An, J. *et al.* A *Medicago truncatula* SWEET transporter implicated in arbuscule maintenance during arbuscular mycorrhizal symbiosis. *New Phytol.* **224**, 396–408 (2019).
214. Kloppholz, S., Kuhn, H. & Requena, N. A Secreted Fungal Effector of Glomus intraradices Promotes Symbiotic Biotrophy. *Curr. Biol.* **21**, 1204–1209 (2011).
215. Zeng, T. *et al.* A lysin motif effector subverts chitin-triggered immunity to facilitate arbuscular mycorrhizal symbiosis. *New Phytol.* **225**, 448–460 (2020).
216. Wang, P. *et al.* A nuclear-targeted effector of *Rhizophagus irregularis* interferes with histone 2B mono-ubiquitination to promote arbuscular mycorrhization. *New Phytol.* **230**, 1142–1155 (2021).
217. Teulet, A. *et al.* A pathogen effector FOLD diversified in symbiotic fungi. *New Phytol.* **239**, 1127–1139 (2023).
218. Marx, V. Method of the Year: spatially resolved transcriptomics. *Nat. Methods* **18**, 9–14 (2021).
219. Oh, J.-M. *et al.* Comparison of cell type distribution between single-cell and single-nucleus RNA sequencing: enrichment of adherent cell types in single-nucleus RNA sequencing. *Exp. Mol. Med.* **54**, 2128–2134 (2022).
220. Asp, M., Bergenstråhle, J. & Lundeberg, J. Spatially Resolved Transcriptomes—Next Generation Tools for Tissue Exploration. *BioEssays* **42**, 1900221 (2020).
221. Minerdi, D., Savoi, S. & Sabbatini, P. Role of Cytochrome P450 Enzyme in Plant Microorganisms' Communication: A Focus on Grapevine. *Int. J. Mol. Sci.* **24**, (2023).
222. Ji, L., Yang, X. & Qi, F. Distinct Responses to Pathogenic and Symbionic Microorganisms: The Role of Plant Immunity. *Int. J. Mol. Sci.* **23**, (2022).
223. Walker, C., Schüßler, A., Vincent, B., Cranenbrouck, S. & Declerck, S. Anchoring the species Rhizophagus intraradices (formerly Glomus intraradices). *Fungal Syst. Evol.* (2021) doi:10.3114/fuse.2021.08.14.
224. Muñoz, I. V., Sarrocco, S., Malfatti, L., Baroncelli, R. & Vannacci, G. CRISPR-Cas for Fungal Genome Editing: A New Tool for the Management of Plant Diseases. *Front. Plant Sci.* **10**, 135 (2019).
225. Voß, S., Betz, R., Heidt, S., Corradi, N. & Requena, N. RiCRN1, a Crinkler Effector From the Arbuscular Mycorrhizal Fungus Rhizophagus irregularis, Functions in Arbuscule Development. *Front. Microbiol.* **9**, 2068 (2018).
226. Zhang, S. *et al.* A transcriptional activator from Rhizophagus irregularis regulates phosphate uptake and homeostasis in AM symbiosis during phosphorous starvation. *Front. Microbiol.* **13**, 1114089 (2023).
227. Trouvelot, A. Mesure Du Taux de Mycorhization VA D'un Systeme Radiculaire. Recherche de Methodes D'estimation Ayant Une Signification Fonctionnelle. *Physiological And Genetical Aspects of Mycorrhizae* **In Proceedings of the 1st European Symposium on Mycorrhizae**, 217–221 (1986).

228. Giacomello, S. & Lundeberg, J. Preparation of plant tissue to enable Spatial Transcriptomics profiling using barcoded microarrays. *Nat. Protoc.* **13**, 2425–2446 (2018).
229. Butler, A., Hoffman, P., Smibert, P., Papalexi, E. & Satija, R. Integrating single-cell transcriptomic data across different conditions, technologies, and species. *Nat. Biotechnol.* **36**, 411–420 (2018).
230. Biała, W., Banasiak, J., Jarzyniak, K., Pawela, A. & Jasiński, M. Medicago truncatula ABCG10 is a transporter of 4-coumarate and liquiritigenin in the medicarpin biosynthetic pathway. *J. Exp. Bot.* **68**, 3231–3241 (2017).
231. Nadal, M. *et al.* An N-acetylglucosamine transporter required for arbuscular mycorrhizal symbioses in rice and maize. *Nat. Plants* **3**, 17073 (2017).
232. Roy, S. *et al.* Three Common Symbiotic ABC Subfamily B Transporters in *Medicago truncatula* Are Regulated by a NIN-Independent Branch of the Symbiosis Signaling Pathway. *Mol. Plant-Microbe Interactions®* **34**, 939–951 (2021).
233. Franssen, H. J. *et al.* Root developmental programs shape the Medicago truncatula nodule meristem. *Dev. Camb. Engl.* **142**, 2941–2950 (2015).
234. Cao, X. *et al.* The Roles of Auxin Biosynthesis YUCCA Gene Family in Plants. *Int. J. Mol. Sci.* **20**, 6343 (2019).
235. Marsh, J. F. *et al. Medicago truncatula NIN* Is Essential for Rhizobial-Independent Nodule Organogenesis Induced by Autoactive Calcium/Calmodulin-Dependent Protein Kinase. *Plant Physiol.* **144**, 324–335 (2007).
236. Chapman, J., Muhlemann, J., Gayomba, S. & Muday, G. RBOH-Dependent ROS Synthesis and ROS Scavenging by Plant Specialized Metabolites To Modulate Plant Development and Stress Responses. *Chem Res Toxicol* (2019).
237. Dong, W. *et al.* An SHR–SCR module specifies legume cortical cell fate to enable nodulation. *Nature* **589**, 586–590 (2021).
238. Miyashima, S. *et al.* Mobile PEAR transcription factors integrate positional cues to prime cambial growth. *Nature* **565**, 490–494 (2019).
239. Karlo, M. *et al.* The CLE53–SUNN genetic pathway negatively regulates arbuscular mycorrhiza root colonization in Medicago truncatula. *J. Exp. Bot.* **71**, 4972–4984 (2020).
240. Kim, J.-Y. *et al.* Distinct identities of leaf phloem cells revealed by single cell transcriptomics. *Plant Cell* **33**, 511–530 (2021).
241. Love, M. I., Huber, W. & Anders, S. Moderated estimation of fold change and dispersion for RNA-seq data with DESeq2. *Genome Biol.* **15**, 550 (2014).
242. Pecrix, Y. *et al.* Whole-genome landscape of Medicago truncatula symbiotic genes. *Nat. Plants* **4**, 1017–1025 (2018).
243. Thomas, P. D. *et al.* PANTHER : Making genome-scale phylogenetics accessible to all. *Protein Sci.* **31**, 8–22 (2022).
244. Conesa, A. *et al.* Blast2GO: a universal tool for annotation, visualization and analysis in functional genomics research. *Bioinformatics* **21**, 3674–3676 (2005).
245. Houston, K., Tucker, M. R., Chowdhury, J., Shirley, N. & Little, A. The Plant Cell Wall: A Complex and Dynamic Structure As Revealed by the Responses of Genes under Stress Conditions. *Front. Plant Sci.* **7**, (2016).
246. Ishida, K. & Noutoshi, Y. The function of the plant cell wall in plant–microbe interactions. *Plant Physiol. Biochem.* **192**, 273–284 (2022).
247. Burton, R. A., Gidley, M. J. & Fincher, G. B. Heterogeneity in the chemistry, structure and function of plant cell walls. *Nat. Chem. Biol.* **6**, 724–732 (2010).

248. Keegstra, K. Plant Cell Walls. *Plant Physiol.* **154**, 483–486 (2010).
249. Scheller, H. V. & Ulvskov, P. Hemicelluloses. *Annu. Rev. Plant Biol.* **61**, 263–289 (2010).
250. Shin, Y., Chane, A., Jung, M. & Lee, Y. Recent Advances in Understanding the Roles of Pectin as an Active Participant in Plant Signaling Networks. *Plants* **10**, 1712 (2021).
251. Albenne, C., Canut, H. & Jamet, E. Plant cell wall proteomics: the leadership of Arabidopsis thaliana. *Front. Plant Sci.* **4**, (2013).
252. Wang, Y., Chantreau, M., Sibout, R. & Hawkins, S. Plant cell wall lignification and monolignol metabolism. *Front. Plant Sci.* **4**, (2013).
253. Ralph, J. *et al.* Lignins: Natural polymers from oxidative coupling of 4-hydroxyphenyl-propanoids. *Phytochem. Rev.* **3**, 29–60 (2004).
254. Liu, Q., Luo, L. & Zheng, L. Lignins: Biosynthesis and Biological Functions in Plants. *Int. J. Mol. Sci.* **19**, 335 (2018).
255. Zoghlami, A. & Paës, G. Lignocellulosic Biomass: Understanding Recalcitrance and Predicting Hydrolysis. *Front. Chem.* **7**, 874 (2019).
256. Loqué, D., Scheller, H. V. & Pauly, M. Engineering of plant cell walls for enhanced biofuel production. *Curr. Opin. Plant Biol.* **25**, 151–161 (2015).
257. Bartley, L. E. *et al.* Overexpression of a BAHD Acyltransferase, *OsAt10* , Alters Rice Cell Wall Hydroxycinnamic Acid Content and Saccharification. *Plant Physiol.* **161**, 1615–1633 (2013).
258. Lanoue, A. *et al. De novo* biosynthesis of defense root exudates in response to *Fusarium* attack in barley. *New Phytol.* **185**, 577–588 (2010).
259. Xu, D., Wang, Z., Zhuang, W., Wang, T. & Xie, Y. Family characteristics, phylogenetic reconstruction, and potential applications of the plant BAHD acyltransferase family. *Front. Plant Sci.* **14**, 1218914 (2023).
260. Withers, S. *et al.* Identification of Grass-specific Enzyme That Acylates Monolignols with p-Coumarate. *J. Biol. Chem.* **287**, 8347–8355 (2012).
261. Li, G. *et al.* Overexpression of a rice BAHD acyltransferase gene in switchgrass (Panicum virgatum L.) enhances saccharification. *BMC Biotechnol.* **18**, 54 (2018).
262. Tian, Y. *et al.* Overexpression of the rice BAHD acyltransferase AT10 increases xylan-bound p-coumarate and reduces lignin in Sorghum bicolor. *Biotechnol. Biofuels* **14**, 217 (2021).
263. Varalakshmi, B. *et al.* Manipulation of cell wall components and enzymes on plant-microbe interactions. in *Plant-Microbe Interaction - Recent Advances in Molecular and Biochemical Approaches* 303–326 (Elsevier, 2023). doi:10.1016/B978-0-323-91875-6.00010-4.
264. Dora, S., Terrett, O. M. & Sánchez-Rodríguez, C. Plant–microbe interactions in the apoplast: Communication at the plant cell wall. *Plant Cell* **34**, 1532–1550 (2022).
265. Li, P. *et al.* Spatial Expression and Functional Analysis of Casparian Strip Regulatory Genes in Endodermis Reveals the Conserved Mechanism in Tomato. *Front. Plant Sci.* **9**, 832 (2018).
266. Balestrini, R. & Bonfante, P. Cell wall remodeling in mycorrhizal symbiosis: a way towards biotrophism. *Front. Plant Sci.* **5**, (2014).
267. Genre, A., Lanfranco, L., Perotto, S. & Bonfante, P. Unique and common traits in mycorrhizal symbioses. *Nat. Rev. Microbiol.* **18**, 649–660 (2020).
268. Gao, M. Y. *et al.* Cell wall modification induced by an arbuscular mycorrhizal fungus enhanced cadmium fixation in rice root. *J. Hazard. Mater.* **416**, 125894 (2021).

269. Chen, X. W., Kang, Y., So, P. S., Ng, C. W. W. & Wong, M. H. Arbuscular mycorrhizal fungi increase the proportion of cellulose and hemicellulose in the root stele of vetiver grass. *Plant Soil* **425**, 309–319 (2018).
270. Vangelisti, A. *et al.* Transcriptome changes induced by arbuscular mycorrhizal fungi in sunflower (Helianthus annuus L.) roots. *Sci. Rep.* **8**, 4 (2018).
271. Matsubayashi, Y. Posttranslationally Modified Small-Peptide Signals in Plants. *Annu. Rev. Plant Biol.* **65**, 385–413 (2014).
272. Ogawa-Ohnishi, M. *et al.* Peptide ligand-mediated trade-off between plant growth and stress response. *Science* **378**, 175–180 (2022).
273. Amano, Y., Tsubouchi, H., Shinohara, H., Ogawa, M. & Matsubayashi, Y. Tyrosine-sulfated glycopeptide involved in cellular proliferation and expansion in *Arabidopsis*. *Proc. Natl. Acad. Sci.* **104**, 18333–18338 (2007).
274. Wang, Y., Chen, W., Ou, Y., Zhu, Y. & Li, J. *Arabidopsis* ROOT ELONGATION RECEPTOR KINASES negatively regulate root growth putatively via altering cell wall remodeling gene expression. *J. Integr. Plant Biol.* **64**, 1502–1513 (2022).
275. Tost, A. S., Kristensen, A., Olsen, L. I., Axelsen, K. B. & Fuglsang, A. T. The PSY Peptide Family—Expression, Modification and Physiological Implications. *Genes* **12**, 218 (2021).
276. Mosher, S. & Kemmerling, B. PSKR1 and PSY1R-mediated regulation of plant defense responses. *Plant Signal. Behav.* **8**, e24119 (2013).
277. Pruitt, R. N. *et al.* A microbially derived tyrosine-sulfated peptide mimics a plant peptide hormone. *New Phytol.* **215**, 725–736 (2017).
278. Yimer, H. Z. *et al.* Root-knot nematodes produce functional mimics of tyrosine-sulfated plant peptides. *Proc. Natl. Acad. Sci.* **120**, e2304612120 (2023).
279. Tsuzuki, S., Handa, Y., Takeda, N. & Kawaguchi, M. Strigolactone-Induced Putative Secreted Protein 1 Is Required for the Establishment of Symbiosis by the Arbuscular Mycorrhizal Fungus *Rhizophagus irregularis*. *Mol. Plant-Microbe Interactions®* **29**, 277–286 (2016).
280. Serrano, K. *et al. Spatial Co-Transcriptomics Reveals Discrete Stages of the Arbuscular Mycorrhizal Symbiosis*. http://biorxiv.org/lookup/doi/10.1101/2023.08.02.551648 (2023) doi:10.1101/2023.08.02.551648.
281. Yamaguchi, Y. L., Ishida, T. & Sawa, S. CLE peptides and their signaling pathways in plant development. *J. Exp. Bot.* **67**, 4813–4826 (2016).
282. Sasaki, T. *et al.* Shoot-derived cytokinins systemically regulate root nodulation. *Nat. Commun.* **5**, 4983 (2014).
283. Müller, L. M. *et al.* A CLE–SUNN module regulates strigolactone content and fungal colonization in arbuscular mycorrhiza. *Nat. Plants* **5**, 933–939 (2019).
284. Roy, S. & Müller, L. M. A rulebook for peptide control of legume–microbe endosymbioses. *Trends Plant Sci.* **27**, 870–889 (2022).
285. Le Marquer, M., Bécard, G. & Frei Dit Frey, N. Arbuscular mycorrhizal fungi possess a CLAVATA3/embryo surrounding region-related gene that positively regulates symbiosis. *New Phytol.* **222**, 1030–1042 (2019).
286. Patel, N. *et al.* Diverse Peptide Hormones Affecting Root Growth Identified in the Medicago truncatula Secreted Peptidome. *Mol. Cell. Proteomics* **17**, 160–174 (2018).
287. Downie, J. A. & Kondorosi, E. Why Should Nodule Cysteine-Rich (NCR) Peptides Be Absent From Nodules of Some Groups of Legumes but Essential for Symbiotic N-Fixation in Others? *Front. Agron.* **3**, 654576 (2021).

288. Yang, S. *et al.* Microsymbiont discrimination mediated by a host-secreted peptide in *Medicago truncatula*. *Proc. Natl. Acad. Sci.* **114**, 6848–6853 (2017).
289. Uhe, M. Functional analysis of arbuscular mycorrhiza-related membrane transporter and defensin genes of Medicago truncatula. (2018) doi:10.15488/3580.
290. Uhe, M., Hogekamp, C., Hartmann, R. M., Hohnjec, N. & Küster, H. The mycorrhiza-dependent defensin MtDefMd1 of Medicago truncatula acts during the late restructuring stages of arbuscule-containing cells. *PLOS ONE* **13**, e0191841 (2018).
291. Walder, F. *et al.* Plant phosphorus acquisition in a common mycorrhizal network: regulation of phosphate transporter genes of the Pht1 family in sorghum and flax. *New Phytol.* **205**, 1632–1645 (2015).
292. Fang, L. *et al.* Analysis of the AMT gene family in chili pepper and the effects of arbuscular mycorrhizal colonization on the expression patterns of CaAMT2 genes. *BMC Genomics* **24**, 158 (2023).
293. Liu, J. *et al.* The Potassium Transporter SlHAK10 Is Involved in Mycorrhizal Potassium Uptake. *Plant Physiol.* **180**, 465–479 (2019).
294. Watts-Williams, S. J. *et al.* Diverse *SORGHUM BICOLOR* accessions show marked variation in growth and transcriptional responses to arbuscular mycorrhizal fungi. *Plant Cell Environ.* **42**, 1758–1774 (2019).
295. Kameoka, H. & Gutjahr, C. Functions of Lipids in Development and Reproduction of Arbuscular Mycorrhizal Fungi. *Plant Cell Physiol.* **63**, 1356–1365 (2022).
296. Paszkowski, U., Kroken, S., Roux, C. & Briggs, S. P. Rice phosphate transporters include an evolutionarily divergent gene specifically activated in arbuscular mycorrhizal symbiosis. *Proc. Natl. Acad. Sci.* **99**, 13324–13329 (2002).
297. Yang, S.-Y. *et al.* Nonredundant Regulation of Rice Arbuscular Mycorrhizal Symbiosis by Two Members of the *PHOSPHATE TRANSPORTER1* Gene Family. *Plant Cell* **24**, 4236–4251 (2012).
298. Moore, W. M. *et al.* Reprogramming sphingolipid glycosylation is required for endosymbiont persistence in Medicago truncatula. *Curr. Biol.* **31**, 2374-2385.e4 (2021).
299. Panneerselvam, P. *et al.* Arbuscular Mycorrhizal Fungi (AMF) for Sustainable Rice Production. in *Advances in Soil Microbiology: Recent Trends and Future Prospects* (eds. Adhya, T. K., Mishra, B. B., Annapurna, K., Verma, D. K. & Kumar, U.) vol. 4 99–126 (Springer Singapore, Singapore, 2017).
300. Wang, Y., Bao, X. & Li, S. Effects of Arbuscular Mycorrhizal Fungi on Rice Growth Under Different Flooding and Shading Regimes. *Front. Microbiol.* **12**, 756752 (2021).
301. Watts-Williams, S. J. *et al.* Enhancement of sorghum grain yield and nutrition: A role for arbuscular mycorrhizal fungi regardless of soil phosphorus availability. *PLANTS PEOPLE PLANET* **4**, 143–156 (2022).
302. Cobb, A. B. *et al.* The role of arbuscular mycorrhizal fungi in grain production and nutrition of sorghum genotypes: Enhancing sustainability through plant-microbial partnership. *Agric. Ecosyst. Environ.* **233**, 432–440 (2016).
303. Montero, H., Choi, J. & Paszkowski, U. Arbuscular mycorrhizal phenotyping: the dos and don'ts. *New Phytol.* **221**, 1182–1186 (2019).
304. Müller, A., Ngwene, B., Peiter, E. & George, E. Quantity and distribution of arbuscular mycorrhizal fungal storage organs within dead roots. *Mycorrhiza* **27**, 201–210 (2017).
305. Garcia-Garrido, J. M. Regulation of the plant defence response in arbuscular mycorrhizal symbiosis. *J. Exp. Bot.* **53**, 1377–1386 (2002).

306. Muro, K., Kamiyo, J., Wang, S., Geldner, N. & Takano, J. Casparian strips prevent apoplastic diffusion of boric acid into root steles for excess B tolerance. *Front. Plant Sci.* **14**, (2023).
307. Tang, W. & Thompson, W. A. Role of the Rice BAHD Acyltransferase Gene OsAt10 in Plant Cold Stress Tolerance. *Plant Mol. Biol. Report.* **40**, 482–499 (2022).
308. Muroi, A. *et al.* Accumulation of hydroxycinnamic acid amides induced by pathogen infection and identification of agmatine coumaroyltransferase in Arabidopsis thaliana. *Planta* **230**, 517–527 (2009).
309. Barceló, M. *et al.* The abundance of arbuscular mycorrhiza in soils is linked to the total length of roots colonized at ecosystem level. *PLOS ONE* **15**, e0237256 (2020).
310. Maherali, H. Is there an association between root architecture and mycorrhizal growth response? *New Phytol.* **204**, 192–200 (2014).